Experimental and Numerical Modeling of a Tidal Energy Channeling Structure

Derek Foran

Thesis submitted to the

Faculty of Graduate and Postdoctoral Studies

in partial fulfillment of the requirements for the degree of

Master of Applied Science in Civil Engineering

Under the auspices of the Ottawa-Carleton Institute for Civil Engineering

Academic advisors: Dr. Majid Mohammadian and Dr. Ioan Nistor

University of Ottawa

Ottawa, Ontario, Canada

January 2015

Abstract

Tidal power, or the use of tides for electricity production, exists in many forms including tidal barrages, which exploit tidal head differentials, and turbines placed directly in regions with large tidal current velocities. The latter is actively being investigated in many countries around the world as a means of providing renewable and wholly predictable electricity (cf. wind, solar and wave power). The expansion of the in-stream tidal industry is hindered however by several factors including: turbine durability, deployment and maintenance costs, and the lack of abundant locations which meet the necessary current velocities for turbine start-up and economic power production. A new novel type of augmentation device, entitled the 'Tidal Acceleration Structure' or *TAS* (Canadian patent pending 2644792), has been proposed as a solution to the limited number of coastal regions which exhibit fast tidal currents. In preliminary investigations, the *TAS*, a simple Venturi section consisting of walls extending from the seafloor to above the high water mark in an hourglass shape, was found as able to more than double current velocities entering the device. The results indicated a significant advantage over other current channeling technologies and thus the need for more in-depth investigations.

The main objective of the present study was to optimise the design of the *TAS* and to predict the power that a turbine placed within it could extract from flow. To do this, two principal methods were employed. Firstly, a 1:50 scale model of the *TAS* was tested and its shape optimised in a 1.5 m wide flume. Secondly, a 3D numerical model (ANSYS Fluent) was used for comparison with the experimental results. During the tests, a *TAS* configuration was found that could accelerate upstream velocities by a factor of 2.12. In separate tests, turbines were simulated using Actuator Disc Theory and porous plates. The *TAS*-plate combination was found to be able to extract up to 4.2 times more power from flow than the stand-alone plate, demonstrating that the *TAS* could provide turbines with a significant advantage in slower currents.

Though further research is needed, including the testing of a larger *TAS* model in conjunction with a small in-stream turbine, the results of this thesis clearly demonstrate the potential of the *TAS* concept to unlock vast new areas for tidal energy development.

Résumé

L'énergie marémotrice, ou l'utilisation des marées pour la production d'électricité, existe sous plusieurs formes, incluant l'exploitation de l'énergie potentielle des variations du niveau de la mer, et l'énergie cinétique qui peut être captée par des turbines (hydroliennes). Ces dernières sont le sujet d'études dans plusieurs pays autour du monde afin de produire de l'électricité renouvelable et prévisible (cf. éolienne, solaire, houlomotrice). Désormais, l'expansion de l'industrie d'énergie marémotrice cinétique est gênée par plusieurs facteurs incluant : la durabilité des turbines, les coûts de lancement et d'entretien des machines, et le nombre d'emplacements limités ayant des courants avec la vélocité requise pour à la fois démarrer les turbines ainsi que produire l'électricité de façon économique. Un nouveau type de structure augmentative, appelée le 'Tidal Acceleration Structure' ou *TAS* (en attente du brevet Canadien 2644792), a été proposée comme solution au manque de régions qui démontrent des courants maritimes suffisamment élevés. Dans des études préliminaires, le *TAS*, une structure simple exploitant l'effet Venturi ayant des murs qui passent du fond à la surface de l'océan, a démontré sa capacité de plus de doubler le courant qui entre dans l'appareil. Les résultats indiquent un avantage significatif par rapport à d'autres structures augmentatives, et par conséquent, la nécessité d'enquêtes supplémentaires.

L'objectif principal de la recherche actuelle était d'optimiser le plan du *TAS* et de prédire la puissance qu'on peut extraire du champ d'écoulement. Pour faire ceci, deux méthodes ont été employées. Premièrement, une maquette de 1:50 du *TAS* a été examinée et sa forme optimisée dans un canal d'eau de 1.5 m de large. Deuxièmement, un modèle numérique 3D (ANSYS Fluent) a été utilisé pour comparer avec les résultats expérimentaux. Durant les tests, une configuration du *TAS* a démontré sa capacité d'accélérer le courant d'un facteur de plus de 2.12 comparativement à la vélocité en amont. Dans d'autres tests, des turbines ont été simulées en utilisant la Théorie de Froude et des plaques trouées. La combinaison *TAS*-plaque a été capable d'extraire jusqu'à 4.2 fois plus d'énergie que la plaque par elle-même, démontrant que le *TAS* pourrait accorder un avantage important aux turbines exploitant des courants d'eau lents.

Bien que des recherches supplémentaires soient requises, incluant la simulation d'un *TAS* plus large en conjonction avec une petite turbine, les résultats de cette thèse démontrent clairement le potentiel du concept *TAS* pour déchaîner le développement de l'énergie marémotrice dans de nouvelles régions.

Remerciements

En premier lieu, je voudrais remercier Dr. Ioan Nistor et Dr. Majid Mohammadian, mes superviseurs et professeurs à l'Université d'Ottawa, pour leur soutien et direction durant notre projet de recherche. Depuis qu'ils ont exprimé un intérêt dans mon idée d'énergie marémotrice tôt durant mon baccalauréat de Génie Civil, ils ont été fermes dans leur croyance en moi et dans le projet. Pour ceci, je suis sincèrement reconnaissant. Avoir eu le privilège de travailler avec vous deux a vraiment été la meilleure partie de mon expérience universitaire et je n'oublierai pas tout ce que m'avez appris.

Deuxièmement, je voudrais remercier tous ceux qui m'ont aidés durant mes recherches, particulièrement l'étudiante de l'Université de Technologie à Brauschweig Corinna Hohls et l'étudiant de l'Université d'Ottawa Mathieu Toupin, qui ont contribué énormément à la qualité de ma recherche. Je voudrais aussi remercier Milan Le Du et Marta Calitoiu, parmi d'autres étudiants, pour leur immense aide et amitié durant l'été 2014.

Troisièmement, je voudrais remercier le technicien de Génie Civil Marc Lapointe et l'équipe de l'atelier d'usinage de Génie Mécanique, pour leurs aide et conseils concernant l'installation de mes tests expérimentaux. À ma cohorte d'étudiants en génie civil, merci pour vos gentils conseils et les souvenirs qu'on a pu créer ensemble, c'était un plaisir de rentrer à l'école chaque jour quand vous étiez là. Je voudrais aussi remercier tout le personnel et faculté de Génie Civil qui ont rendu ma recherche et celles de mes collègues possibles. De plus, je veux souligner mon obtention de la bourse d'études supérieures de l'Ontario ainsi que la bourse d'admission de l'Université d'Ottawa ; elles m'ont beaucoup aidée à apprécier mes études.

Finalement, je veux remercier ma famille et mes amis, spécifiquement mes parents. Vous êtes les meilleurs exemples qu'un fils peut avoir.

Acknowledgments

First and foremost, I would like to thank Dr. Majid Mohammadian and Dr. Ioan Nistor, my supervisors and professors at the University of Ottawa, for their support and guidance during the course of our research project together. Since the time they first expressed interest in my tidal energy idea early on in my undergraduate Civil Engineering degree, they have been steadfast in their belief in me, and the project. For this, I am sincerely grateful. Working with both of you has truly been the best part of my university experience and I will not soon forget everything you have taught me.

Secondly, I would like to thank all those who have helped me during the course of my research, particularly Braunschweig University of Technology student Corinna Hohls and University of Ottawa student Mathieu Toupin, who contributed greatly to the quality of my research. I would also like to thank Milan Le Du and Marta Calitoiu, amongst other students, for their help and friendship over the summer of 2014.

Thirdly, I would like to thank Civil Engineering technician Marc Lapointe and the Mechanical Engineering machine shop team for their help and advice in the creation of the experimental testing setup. To my fellow Civil Engineering students, thank you for your kind advice and shared memories, you made it a pleasure to come to school every day. Also, I would like to extend my thanks to all the Civil Engineering Department staff and faculty who help make my and others research possible, often without receiving much formal credit. In addition, I acknowledge receiving the Ontario Graduate Scholarship and the University of Ottawa admission scholarship; these helped me greatly to enjoy my graduate level education.

Finally, I would like to thank my family and friends, especially my parents. You are the best role models a son could ask for.

Table of Contents

List of Figures

List of Tables

List of Notations

α	permeability of the medium
Δm	thickness of the medium
θ	open area ratio or porosity of the porous plate
ρ	fluid density
μ	laminar fluid viscosity
$\bar{\bar{\tau}}$	stress tensor
λ_F	force ratio
λ_L	length ratio
λ_V	velocity ratio
A_{15D}	cross-sectional area 15 cm downstream of the disc
A_{15U}	cross-sectional area 15 cm upstream of the disc
A	cross section area
a	axial flow induction factor
A_D	area of the disc
A_i	cross-sectional area at any point along the stream-tube
AR	acceleration ratio – analogous to the velocity *Speed-Up Factor*
C_2	pressure-jump coefficient in Fluent
C_D	dimensionless drag coefficient
c_f	friction coefficient based on the Manning or Chézy coefficient
C_p	power coefficient or turbine efficiency
C_T	porous disc thrust coefficient
DF	Deviation Factor
d_i	distance to the middle of this sub-section
F_D	drag force
F_{LC}	force measured by the load cell
F_m	force in the model
F_p	force in the prototype
g	gravitational acceleration
h	water depth
I	unit tensor
k	resistance coefficient of the porous disc to flow

L_m	length scale of the model
L_p	length scale of the prototype
$\dot{m}_{pq}$	mass transfer from phase *p* to phase *q*
$\dot{m}_{qp}$	mass transfer phase *q* to phase *p*
MV	Modified Velocity
p	static pressure
p_D^-	pressure just downstream of the disc
p_D^+	pressure just upstream of the disc
P_{ext}	power extracted by the actuator disc
S_{a_q}	mass source term in Fluent
S_m	mass added per unit time to the continuous phase from the dispersed second phase or any other user defined source
TAS	Tidal Acceleration Structure
T	thrust force imparted by flow on the turbine/plate
t	time
U_{15D}	velocity 15 cm downstream of the disc
U_{15U}	velocity 15 cm upstream of the disc
U_∞	velocity far upstream of the disc in Actuator Disc Theory
u	flow velocity vector field
U_D	velocity at the actuator disc
U_i	average velocity at any point along the stream-tube
$\vec{v}$	velocity vector
v	fluid velocity
VC_{mean}	average velocity at the centre of the *TAS* between 10 and 22.5 cm above the bed
v_i	average velocity in this sub-section
V_m	velocity in the model
V_o	in-stream velocity upstream of the turbine
V_p	velocity in the prototype
V_{up}	velocity 2 m upstream of the *TAS* in *Side* profile
W_{15}	width of opening 15 cm upstream or downstream of the disc
W_D	width of the disc
Z	distance between the bed surface and the reference level

Chapter 1. Introduction

1.1. Background

The use of tidal energy to generate electric power is expanding rapidly in many countries around the world, including Canada. Tidal harnessing projects range from tidal barrages, which use water head differentials, to turbines placed directly in fast flowing tidal currents (Bedard et al. 2005; Khan et al. 2009). Several companies and institutions around the world are currently investigating the latter for power production, due to its lower impact on the environment and its advantages over wind, solar and other renewables in terms of power production predictability (see Section 2.2.3).

The in-stream tidal industry is still relatively un-developed, with most companies either still proving their prototypes merits or having only small commercial deployments. Deployment cost and reliability of the turbines are still the primary concerns for the development of tidal energy and therefore the sector still suffers a competitive disadvantage over other renewable energy sources (Robertson 2014). Primarily, in-stream tidal is being investigated in countries with public mandates to invest in clean energy and which also have a multitude of ocean sites with fast tidal currents. These include the UK, Canada, France, the USA and Ireland amongst others. Because sites must match all necessary criteria for tidal development whilst taking into account other concerns (proximity to market/electrical grid, water bathymetry and ocean bottom conditions, water use conflicts, etc.), besides the primary concern for a high energy current environment, the potential for development in many locations around the world is limited. The elimination of any of these requirements, or an alleviation of one of them, could be the key to bringing down tidal project costs and allow for competitive electricity prices as compared to other sources of clean energy.

1.2. Significance and Novelty of the Study

The subject of this research project was the development of a new method of extracting energy from the tides. The idea, invented by the author and pending under Canadian patent 2644792, uses a constriction to accelerate flow (Venturi effect) and in turn increase the energy which can be extracted with a turbine. The structure in question is named the Tidal Acceleration Structure (*TAS*) and was designed to be constructed for either two-way (ebb and flood tides) or one-way capture of fluid kinetic energy. Though the wind energy sector (MacQuarrie 2011; Ohya and Karasudani 2010; Setoguchi et al. 2004) and other tidal/river concepts (Sireli 2014; Gaden and Bibeau 2010; Ponta and Shankar Dutt 2000) have utilised the Venturi effect, the tidal design presented herein is novel in many respects. Therefore, to the best of the author's knowledge, no published research exists on the specific design. A pictorial showing the basic configuration of the concept is presented in Figure 1-1 below.

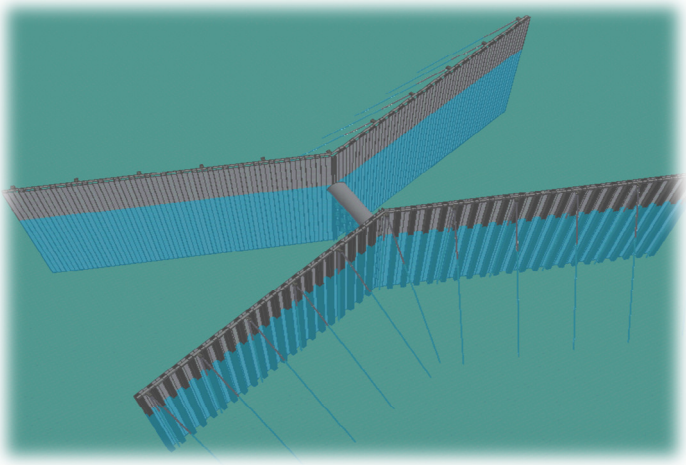

Figure 1-1: Perspective View of the Tidal Acceleration Structure

What makes the *TAS* different than existing patents and published paper embodiments is that it utilises containment walls extending from the seafloor to above the water surface to funnel the flow into a central section where a turbine or group of turbines would be located. The scale of the structure is also larger than most other duct systems as the four walls shown in Figure 1-1 above were envisioned as being 30 m in length (Foran et al. 2012). Though unverified in the current research project, it is

suspected that the *TAS* is able to reduce the peak forces acting on the turbines by straightening the incoming flow and eliminating some of the random directional change that occurs over a tidal cycle. This could be a major advantage for the *TAS* design, compared to conventional in-stream turbines, as turbine construction and lifespan are currently limited by these peak flow forces (Bedard et al. 2005). The *TAS* is also distinctive in that it is not a turbine-specific design, but instead creates a channel of increased flow velocity where any turbine could theoretically be placed for enhanced power production. This is an important improvement as the primary limitation for many potential tidal berths is that the average flow velocity is too low and the turbines cannot produce power for part of the tidal cycle due to their minimum start-up or cut-in speed (Bedard et al. 2005). Sites that are currently being investigated for in-stream tidal turbine development, such as the Minas Passage in Nova Scotia, are in remote locations far from electricity grids and therefore there are additional costs associated with bringing the electricity from these sites to market. By increasing the current magnitudes and in effect lowering the required magnitudes for turbine start-up, the *TAS* could greatly increase the number of viable tidal development locations.

The structure described herein has the potential to become an important and viable renewable energy alternative which would expand worldwide use of water flows as a source of energy. However, before any large prototypes or commercial structures can be built, the specific impacts on water flow conditions and potential power generation must be investigated.

1.3. Objectives of the Study

The development of the Tidal Acceleration Structure can be separated into long and short term goals. Long term, the final objective is to have a full-scale working prototype operating in a region of medium tidal current velocity somewhere in Canada or elsewhere in the world. At this stage, the project would be in partnership with a major turbine developer. This final project phase would require a sizable

monetary investment therefore more modest research steps must be taken first to verify the feasibility of the concept. The knowledge gained during the current research project was thought to be a vital first stage in making the final prototype deployment a reality.

The experimental objectives of the current research project were relatively straightforward:

1. **To build a scaled *TAS* and test its hydrodynamic performance in a flume**
2. **To test the *TAS* design using a 3D numerical model**
3. **To compare the results of the experimental and numerical tests for the purpose of calibrating the numerical model for future *TAS* simulations**

Underscoring all of the above, the main objective of the study was to optimise the design of the *TAS* and to predict the power that a turbine placed within its contraction could extract from flow.

To attain these goals, more specific objectives were also laid forth. The velocities generated within and around the structure in the experimental flume tests were sought in order to compute the power production potential and for comparison with velocity profiles from the numerical model. To estimate the power production potential, a porous plate placed at the centre of the structure was envisioned to be used in conjunction with the principles of Actuator Disc Theory (see Section 2.4.1). To determine the best possible wall shape for power capture, several different *TAS* configurations were planned for testing with and without the porous plates. As the current project was the first in-depth exploration of the *TAS* concept, the objectives and ambition of the study evolved slightly as the project progressed. At its core, the objective of the study was simple: to further the knowledge of and perfect the design of the Tidal Acceleration Structure.

1.4. Scope of the Study

As mentioned, the objectives of the study evolved somewhat over time as there were many unknowns associated with the research and some delays and problems occurred. As well, the physical experimentation allowed for the discovery of elements that were not initially pondered and this added to the project deviating somewhat in its specifics from the initial plan. That being said, the scope of the study was focused on the experimental modeling of a 1:50 scale *TAS* model in the 1.5 m wide, 30 m long flume located in the hydraulics lab of the University of Ottawa. The main parameter of interest in the modeling was the velocity field generated by a 14.14 cm/s in-stream current with a depth of 30 cm. This was equivalent to a 1 m/s current with a depth of 15 m at full scale. The velocity field was captured by taking velocity points with a Nortek Vectrino ADV at many points within and around the structure. Points were taken longitudinally through the centre of the structure to capture the flow acceleration caused by the *TAS* and also longitudinally through the centre of the flume to measure the blockage effect of the *TAS* on the overall flow field. Different *TAS* shapes were tested by changing one geometric parameter at a time in a methodic optimisation fashion, with the goal of determining the structure shape which produced the highest velocities at its centre. It was thus deemed that the designs which were "performing" best were those with the highest ratio of *velocity at the centre of the TAS* to *velocity upstream of the TAS* (speed-up factor). One limitation of the physical experimental work was that some physical parameters were fixed and not varied from test to test (only one depth, one in-stream velocity and one wall length were tested). Choosing other parameters would have changed the flow-structure interaction and thus different speed-up factors could have been attained. One side query which was investigated quickly, was the impact of a net placed across the *TAS* entrance on flow. Other issues which could have been beneficial to investigate included the impact of changes in bottom topography, more complex wall shapes, and changes to bed friction both inside and outside of the structure.

Unfortunately, time limitations did not allow for their inquiry and are therefore recommended for future studies.

Another major test component of the project was the impact of using porous plates to simulate the impact of turbines at the *TAS* centre. Using Actuator Disc Theory, the plates were carefully manufactured to the standards of a previous study and tested with numerous *TAS* wall configurations. In total, 23 tests were performed using three plates of different widths. ADV readings were taken in these tests however, the power extracted by the plates was the main objective of concern. A load cell was used to measure the thrust on the plates and, along with the estimated velocity through the plate and Actuator Disc Theory, an extracted power value was computed.

The first numerical model employed in the project was the 2D Hemat program and the work focused on obtaining an initial *TAS* design which could then be used in the experimental modeling. The 3D numerical work discussed herein focused on the simulation of a 10 cm wide contraction, 25 cm opening *TAS* as located in the 1.5 m wide flume. The 3D CFD efforts were performed using ANSYS Fluent and compared to the velocity field observed in the experimental model in the hopes of validating the numerical model. Two original objectives of the numerical work were to simulate the *TAS* at full scale and also to simulate the presence of the actuator disc using Fluent's *Porous Jump Model*. Unfortunately, these objectives could not be completed because of time limitations. Overall, the scope of the study was quite large and it's believed the work will be invaluable to any further investigations into the *TAS* concept.

1.5. Thesis Outline

The following provides a brief outline of the thesis.

- The current chapter, **Chapter 1**, was meant as an introduction to the study without focusing on any details.
- In **Chapter 2**, the relevant literature was reviewed starting with the theoretical background of tidal energy including current in-stream tidal technologies. Tidal channeling devices were explored next and the Tidal Acceleration Structure (*TAS*) introduced. Finally, strategies for modeling turbines experimentally and numerically, both using Actuator Disc Theory, were outlined.
- **Chapter 3** briefly outlined the research methodologies employed including the research objectives, testing parameters and the *TAS* optimisation strategy used during the physical modeling.
- The physical modeling work was detailed in **Chapter 4** and was the most extensive chapter as it represented a significant portion of the study. The experimental setup was reviewed as well as the instrumentation before detailing the specific procedures used in each stage of testing. A sensitivity analysis conducted to justify structure scale was then probed before delving into the main results of the three stages of the experimental testing.
- **Chapter 5** focused on the numerical modeling of the *TAS* concept starting with a 2D numerical study using the Hemat software. The chapter then examined the 3D numerical simulations done using ANSYS Fluent, conducted to calibrate a numerical model against the experimental results which could then be used for simulating the *TAS* at full scale. The comparison of the experimental and Fluent results was also done in the chapter.
- In **Chapter 6**, additional discussion points regarding the *TAS* were made including some regarding the experimental and numerical results which were not discussed in their specific chapters.
- Finally, **Chapter 7** lists the overall conclusions of the study.

Chapter 2. Literature Review

2.1. Introduction

This chapter will begin by introducing tides and tidal energy before delving more in detail to the phenomena which affect the study at hand. Different types of tidal energy extraction methods will be discussed as well as the physics of tides. Channeling devices for use with in-stream turbines will be explored and the novel Tidal Acceleration Structure (*TAS*) introduced. After this, the methods with which one can model a turbine in conjunction with a channeling device will be presented, including physical modeling using porous plates and numerical modeling using a momentum sink model.

2.2. Tidal Energy – Theoretical Background

2.2.1 Tides

Tides are the periodic rise and fall of ocean levels caused by the gravitational effects of the moon and sun and the rotation of the Earth. Due to the liquid nature of water, the oceans are able to bulge and deform towards a gravitational force much more than the solid earth. Throughout the course of history, the methods of predicting tides were secrets passed down from generation to generation due to their importance for coastal navigation. There are generally considered to be two types of tide events: spring tides, the greater or more extreme tidal events, and neap tides, the smaller events. Spring tides occur when the gravitational effects of the moon and sun coincide or align to create large tidal ranges. In comparison, neap tides are the minimum tidal range events and are caused by the gravitational effects of the moon and sun being 90^{o} out of sync (see Figure 2-1 below, note that spring tide does not often occur exactly at the point of perfect sun–earth–moon alignment). Though the gravitational effects of the moon and sun are both important, the moon is 2.16 times more influential than the sun and thus is the major contributor to tidal ranges (Hicks and Szabados 2006).

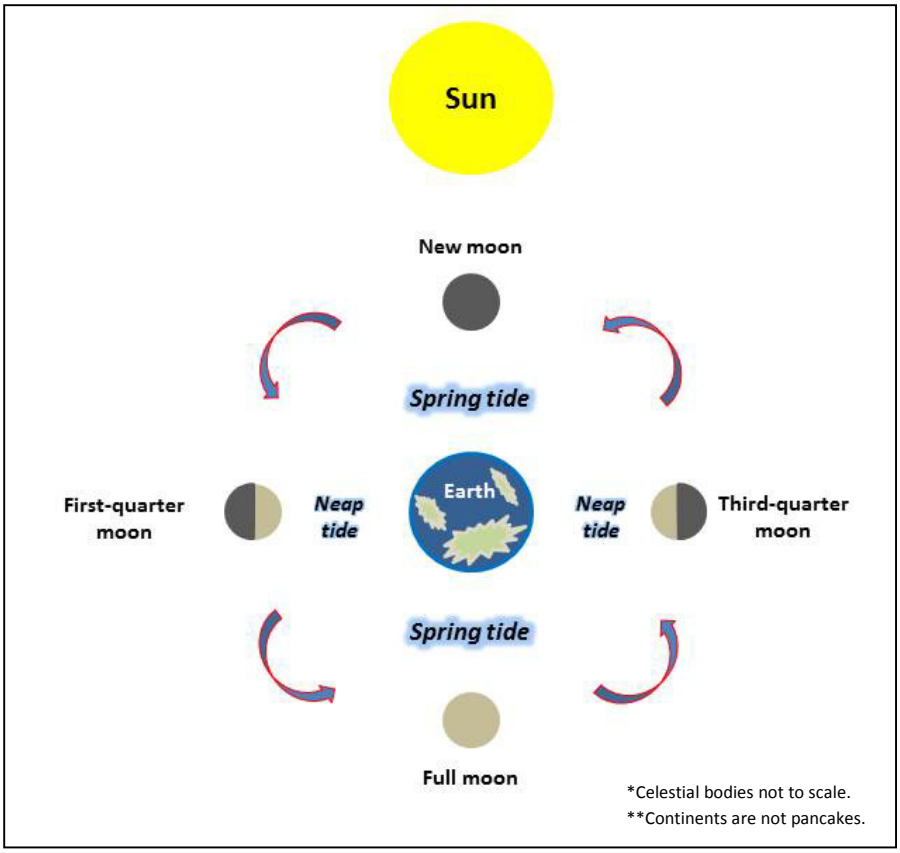

Figure 2-1: Generalised Relationship between Tides and Lunar Cycle

Other factors affecting tidal levels are coastline shape, coastal bathymetry and amphidromic point proximity. The various influences often act with different periods and intensities and these are called tidal constituents (Parker 1991). Amphidromic points are locations where there is zero amplitude for one of the tidal constituents. Usually, the most dominant constituent is the principal lunar semi-diurnal or the *M2 Constituent.* The *M2* has a period of 12.42 hours, half a tidal lunar day, and can be attributed to the time separating one lunar zenith from the next. Other constituents of importance include the solar semi-diurnal (*S2*), the larger lunar elliptic semi-diurnal (*N2*), the luni-solar declinational (*K1*), principal lunar declinational (*O1*) and principal solar declinational (*P1*) amongst many others. In some locations very few constituents are needed to accurately describe the tidal cycle where as in others many more are needed. Depending on the local strength of each constituent the tides can either be semi-diurnal (two equal low and high tides per day), mixed (two low and high tides of different strengths

per day) or diurnal (only one low and high tide per day) (Schwartz 2006). As the *M2* is often the forcing constituent and the lunar day does not match up with the solar day, the time and intensity of low and high tide do not repeat themselves every day but follow a longer, more complex cycle.

The two main phenomena associated with tides are water elevation change, which is quantified in terms of tidal range (high tide minus low tide water levels), and the horizontal component: tidal currents. Tidal currents are either considered as ebb (water receding towards low tide) or flood (water approaching towards high tide) currents and these are often not in opposite directions. The direction, velocity profiles and resulting turbulence are affected by upstream bathymetry and channel shape therefore the ebb and flood currents can be quite asymmetric (Schwartz 2006).

2.2.2 Historical Tide Exploitation – Tidal Lagoons

The first use of tides by man for power purposes was using tide mills. The structures were placed on tidal inlets or river estuaries and functioned by trapping water at high tide in a reservoir via a dam and then storing the water until low tide to drive a water wheel. Tide mills were used quite commonly in the Middle Ages and possibly even dating back as far as Roman times on the River Fleet (Spain 2002).

Figure 2-2: Tide Mill at Olhão, Portugal (Source: Wikipedia.org)

A more modern use of tidal head differentials can be found in tidal barrages. This type of dam structure was first used for electricity production at the La Rance Tidal Power Station in the Brittany region of France. The facility opened in the 1960's and can produce power during both ebb and flood for a total installed capacity of 240 MW (Cousineau 2012). Tidal barrages, like tide mills, function by exploiting the water differential between high and low tides. The water is let in and out using sluices and energy is extracted with turbines placed inside the sluices. Some tidal barrages can produce power during both ebb and flood tide events where as others can only produce electricity in one flow direction. The operational cycle and corresponding water level inside the barrage are usually controlled to maximise power output while providing a stable load to the grid. Currently the largest tidal barrage facility in the world is in Sihwa Lake, South Korea. Completed in 2010, the facility is a retrofitted 11 km barrage with a power capacity of 254 MW, slightly higher than La Rance (Bahaj 2011).

Figure 2-3: Sihwa Lake Tidal Power Plant under Construction, South Korea (Source: Wikipedia.org)

In Canada, the only tidal barrage which is currently in existence is the Annapolis Royal Tidal Power plant which was completed in 1984 and has a 20 MW capacity. Historically there had been some talk of

developing larger barrages in the Minas Basin, Nova Scotia but this was never pursued due to fears over impacts on the surrounding ecosystem and tidal levels over a large area (Garrett 1974).

More recently, a research team at the University of Ottawa led by Julien Cousineau, Dr. Ioan Nistor and Dr. Andrew Cornett, investigated the feasibility of developing tidal lagoons in the Bay of Fundy (Cousineau 2012). Using a calibrated 2D hydrodynamic model, the team investigated the change in tidal ranges and currents due to the construction of several lagoon scenarios including both coastal and offshore options. They concluded that though changes to the local tidal currents would be significant due to the lagoon presence and power extraction, the changes to far-field tidal conditions in the Bay of Fundy and larger Gulf of Maine region could be minimised with careful selection of lagoon location and size. Figure 2-4 below shows the meshing for two of the modeled scenarios.

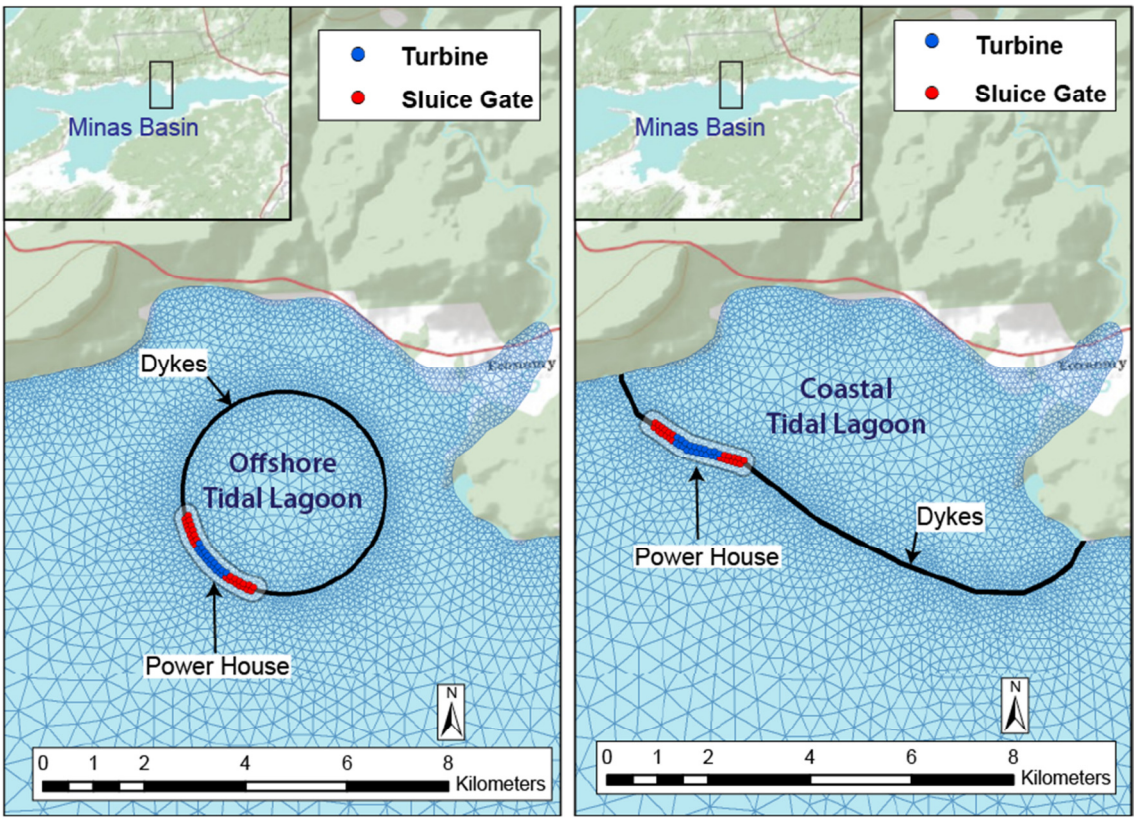

Figure 2-4: Meshing of Tidal Lagoon Modeling in the Bay of Fundy (Cousineau et al. 2012)

2.2.3 In-Stream Tidal Power Generation

Relatively new compared to tidal barrages, in-stream tidal energy devices produce power by extracting kinetic energy from flow. Inspired from wind energy devices which have been around for centuries (i.e. windmills), in-stream turbines are generally considered to be invented in France in 1923 with the vertical axis Darrieus turbine (Bedard et al. 2005).

Hydrokinetic turbine blades move by utilising the lift created on their blades by the ambient flow velocity. The greater the flow velocity, the greater potential for lift and consequently the greater potential for power production. The specific power available to an in-stream turbine is given by (Bahaj 2011):

$$P_o = \frac{1}{2} C_p \rho A V_o^3 \quad \textbf{(2-1)}$$

Where:

- C_p is the power coefficient or turbine efficiency
- ρ is the density of water
- A is the cross-sectional area of the turbine swept area
- V_o is the in-stream velocity upstream of the turbine

The C_p value is limited to 0.593, a theoretically derived limit also known as the Betz limit (Bahaj 2011), as flow is forced around the turbine because of the energy removal (discussed further in Section 2.4.1). Another parameter of interest is the coefficient of thrust which describes the thrust imparted by flow on the hydrodynamic subsystem in comparison to flow conditions.

$$C_t = \frac{T}{\frac{1}{2} \rho A V_o^2} \quad \textbf{(2-2)}$$

Where:

- T is the thrust force imparted by flow on the turbine/plate (equivalent to the drag force acting on the turbine/plate)

- ρ is the density of water
- A is the cross-sectional area of the turbine swept area
- V_o is the in-stream velocity upstream of the turbine

It should be noted that C_t represents the loading of the subsystem and is independent of scale (Bahaj 2011).

Because the in-stream tidal power industry is still relatively undeveloped, the implementation of devices presents many challenges. There are however many advantages to in-stream tidal as compared to other power production technologies (Fraenkel 2006).

Advantages	Challenges
• Predictable power ouput (cf. wind, solar, wave) • Renewable • Environmental impacts thought to be low • Relatively straighforward energy extraction process (cf. wave energy) • Lessons learned from offshore oil & wind energy	• High installation and maintenance costs • Turbine fixing considerations (gravity, pile or floating) • Full impact of devices on marine life unknown • Effects on surrounding and far-field flow conditions • Water-use conflicts (fishing, recreation) • Site specific challenges including waves, tidal range, floating debris (logs, ice, boats) • Locations are quite limited (peak currents > 2-2.5 m/s, proximity to coast, grid & ports)

Figure 2-5: Advantages and Challenges to In-Stream Tidal Power Implementation

Though many sites exhibit challenges when it comes to actual in-stream tidal power installations, there is thought to be vast potential for in-stream tidal energy worldwide. A survey conducted by consulting firm Black and Veatch came up with the estimate of there being about 159 TWh of extractable in-stream tidal power worldwide (Black and Veatch Consulting Ltd. 2004). This number should only be taken as a rough estimate however as there are many uncertainties associated with the prediction. A more thorough analysis was conducted in the same paper but only for United Kingdom waters and the

estimate given for only this jurisdiction was 22 TWh of extractable resource potential. Figure 2-6 shown below, given by the tidal turbine developer Atlantis Resources Ltd, depicts a rough estimate of worldwide tidal in-stream power potential.

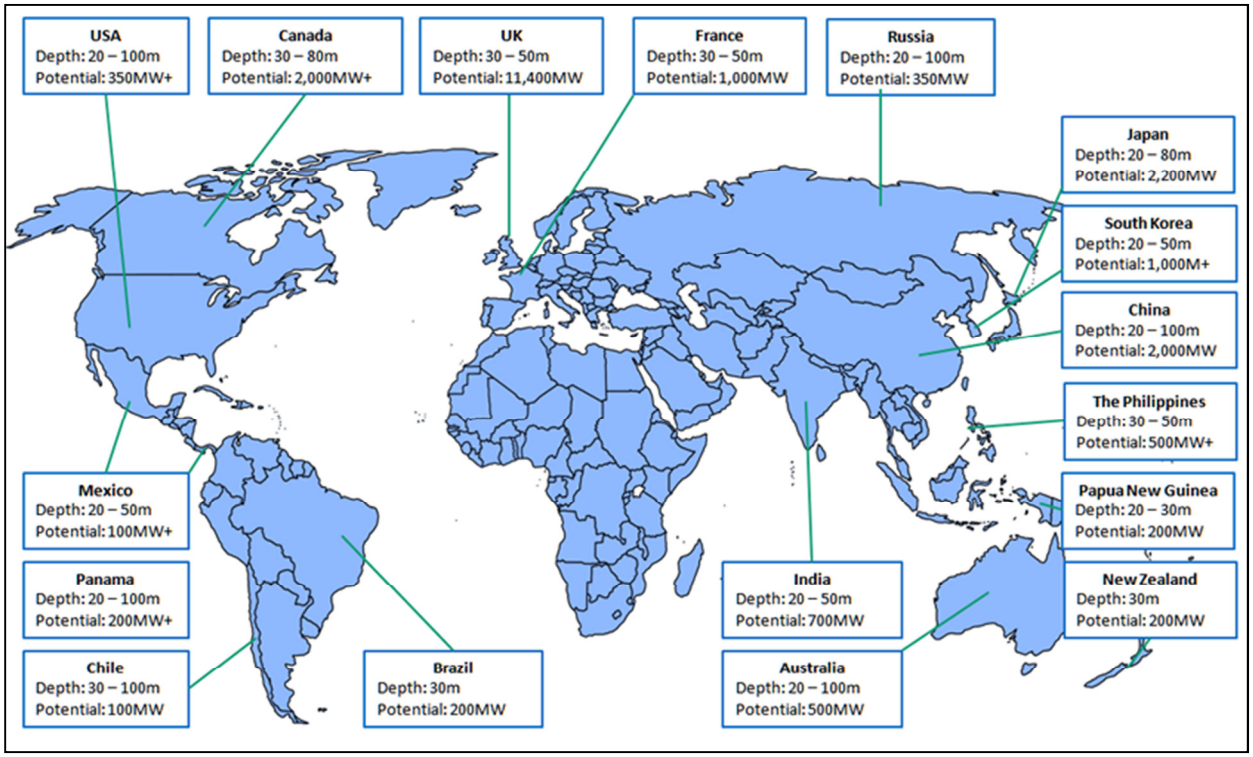

Figure 2-6: Rough Estimate of Worldwide Tidal Stream Resource (Source: atlantisresourcesltd.com)

The power potential estimations of Figure 2-6 above can also be shown in terms of country ranking.

Table 2-1: Country Ranking of Worldwide Tidal Stream Resource (Source: atlantisresourcesltd.com)

Rank	Country	Potential (MW)
1	UK	11 400
2	Japan	2 200
3	Canada	2 000+
4	China	2 000
5	South Korea	1 000+
6	France	1 000

7	India	700
8	The Philippines	500+
9	Australia	500
10	USA	350+
11	Russia	350
12	Panama	200+
13	Brazil	200
14	New Zealand	200
15	Papua New Guinea	200
16	Mexico	100+
17	Chile	100

In terms of Canadian waters, an extensive study was performed by Dr. Andrew Cornett and the National Research Council of Canada to locate potential areas for in-stream tidal development (Cornett 2006). This study did not focus on actual extractability of the resource with all its cost and feasibility aspects, but purely on the power available in the water. With the use of various numerical models from different sources, the researcher identified several locations within Canada with excellent tidal development potential. The following figure depicts the RMS velocities found in the study for two broad regions of interest (amongst others, including Ungava Bay in northern Quebec).

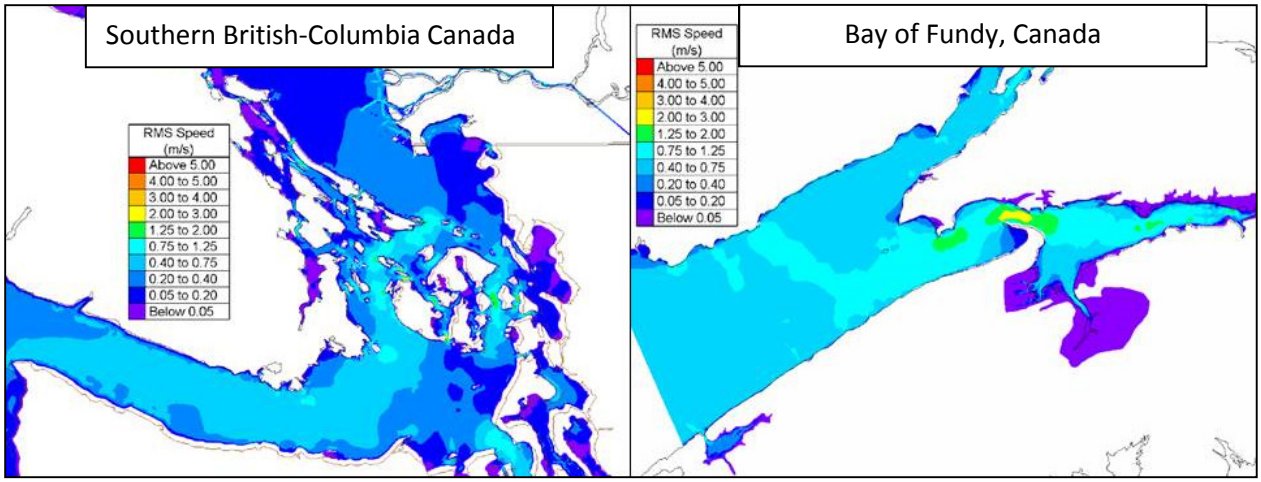

Figure 2-7: RMS Speed - Southern BC and Bay of Fundy (Cornett 2006)

As stated in Figure 2-5, high current velocities are only one part of the puzzle when it comes to tidal power development therefore, site-by-site analysis is required to assess whether tidal turbine installations are viable and realistic at the Canadian locations described above.

As mentioned, the two most conventional types of tidal in-stream devices are vertical and horizontal axis turbines however there are other types. Table 2-2 below presents a list of various turbine manufacturers and their device types along with a picture of the device.

Table 2-2: In-Stream Tidal Types and Device Manufacturers

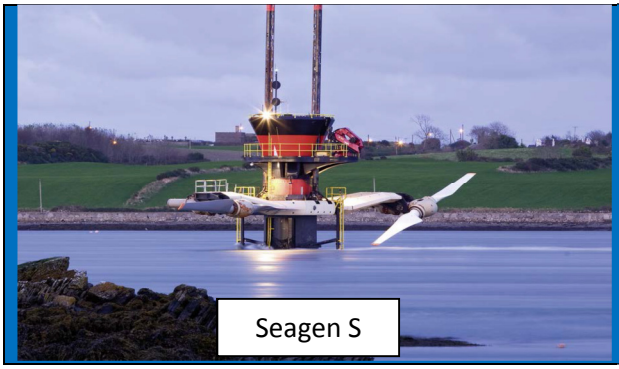 Source: http://www.marineturbines.com/	**Marine Current Turbines (Siemens) – UK** • Horizontal axis turbines • Pile and floating pontoon based designs • Seagen: First commercial tidal in-stream device • Seagen: Generated 10x more power than rest of in-stream industry combined as of 2014

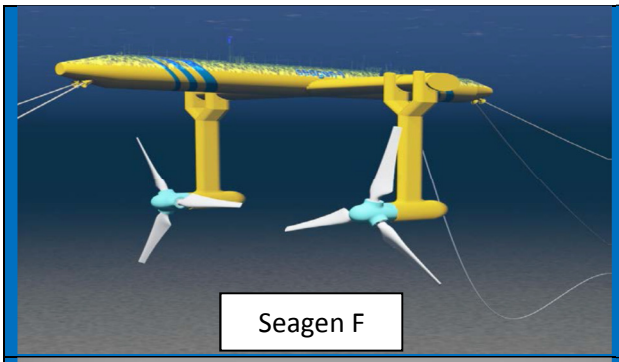

Source: http://www.bluewater.com/

- March 2014: Announced planned installation of Seagen F in conjunction with Bluewater Energy Services and Minas Energy at FORCE, Nova Scotia
- November 2014: Siemens announced they are selling MCT

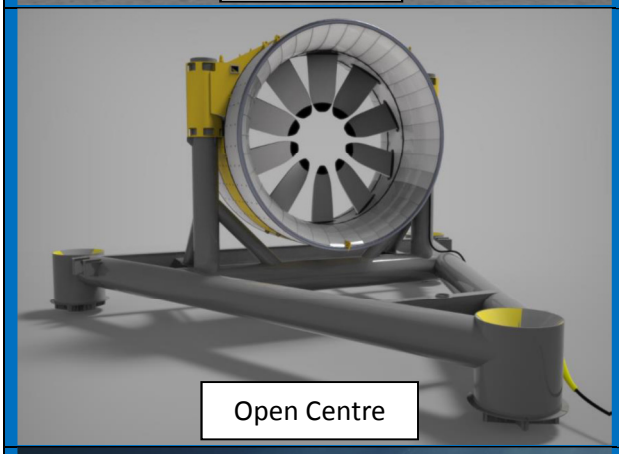

Source: www.openhydro.com

OpenHydro (DCNS) – Ireland

- Augmented/ducted turbine
- Horizontal axis turbine
- Open-centre ducted design
- Gravity base
- First company to deploy turbine in Bay of Fundy – Turbine destroyed in 1 week
- 2015: Planned deployment of 2 turbines at FORCE, Nova Scotia

Source: http://atlantisresourcesltd.com/

Atlantis Resources (Lockheed Martin) – Singapore

- Horizontal axis turbine
- Gravity base
- Owners of MeyGen ltd, consortium to develop 398 MW in Pentland Firth, Scotland
- Berth holder at FORCE, Nova Scotia

Source: http://www.hammerfeststrom.com/

Andritz Hydro Hammerfest – Norway

- Horizontal axis turbine
- Gravity base
- Set to develop 105 MW at Sound of Islay, Scotland
- Turbines set to be installed in MeyGen project

 Source: http://www.cleancurrent.com/	**Clean Current – Canada** - Augmented/ducted turbine - Horizontal axis river and tidal turbines - 2015: Set to deploy a 3.5 m diameter turbine at Grand Passage, NS, Canada - 2006: Deployed a demonstration turbine at Race Rocks, BC, Canada
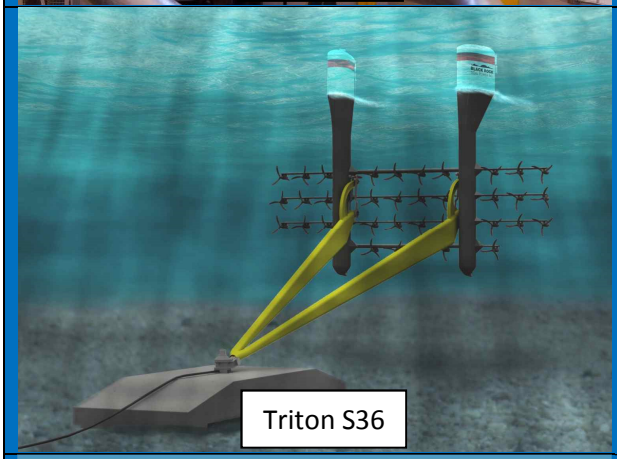 Source: www.blackrocktidalpower.com	**Black Rock Tidal Power – Canada** - Horizontal axis turbines - Gravity base with floating support - Utilises grid of Schottel STG turbines - Turbines can float and rotate to surface for maintenance - Berth holder at FORCE, Nova Scotia
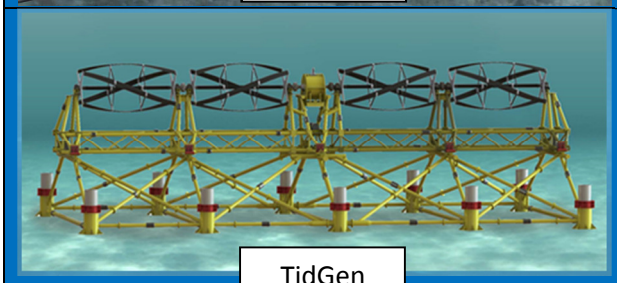 Source: http://www.orpc.co/	**Ocean Renewable Power Company – US** - Vertical axis turbines - Utilisation of Gorlov turbine design - Set to deploy up to 5 MW in Maine, US in the near future - Set to deploy a turbine device at Digby Gut, NS, Canada with Fundy Tidal Inc.
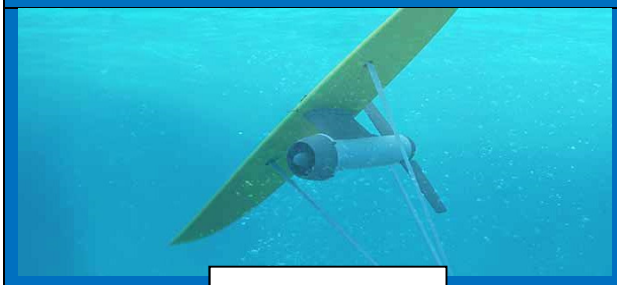 Source: http://minesto.com/	**Minesto – Sweden** - Horizontal axis turbine attached to kite - Kite is propelled in figure eight pattern by tidal currents - Kite travels up to 10 times faster than ambient current velocity - 2016: Goal to produce 1.5 MW array

As seen in Table 2-2 above, there are many different types of in-stream tidal turbines which are currently competing for development in the growing tidal industry. The list of turbine types (vertical and

horizontal axis, kite, ducted horizontal axis) presented is not all-inclusive as there are other types including flutter vane, gravitational vortex, Venturi, vortex-induced-vibration, piezo-electric, sail and oscillating foil (Khan et al. 2009). This is not even including augmentation channel types which can be used along with many of the above energy extraction devices. Though the recommended or ideal device, from those presented in Table 2-2 above, would vary depending on the tidal site, only time will tell whether each or any will progress past prototype and early commercial phase development. At this moment, a thorough comparison of their strengths and deficiencies would be unsubstantial therefore none has been made.

2.3. Tidal Energy Channeling Devices

There are many types of channelling devices which can be used in conjunction with turbines or other tidal stream devices to enhance flow. The ducts around the turbines of OpenHydro and Clean Current shown above in Table 2-2 are some of them. In this section, the function of these devices will be explored and the state-of-the-art technology compared. Lastly, a new channeling device design, the Tidal Acceleration Structure or *TAS* for short, will be introduced and described.

2.3.1 Venturi Effect

Tidal channeling devices function by exploiting a basic fluid phenomenon: the Venturi effect. First studied by and named after Giovanni Battista Venturi (Venturi 1799), the basic principle dictates that when the cross-sectional area through which a fluid passes is reduced, the velocity of the fluid increases and the static pressure decreases. This phenomenon exists because fluids in motion must satisfy continuity as expressed in the following equation (Pedlosky 1987):

$$\frac{\partial \rho}{\partial t} + \nabla * (\rho u) = 0 \qquad \textbf{(2-3)}$$

Where:

- ρ is the fluid density
- t is time
- u is the flow velocity vector field

The Venturi effect is easier to understand when explained in a visual manner as shown in Figure 2-8 below.

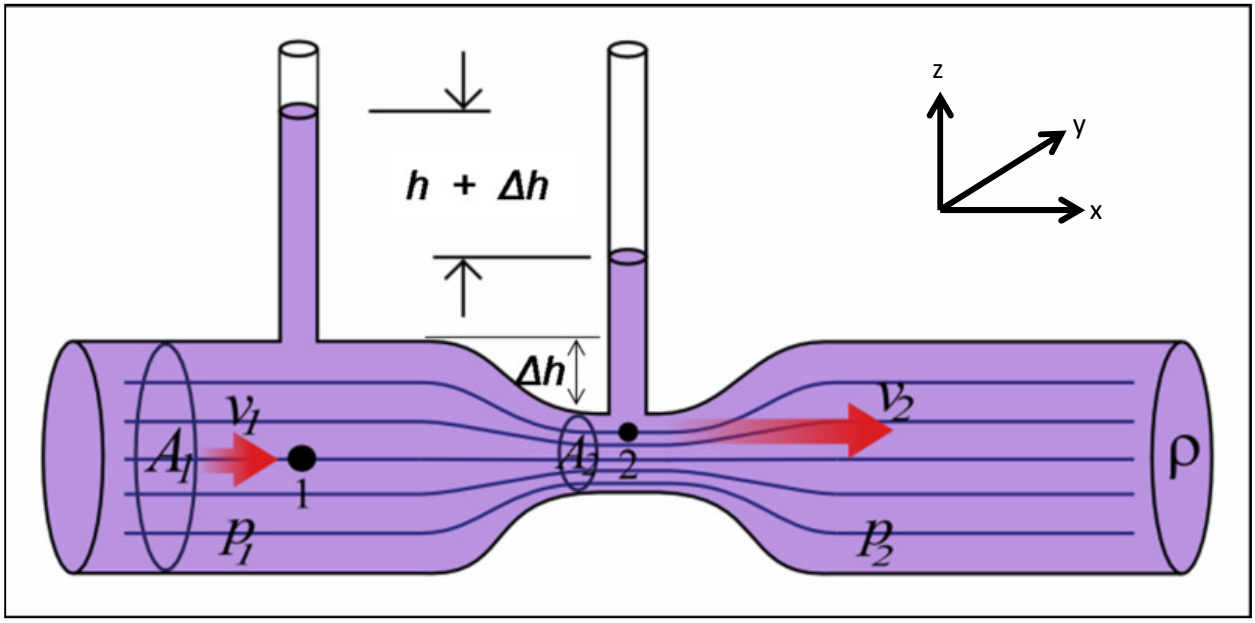

Figure 2-8: Venturi Effect Pictorial for a Pipe – Cross-Section View (Source: Wikipedia.org)

In Figure 2-8 above, two points of reference are compared, *1* on the left and *2* in the middle. As one can see the cross sectional area at *1* (A1) is larger than at *2* (A2). This reduction in area as the flow passes from *1* to *2* causes an increase in fluid velocity, from V_1 to V_2. The decrease in pressure from *1* to *2* is seen as the pressure head differential (h + Δh) between the piezometers.

Although the Venturi effect is a well understood principle, the problem with treating tidal augmentation devices as Venturi sections lies in the fact that the Venturi effect is typically applied to closed sections. Because tidal channeling devices are open to the surrounding ocean, the flow does not react as would be expected in a closed Venturi section and the resulting pressure and velocities at the constrictions of these devices are more difficult to find. Though increased velocities and reduced pressure at the

constrictions do occur (Khan et al. 2009; Sireli 2014) some energy is lost due to a portion of the upstream flow going around the structures. A generalised illustration of this interaction is shown below:

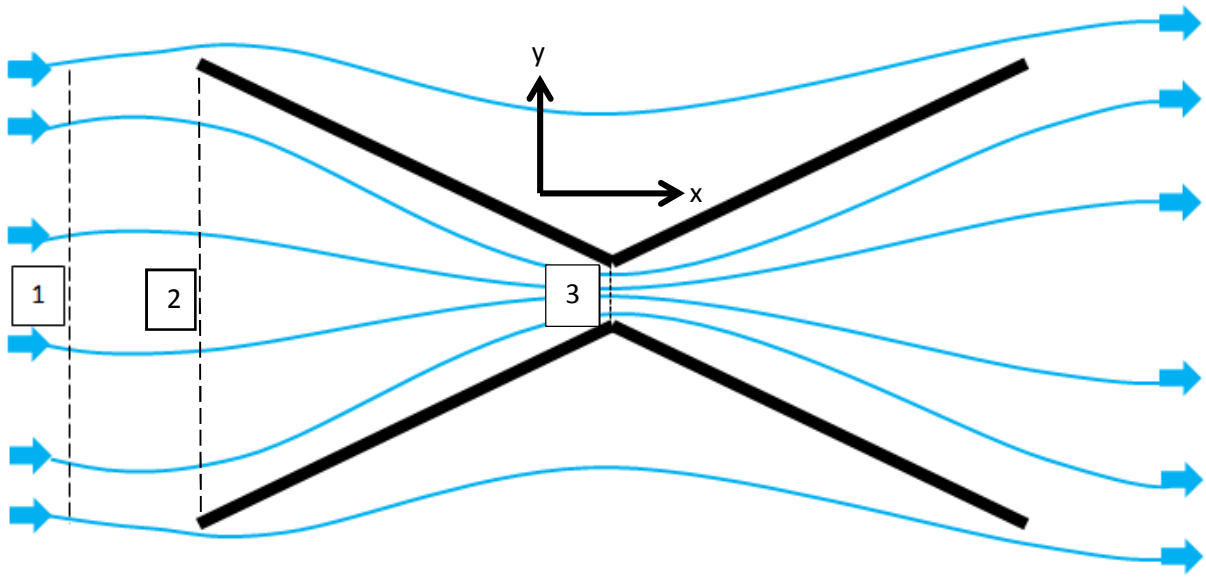

Figure 2-9: Venturi Effect for Open Channeling Devices - Cross-Section View

Because some of flow is expected to go around the structure as shown above in Figure 2-9, it follows to assume that the energy across *1* will be greater than that at *3* and that the principle of continuity described in Equation (2-3) would not be followed as in a closed pipe system. Despite this, it is still expected that the Venturi effect will be observed when comparing sections *2* (inlet) and *3* (contraction) as it is a closed segment between these two sections with no flow escaping the stream-tube (see Section 2.4.1 for more information). As shown, even for open channeling devices, there is still expected to be increased velocity and decreased static pressure (or water surface elevation) at the contracted section compared to the inlet therefore the Venturi Effect applies.

2.3.2 State-of-the-Art Channeling Devices

As mentioned earlier, the turbines of OpenHydro and Clean Current shown in Table 2-2 are examples of channeling devices for use with in-stream energy converters. Though designs can vary quite widely, the purpose of all augmentation channels is in fact to induce a sub-atmospheric pressure within a constrained area to increase the velocity within the constriction (Khan et al. 2009); hence, to exploit the

Venturi effect. Several researchers have investigated the effects of channeling devices on flow for use with turbines. (Ponta and Jacovkis 2008) investigated the effects of channel shape on flow acceleration through a contraction, for use with a floating tidal structure. Both (Gaden and Bibeau 2010) and (Sireli 2014) investigated the effect of duct design around horizontal axis turbines. (Kim et al. 2012) performed numerical simulations on the power increase when using a vertical axis turbine submerged with bi-directional augmentation channel. These are but few of the studies done on augmentation channels as others exist including studies on augmentation devices for wind applications (Ohya and Karasudani 2010; MacQuarrie 2011). Several terms have been used to describe a channelling device including: shroud, concentrator, duct, nozzle and lens amongst others but their differences are often not fully described by these expressions. A branched classification tree is presented below in Figure 2-10 to help classify the different types of augmentation channels.

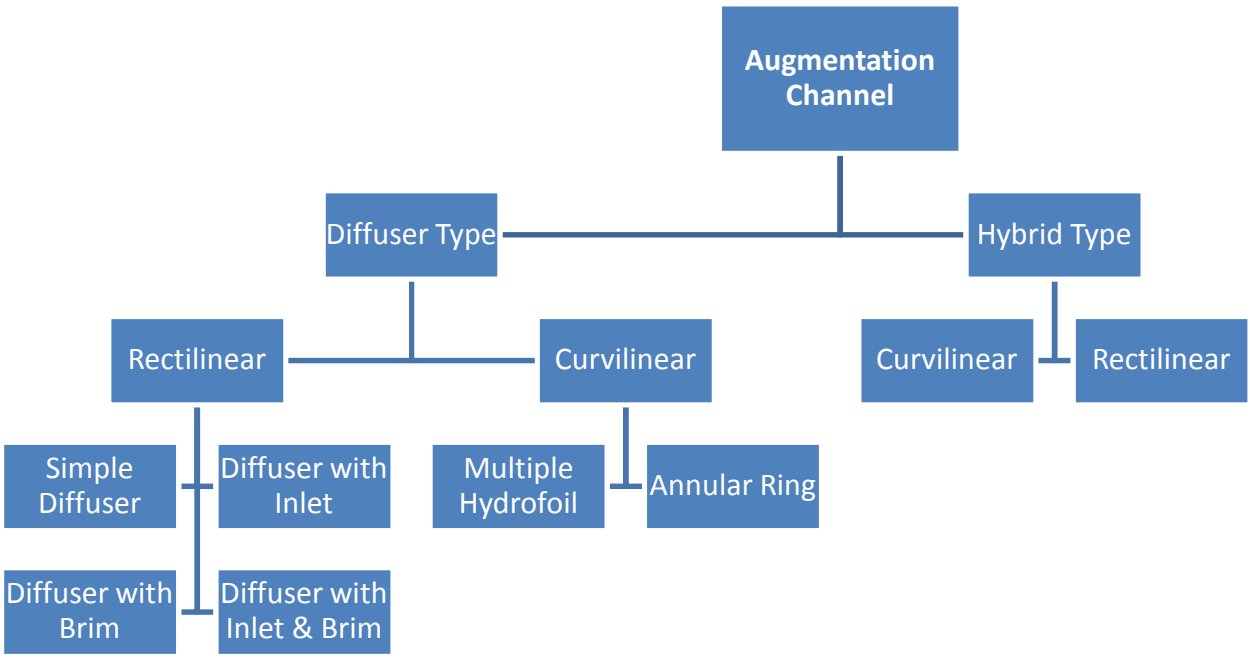

Figure 2-10: Classification Tree of Augmentation Channel Types (Khan et al. 2009)

Because turbines are mostly separated into horizontal axis with circular cross-section or vertical axis with rectangular cross-section, the shape of the augmentations channels usually correspond to these

dimension types. Figure 2-11 below shows generic designs for some of the types described in Figure 2-10 above.

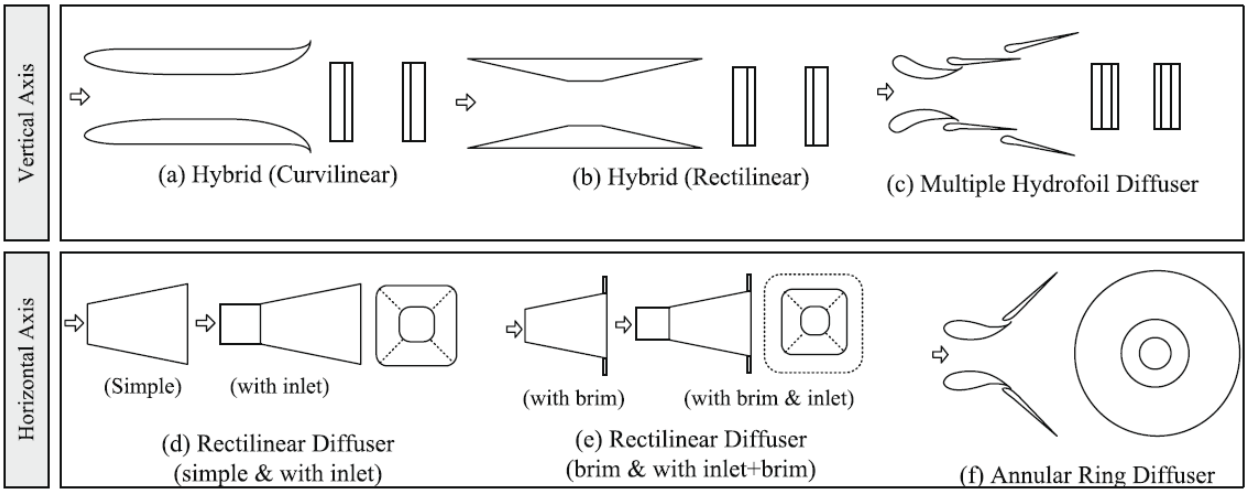

Figure 2-11: Augmentation Channel Shapes (Khan et al. 2009)

It should be noted that the augmentation channels for horizontal axis turbines and the multiple hydrofoil diffuser of Figure 2-11 are all depicted as unidirectional. This does not necessarily have to be the case except for the multiple hydrofoil and annular ring diffuser which would not function properly if used for bidirectional flow. Though it is a bit counter-intuitive, the augmentation device types shown in Figure 2-11 all function by siphoning flow from upstream. This accelerates flow as it passes through the contraction as opposed to funneling the flow from a large opening to a small contraction. This phenomenon is demonstrated using red dye tracer for flow around a multiple hydrofoil diffuser in Figure 2-12 below.

Figure 2-12: Multiple Hydrofoil Diffuser Drawing in Upstream Flow - Plan View (Kirke 2006)

The diffuser shown in Figure 2-12 functions by creating a low-pressure region behind the structure, this draws water through the channel opening as the pressure inside the structure is lower than the ambient in-stream pressure (Kirke 2006). One particular hybrid curvilinear channeling device of interest is the FIUBA vertical-axis water current turbine, developed at the University of Buenos Aires. In (Ponta and Jacovkis 2008), the authors describe a design for a floating channelling device which can be integrated with a river turbine. An artist's sketch of their channeling device (E1A6 model) is depicted in Figure 2-13 below.

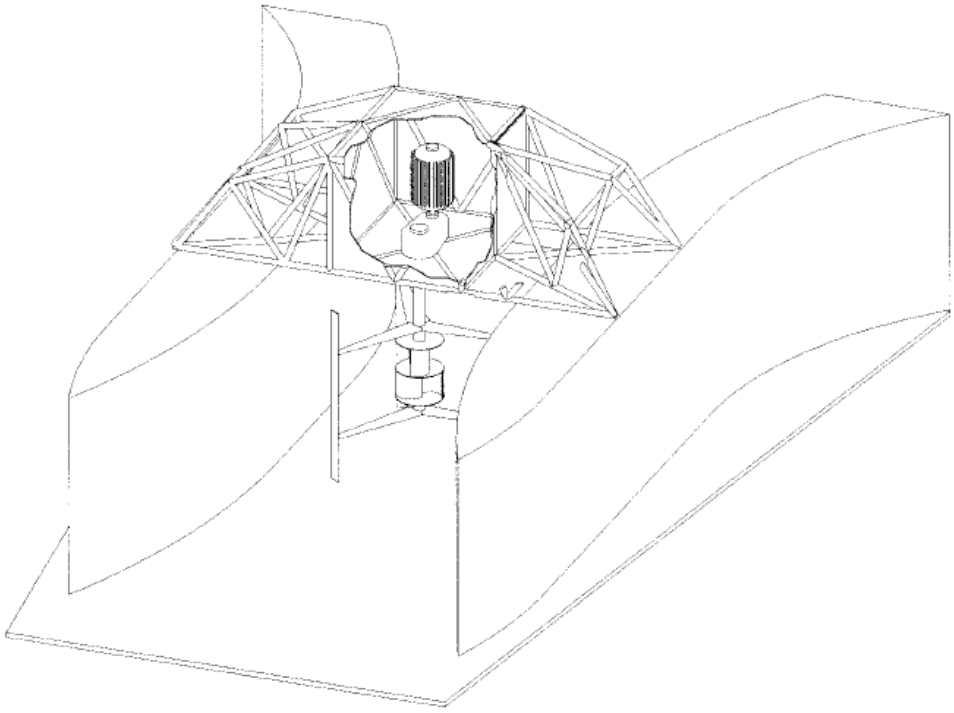

Figure 2-13: E1A6 Model of the FIUBA Floating Channeling Device (Ponta and Shankar Dutt 2000)

The E1A6 design in Figure 2-13 above and others were tested by the researchers using small-scale models in a hydrodynamic test canal and compared with the results of a theoretical model. The main parameter of concern in their modeling was to compare the flow speed through the area where a vertical axis turbine would be placed to the in-stream current speed in the river or tidal environment. As it is desirable to regulate the max power output from a tidal turbine and maximise the ratio of average power output to max power output for project cost reduction (Clarke et al. 2006), the results which are compared in Figure 2-14 below are noteworthy as they show that their design can accomplish this feat.

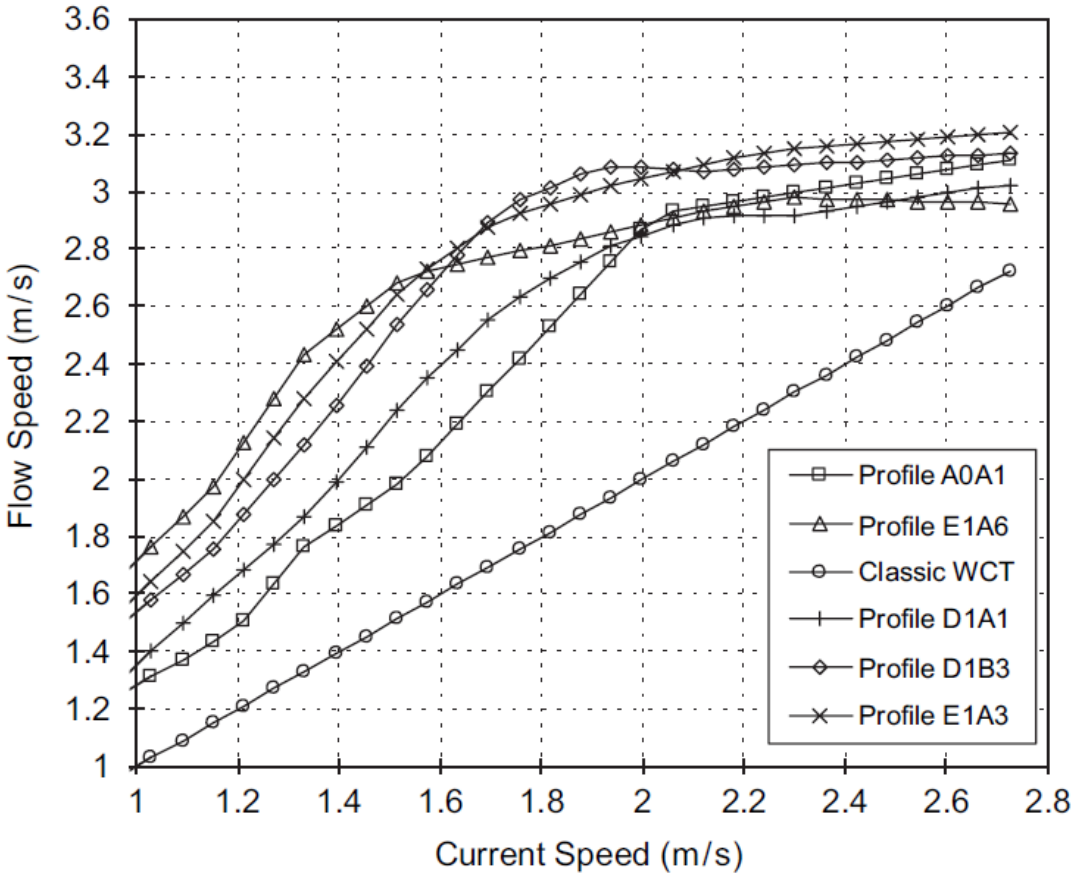

Figure 2-14: Flow Speed Rotor Section vs. In-Stream Current (Ponta and Jacovkis 2008)

Though the flow augmentation results found by Ponta et al. in Figure 2-14 above are promising, the way they are presented is a bit misleading as the true flow augmentation would be reduced due to the presence of the water current turbine (WCT). Discussed further in Section 2.4.1, turbines exert blockage on flow due to their removal of energy and also due to their physical volume. In Figure 2-14 this was obviously not accounted for as the *Flow Speed Rotor Section* to *In-Stream Current Speed* has a 1:1 relationship for the *Classic WCT* which is never the case due to the blockage effect which is necessary for a turbine to extract energy from flow. Though they stated that their work will continue, the flow augmentation factors presented above, and the maximum current acceleration of 1.8 which is shown in Figure 10 of (Ponta and Jacovkis 2008), must be considered as incomplete and unrealistic to actual in-stream power production.

2.3.3 The Tidal Acceleration Structure (*TAS*) Concept

The Tidal Acceleration Structure (*TAS*) is a new innovative structure capable of accelerating tidal or river currents for increased power extraction by in-stream turbines. The patent pending (CA 2644792, author Derek Foran) design consists of walls, extending from the seafloor to above the high water mark, which channel water by utilising the Venturi effect, the well-documented fluid phenomenon discussed in Section 2.3.1 above.

Figure 2-15: Artist Rendering of a Tidal Acceleration Structure in Vancouver Harbour

Initial numerical testing (see Section 5.2) and engineering designs were performed for the concept in 2012 by five undergraduate students under the supervision of Drs. Nistor, Mohammadian and Infante at the University of Ottawa (Foran et al. 2012). This project, though preliminary in many respects, returned the conclusion that a 1.3 MW structure could be constructed at a cost of $7.7 million and become profitable after 7 years in operation.

2.4. Modeling of In-Stream Tidal Turbines

Though there are more precise methods of simulating turbines both for physical and numerical studies, the study at hand did not require precise computation of forces on turbine blades or detailed wake analysis. The main goal of the turbine modeling was to account for the presence of a turbine in simulating the Tidal Acceleration Structure (*TAS*) with respect to its impact on flow velocities in and around the structure, particularly the flow-rate through the *TAS* contraction.

2.4.1 Introduction to Actuator Disc Theory

Actuator Disc Theory was first proposed by Froude (Froude 1889) in 1889 and since has formed the basis of in-stream wind and water turbine theory. The basic assumption of the theory is that water or wind which passes through a turbine must slow down if energy is to be extracted. If the flow did not lose momentum then no energy would be lost from flow and no energy would be captured by the turbines. To analyse the fluid which passes through a turbine one can consider a stream-tube of affected fluid or the volume of fluid which passes through a turbine (Burton et al. 2011).

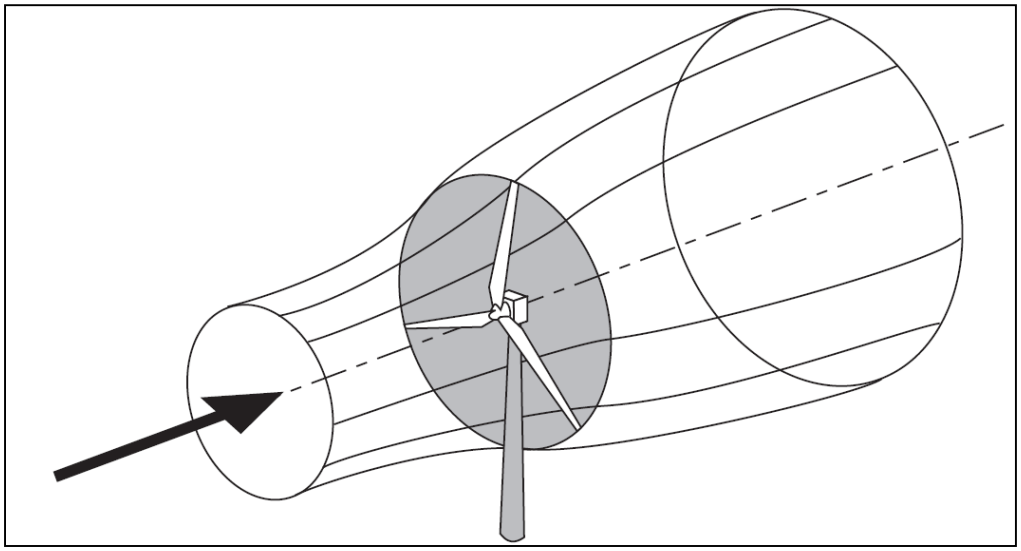

Figure 2-16: The Stream-Tube of a Turbine (Burton et al. 2011)

In Figure 2-16 above, one can see that the cross-sectional area of the stream-tube at the area of the turbine is also the swept area of the turbine. To be noted also is that the cross-sectional area does not change suddenly in the longitudinal direction but instead a gradual increase in cross-sectional area of the stream-tube is observed throughout. This results in a gradual reduction of velocity as flow passes through the disc as sudden changes in velocity would not be possible (Burton et al. 2011). The expansion in the cross-sectional area of the stream-tube is caused by the necessity for conservation of mass flow rate at any section as expressed by:

$$\dot{m} = \rho A_i U_i \qquad \textbf{(2-4)}$$

Where:

- ρ is the density of water
- A_i is the cross-sectional area at any point along the stream-tube
- U_i is the average velocity at any point along the stream-tube

For the fluid to observe Equation **(2-4)** above and because the fluid is slowing down from longitudinally, the increase in cross-sectional area naturally follows. This interaction as well as the change in pressure across the disc can be visualised in the following figure.

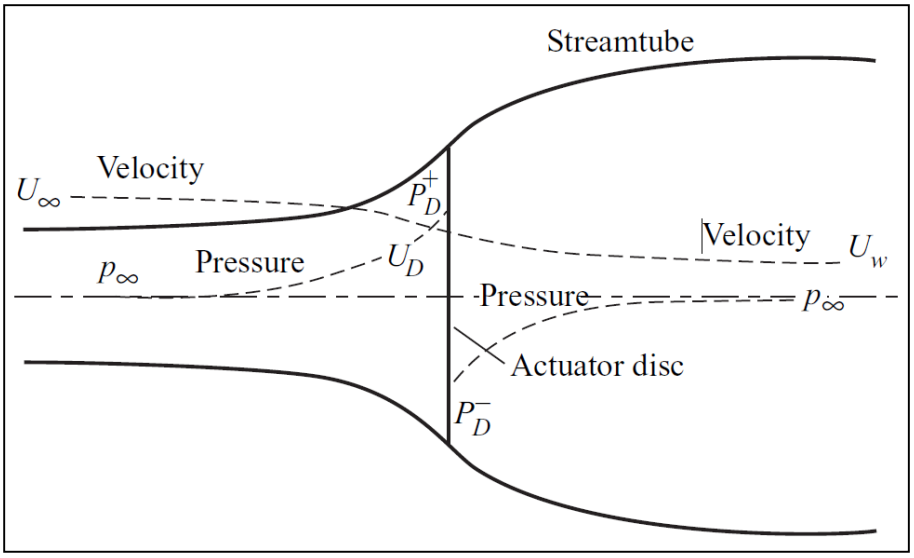

Figure 2-17: Energy Extracting Actuator Disc and Flow Stream-Tube (Burton et al. 2011)

By observing Figure 2-17 above, one can note that both the velocity and stream-tube area change gradually from longitudinally however the pressure drops suddenly at the actuator disc. To be noted also is the uniformity of static pressure far upstream and downstream of the disc. The mass flow rate continuity at the sections can also be compared using the following formula:

$$\rho A_\infty U_\infty = \rho A_D U_D = \rho A_W U_W \quad \textbf{(2-5)}$$

Where Equation **(2-5)** is analogous to Equation **(2-4)** and:

- ∞ refers to the conditions far upstream of the actuator disc
- D refers to the conditions at the actuator disc
- W refers to the conditions in the far wake

This sudden drop in pressure seen in Figure 2-17 is responsible for the force exerted on the disc/turbine necessary for power production. This thrust force (equivalent to drag on the disc/turbine) can be expressed by the following equation.

$$T = (p_D^+ - p_D^-)A_D = 2\rho A_D U_\infty^2 a(1-a) \quad \textbf{(2-6)}$$

Where:

- T is the thrust force on actuator disc (equivalent to drag force felt by the disc/turbine)

- p_D^+ is the pressure just upstream of the disc
- p_D^- is the pressure just downstream of the disc
- ρ is the fluid density
- A_D is the area of the disc
- U_∞ is the velocity far upstream of the disc or unblocked in-stream velocity
- a is the axial flow induction factor, a measure of velocity reduction through the disc

The power extracted from the fluid is then equivalent to the rate of work done by the thrust force (Burton et al. 2011) and is given by:

$$Power = TU_D \quad \textbf{(2-7)}$$

Where:

- T is the thrust force on actuator disc (equivalent to drag force felt by the disc/turbine)
- U_D is the velocity at the actuator disc

Many studies have utilised Actuator Disc Theory for turbine simulation in both the wind and in-stream water (tidal and river) industries. The formulation of Actuator Disc Theory in the *Wind Energy Handbook* (Burton 2011) is an oft-cited and well-written explanation of the theory and was the principle source of information for this study as well. Other significant studies relevant to Actuator Disc Theory in the wind sector to note include those focusing on: a general momentum theory for wind turbines (Sharpe 2004), 3D numerical investigations of the theory's application to turbine rotors (Mikkelsen 2003) and, a non-linear and unsteady actuator disc model for horizontal axis wind turbines (Sørensen and Myken 1992), amongst others.

In the in-stream tidal/river turbine industry, Actuator Disc Theory has been used often as well. (Sun 2008) compared the 3D numerical simulation of a generalised actuator disc with experimental testing of thin porous metal discs in terms of effects on free water surface and wake recovery with good qualitative agreement. (Roc 2013) successfully utilised Actuator Disc Theory to simulate 3D large-scale

ocean circulation models for both stand-alone devices and arrays. (Harrison et al. 2010) compared experimental (porous discs) and numerical simulations for a range of disc thrust coefficients. (Whelan et al. 2007) compared theoretical results with open channel flow experiments using porous discs and also found good agreement particularly in reference to the impacts of disc porosity on turbine/disc efficiency. Another important study was (Bahaj et al. 2007), focused on characterising the wake of a tidal turbine using an eddy-viscosity model and comparing with small-scale mesh disc rotor simulations. Though the above studies and others have found that the Actuator Disc Theory can be extremely useful in modeling in-stream tidal turbines, the following have been identified as deficiencies with applying the theory (Bahaj et al. 2007; Roc 2013):

- No swirl imparted on flow due to actuator disc as compared to actual rotor blades of a turbine
- Vortex shedding is not off of rotating blades but rather disc edges
- Energy is extracted due to creation of small-scale turbulence instead of mechanical motion

2.4.2 Physical Modeling: Porous Plates

As mentioned in Section 2.4.1 above, several studies have utilised Actuator Disc Theory and porous plates to model turbines. The primary design parameter for these porous plates is their porosity or open area to solid area ratio. A first study on the relationship between turbine simulation parameters and porosity was published by Sir Geoffrey Ingram Taylor (Taylor 1971) and has been cited in reference to Actuator Disc Theory (Whelan et al. 2007). It describes the relationship between open area ratio and resistance coefficient as:

$$\theta^2 = \frac{1}{1+k} \qquad \textbf{(2-8)}$$

Where:

- θ is the open area ratio or porosity of the porous plate
- k is the resistance coefficient of the porous disc to flow

In their study on the effects of varying disc resistance, (Whelan et al. 2007) found good agreement between their experimental results and Equation **(2-8)** above. Figure 2-18 below shows their results as compared to the Taylor approximation.

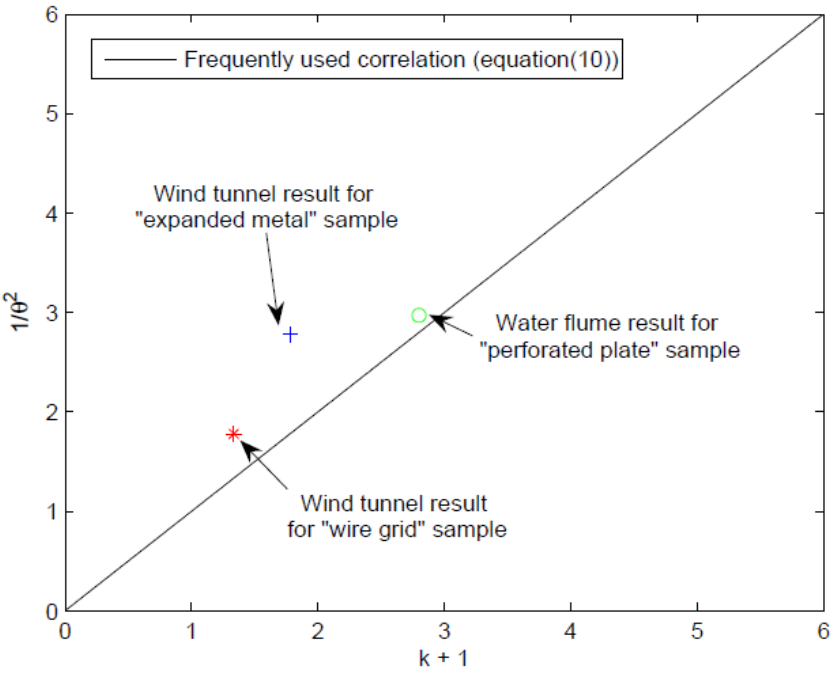

Figure 2-18: Porosity vs Resistance Coefficient (Whelan et al. 2007)

Another important modeling parameter for applying Actuator Disc Theory which was mentioned earlier (see Section 2.2.3) is the coefficient of thrust (C_T) or the thrust imparted on the actuator disc/turbine by flow (equivalent to drag force felt by the disc/turbine). This value can be related to the resistance coefficient using the following formula (Whelan et al. 2007).

$$C_T = \frac{k}{(1 + \frac{1}{4}k)^2} \qquad \textbf{(2-9)}$$

Where:

- C_T is the porous disc thrust coefficient
- k is the resistance coefficient of the porous disc to flow

Knowing that the optimum value of C_T is 0.9 – corresponding to a turbine operating in open-flow at the Betz limit (Myers and Bahaj 2010) - and using equations **(**2-8) and **(**2-9) above, the authors of (Whelan et

al. 2007) were able to deduce that the optimum porosity or open area ratio of a porous plate is 0.58. This value is somewhat unreliable because it is based on the assumption that Equation **(**2-8) is valid however, it provides a good baseline for porous plate modeling as the results of Figure 2-18 show. Examples of a porous plate used to model a turbine and the setup of the support apparatus from (Sun 2008) are shown below in Figure 2-19.

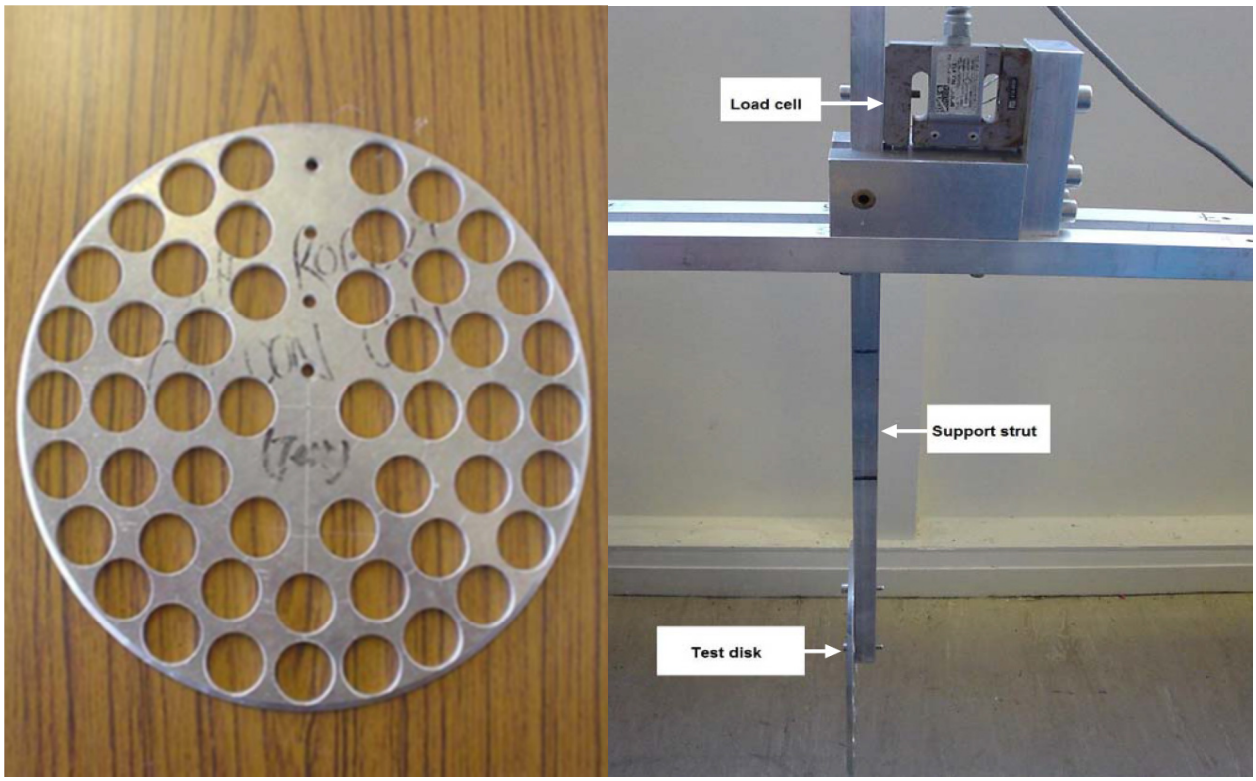

Figure 2-19: Porous Plate and Support Apparatus (Sun 2008)

2.4.3 Numerical Modeling: Porous Jump

The numerical model chosen for the current study was ANSYS Fluent. Within Fluent the actuator disc can be simulated using a momentum sink model entitled the *Porous Jump Model*. Other researchers have used this model in the past with good agreement being found compared to experimentally tested porous plates in regions greater than four diameters downstream from the discs (Sun 2008). Of course the accuracy of using Fluent to model actuator discs is dependent on many factors besides the CFD program itself including: meshing, the solver and the turbulence model selected, amongst many others.

The *Porous Jump Model* imposes a sudden pressure drop on flow similar to that of a theoretical actuator disc (see Figure 2-17). The pressure drop is defined in Fluent over a finite thickness and can be specified as a combination of Darcy's Law and an inertial loss term as follows (ANSYS 2010):

$$\Delta p = -(\frac{\mu}{\alpha} + C_2 \frac{1}{2}\rho v^2)\Delta m \qquad \textbf{(2-10)}$$

Where:

- μ is the laminar fluid viscosity
- α is the permeability of the medium
- C_2 is the pressure-jump coefficient
- ρ is the fluid density
- v is the velocity normal to the porous face
- Δm is the thickness of the medium

For the purposes of applying Actuator Disc Theory, only the inertial loss term or the right half of Equation **(**2-10**)** above is relevant therefore, the viscous term $\left(\frac{\mu}{\alpha}\right)$ can be ignored or set to zero.

2.5. Summary

The existing literature on tides and tidal energy is extensive. Though the in-stream tidal energy industry is still in its adolescence compared to other renewable sectors, several energy extraction devices have been proposed which are at various stages of prototype and commercial development. Channeling devices as a means of enhancing and regulating the velocity field around in-stream turbines have been studied by turbine developers and researchers with some promising results found. Preliminary studies on a new channeling device, entitled the Tidal Acceleration Structure (*TAS*), have also been explored. A method for simulating the energy extraction of in-stream turbines, named Actuator Disc Theory, has been reviewed, with the work of previous researchers establishing agreement between theory and both experimental and numerical results. In terms of physical modeling, the use of porous discs has been

found as a reasonably accurate method for simulating the energy extraction and flow blockage which turbines impart on flow. In regard to numerical modeling, the *Porous Jump Model*, part of ANSYS Fluent's software and a simple momentum sink model, was found in one study as being capable of replicating the physical modeling results with relatively good precision in the far wake area and in terms of its overall effect on flow.

Chapter 3. Research Methodology

3.1. Objectives and Expected Outcomes

As mentioned previously, the main objective of the study was to experimentally test the *TAS* and optimise the design. The design variations for the purposes of the current research project were limited to the opening width, contraction width and basic wall curvature. In testing the structure experimentally, two aspects were of concern: the velocity field around the *TAS* and the power extracted by plates placed at the centre of the contractions. The goal was to test these facets for various structure configurations in the hopes of finding an optimised design. It was expected that certain configurations would be able to accelerate flow through the contraction more than others and that therefore some designs would perform better. The objective of finding better structure configurations was also balanced with the knowledge that the optimised structure would only be for one set of flow parameters. The choice of initial conditions was therefore very important and will be reviewed in the following sections. Another objective was to calibrate a 3D numerical model using ANSYS Fluent that could then be used in the future to simulate the *TAS* at full-scale and with known numerical Actuator Disc Theory models such as the *Porous Jump Model* available in Fluent. These numerical testing options were initially objectives of the present study however, they could not be completed because of time limitations. Plans are underway to complete them as part of a future project. Overall, it was expected that from both the experimental and numerical work, and also from the literature review of similar studies, that appreciable knowledge would be found towards determining the viability of constructing a *TAS* for future tidal or river power production.

3.2. Site Selection and Flow Parameters

Due to the limited timeframe of the present project and the fact that all tidal sites are inherently different, it was decided that the optimisation procedure would only be done for one set of conditions. The optimisation therefore had to be for a very generic location or set of parameters, one that would be the most likely site for a future *TAS* prototype construction. As most tidal turbines ideally operate in around 2 to 3 m/s and have cut in-speeds from around 0.5 to 1 m/s (Bedard et al. 2005), it was determined that an in-stream velocity of 1 m/s would be a good baseline to use for the experimental testing. At an average velocity of 1 m/s conventional in-stream turbines would not be viable therefore, if the *TAS* could be proven to accelerate the flows to above 2 m/s [as found in (Foran et al. 2012)] then locations which could not previously be used for tidal energy exploitation could become technologically feasible. At 1:50 scale and using Froude scaling an in-stream velocity of 1 m/s corresponds to 14.14 cm/s (see Appendix I). The average in-stream velocity during the flume tests was therefore calibrated to this value. It should be noted that larger velocities could have also been tested as the max flow velocity in the flume was above 50 cm/s with a flow depth of 30 cm.

Although it was thought that it wouldn't have as big of an impact on the flow field around the *TAS*, another parameter which had to be chosen was the flow depth. A big concern when considering depth for potential tidal sites for a *TAS* would be the increased construction cost associated with greater depths. In (Foran et al. 2012), the chosen site had a mean high water mark of 20.6 m and the design yielded *TAS* walls of 22 m in height. The cost associated with constructing walls of this height that totally enclose the inside of the *TAS* from the outside would be very significant. Also, the thickness of the walls near the seabed would have to increase with *TAS* height due to the high moments produced by wave and other impact forces acting on the top portions of the structure. Though not always the case, it was also thought that increasing the depths would limit the possible locations close to shore, thus also increasing the associated power transmission costs. For these reasons, it was decided that limiting the

depth would be prudent and would likely result in reduced overall project costs and possible exploitation of shallower, more accessible tidal areas. The depth was therefore set to 15 m or 30 cm at 1:50 scale (see Appendix I).

3.3. Design Criteria and Testing Methods

From a previous 2D numerical study, it was found that a structure with a width 30 m, a length of 60 m and a contraction of 9 m would produce an acceleration ratio of 2.058 (see Section 5.2 and Table 5-2). This was the starting point for the current design but was modified slightly to give the following base structure dimensions.

Table 3-1: Design Criteria for the Experimental Work

Parameter	Prototype Value – Model Value
Wall length	30 m – 60 cm
Wall height	20 m – 40 cm
Contraction width	10 to 20 m – 10 to 20 cm
Opening width	20 to 50 m – 20 to 50 cm
Note: Only half of the *TAS* was modeled in the flume, therefore accounting for the discrepancy in the contraction and opening widths for prototype and model.	

For the experimental optimisation of the *TAS* design, a fairly simple approach was used. In Stage 1, a series of initial tests were conducted for the *TAS* model with straight walls. Contraction widths of 10, 15 and 20 cm were tested with structure openings of 20, 25, 30, 40 and 50 cm for a total of 14 tests. After these tests were analysed, the best two opening widths were taken for each contraction width and 6 more tests were conducted for two wall curvature types for a total of 12 more tests. Two more additional tests with nets across the structure openings were also conducted summing to a total of 28 tests in Stage 1.

The best designs (in terms of flow acceleration through the *TAS*) were tested with the three porous plates in Stage 2. As discussed in section 4.3.2, the porosity of all three plates were 58% (open area to total area ratio) as this was suggested by the results of (Whelan et al. 2007). Similarly to the tests with

curved walls of stage 1, the best two opening widths for each contraction (10, 15 and 20 cm wide) were tested for the three wall curvatures (straight, 7.5 cm and 10 cm out of plane) making a total of 18 tests. In addition, each porous plate (10, 15 and 20 cm wide) was tested on its own without the presence of the *TAS* to have a benchmark to compare the increased power extraction enabled by the *TAS*.

In stage 3, one structure was chosen for more in-depth modeling to form the basis for the comparison with the numerical results. The *TAS* model with an opening of 25 cm, 10 cm contraction and straight walls was taken for this and was tested with and without the presence of the 10 cm wide plate. As these two tests were going to be evaluated in greater detail than the rest, more ADV points and load cell measurements were taken than in Stages 1 and 2. This way, a very precise image of the velocity field around the structure was created for fine tuning of the numerical simulations. In addition to these two tests, a structure with an opening of 35 cm and a contraction of 17.5 cm was tested alongside the 10 cm wide porous plate. This was done as it was thought that the plates were causing too much blockage on flow through the *TAS* therefore the porous or non-solid area in the contraction had to decrease in order to maximise the extracted power. This ended up being the case as discussed in section 4.6.2.

The numerical modeling using ANSYS Fluent was done to calibrate a model which could be used to simulate the *TAS* at full scale. The numerical model tested was therefore setup to replicate the flume conditions as it had to be verified against the experimental results. As mentioned, the test with an opening of 25 cm, a contraction width of 10 cm and straight walls was chosen for the calibration as it was one of the tests with the best *TAS* flow accelerations and it was also simple to model as the walls were straight. Though discussed in greater detail in section 5.3, the main goal of the numerical modeling using Fluent was to match the velocity field of the simulation to that which was observed in the stage 3 test without the plate. This was done by comparing the longitudinal velocity profiles and vertical velocity profile of the stage 3 test with the converged Fluent simulation.

Chapter 4. Physical Modeling of the *TAS*

4.1. Introduction

The physical modeling of the Tidal Acceleration Structure was one of the main goals of the research project as it was essential in proving the merits of the *TAS* concept. The *TAS*'s raison-d'être is to accelerate the flow velocity as it passes through the structure. Several facilities can be used for physical testing of tidal devices however the most common facilities used are flumes, tow-tanks and rivers. A 1.5 m wide by 30 m long flume located in the University of Ottawa's Hydraulics Laboratory was used for the physical modeling. The experimental equipment included an Acoustic Doppler Velocimeter (ADV) on a support frame which could be easily moved around for velocity measurements during testing. In this chapter, the modeling methods and the results of all experimental testing are presented. The later will then be compared with the numerical results presented in section 5.3 for validation.

4.2. Experimental Setup

4.2.1 Design scaling - Froude Scaling

Though ideally the *TAS* concept would be tested at large scale to measure the hydrodynamics of the structure, this was obviously not possible due to cost and facilities limitations. Scaling was therefore necessary, and adequate planning needed, before construction of the structure model could begin. There are generally thought to be three types of similitude: geometric, kinematic and dynamic similarity (Ettema 2000). Geometric similarity requires that each physical length dimension have the same relationship between model and prototype. This is described by the length ratio:

$$\lambda_L = \frac{L_m}{L_p} \qquad \textbf{(4-1)}$$

Where:

- λ_L is the length ratio

- L_m is the length scale of the model
- L_p is the length scale of the prototype

Kinematic similarity on the other hand requires that velocities have a constant ratio between model and prototype and directions are the same. This is described by the velocity ratio:

$$\lambda_V = \frac{V_m}{V_p} \quad \textbf{(4-2)}$$

Where:

- λ_V is the velocity ratio
- V_m is velocity in the model
- V_p is the velocity in the prototype

The third type of similitude when it comes to scaling is dynamic similarity; when forces in the model and prototype have a constant ratio. This is described by the force ratio:

$$\lambda_F = \frac{F_m}{F_p} \quad \textbf{(4-3)}$$

Where:

- λ_F is the force ratio
- F_m is the force in the model
- F_p is the force in the prototype

It should be noted that when two scenarios are dynamically similar they are kinematically similar and when two scenarios are kinematically similar they will be geometrically similar.

As there are different forces at work in fluid dynamics one has to choose which forces to scale. This is often a choice between keeping the Froude number (Fr: ratio of inertia and gravity forces) or the Reynolds number (Re: ratio of inertia and viscous forces) constant between model and prototype. Having equal values for both Re and Fr is not possible therefore it was chosen to keep Fr constant (Froude scaling) due to the importance of gravity in our testing case.

Because velocity was the main parameter to be measured in the flume testing, the only ratio which was calculated was the velocity ratio. This is defined as follows:

$$\lambda_V = \sqrt{\lambda_L} \quad \textbf{(4-4)}$$

Where:

- λ_V is the velocity ratio
- λ_L is the length ratio

As described in detail in Section 4.5, a scale sensitivity analysis was performed using ANSYS Fluent and it was determined that a Froude scale of 1:50 was adequate for the flume dimensions. The prototype and model dimensions and flow properties are as follows:

Table 4-1: Structure Dimensions and Flow Properties for Froude Scaling

	Flow depth	Mean in-stream velocity	Wall length (each)
Prototype	15 m	1 m/s	30 m
Model	30 cm	0.14142 m/s	60 cm

Notes:
1. See Section 3.2 for reasons behind parameter selections.
2. See Appendix I for Froude scale calculations.

4.2.2 Model Construction

The structure model walls were constructed out of marine grade plywood. Marine plywood, often made from mahogany, is a great material for testing shapes in water environments as it is resistant to water damage, is relatively inexpensive compared to metal or plastic, can be shaped using heat and pressure and can be cut and handled with relative ease. Additionally, the author had extensive experience with using this material as he had previously constructed a sailboat, named *Duncan*, out of the same material. Though a tidal environment *TAS* prototype would not be constructed out of wood, marine plywood was suitable for studying the structure-flow interactions in a laboratory environment. As mentioned earlier, the model wall lengths were chosen to be 60 cm and the model water depth 30 cm therefore sheets of marine plywood were cut in 60 cm x 40 cm rectangles to be safely above the water

level. To be able to change the structure setup dimensions easily and rapidly, the plywood pieces were attached to a setup of hollow metal bars which could then slide on threaded bars fixed between the two walls of the flume. The two plywood pieces were attached at the centre using door hinges to allow for modification of the opening angle. To reduce the friction caused by the centre joint and the screws on flow, a sheet of neoprene (rubber) was attached to the inner side of the walls using staples on the outer side. The following figure shows the structure at various periods of construction.

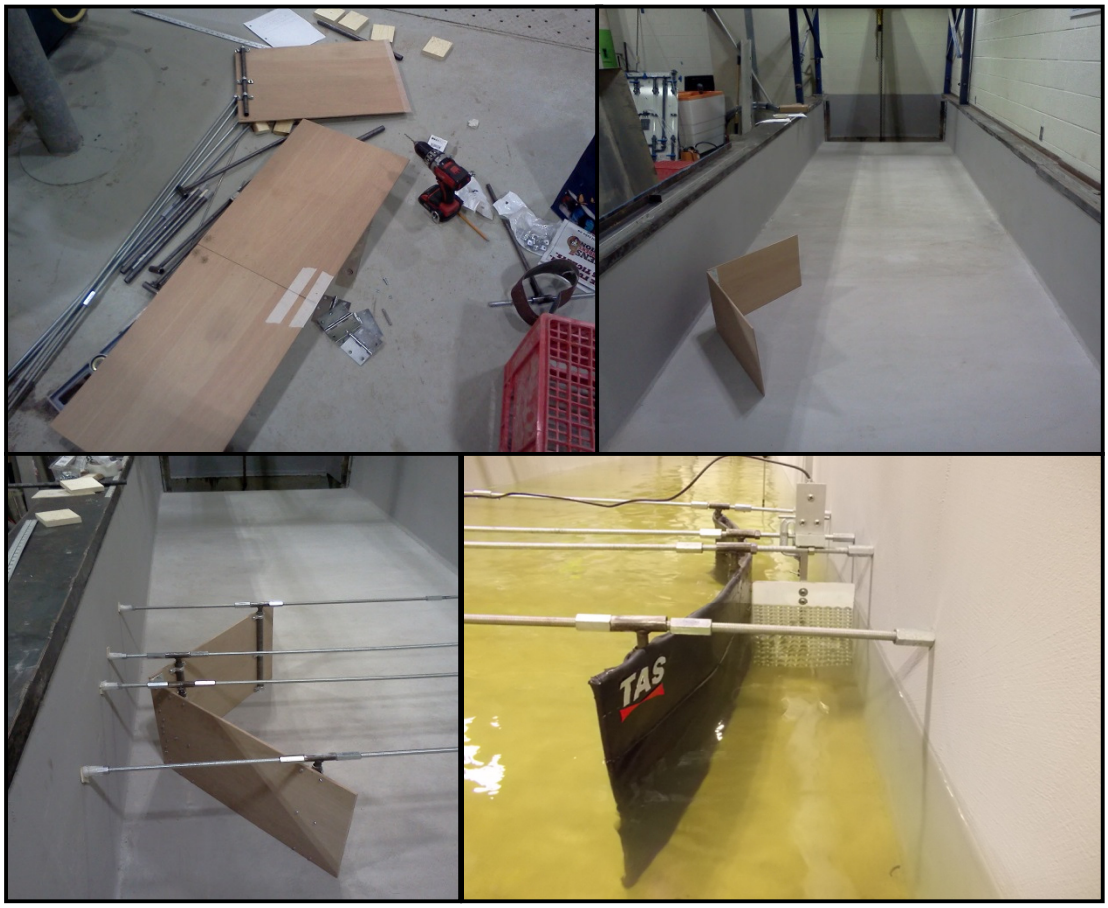

Figure 4-1: Various Stages of Model Construction

4.2.3 Model Modification

To be able to change the structure setup dimensions easily and rapidly, the plywood pieces were attached to a setup of threaded bars as shown in Figure 4-1 above. The orientation of the *TAS* walls, in terms of opening and contraction widths, could then be changed by screwing and un-screwing nuts on

the threaded bars. These dimensions were measured with rulers from the side wall of the flume for each test setup and it was ensured the *TAS* walls were vertical by using a level. The method of modifying the *TAS* model for different test runs was extremely easy and it allowed many different configurations to be tested without having to remove the structure or stop the flume pump. As mentioned earlier, the walls were constructed from mahogany marine-grade plywood and these were curved for certain test runs using boiling water and pressure. The following figure shows the changing of the *TAS* structure to a new wall configuration setup.

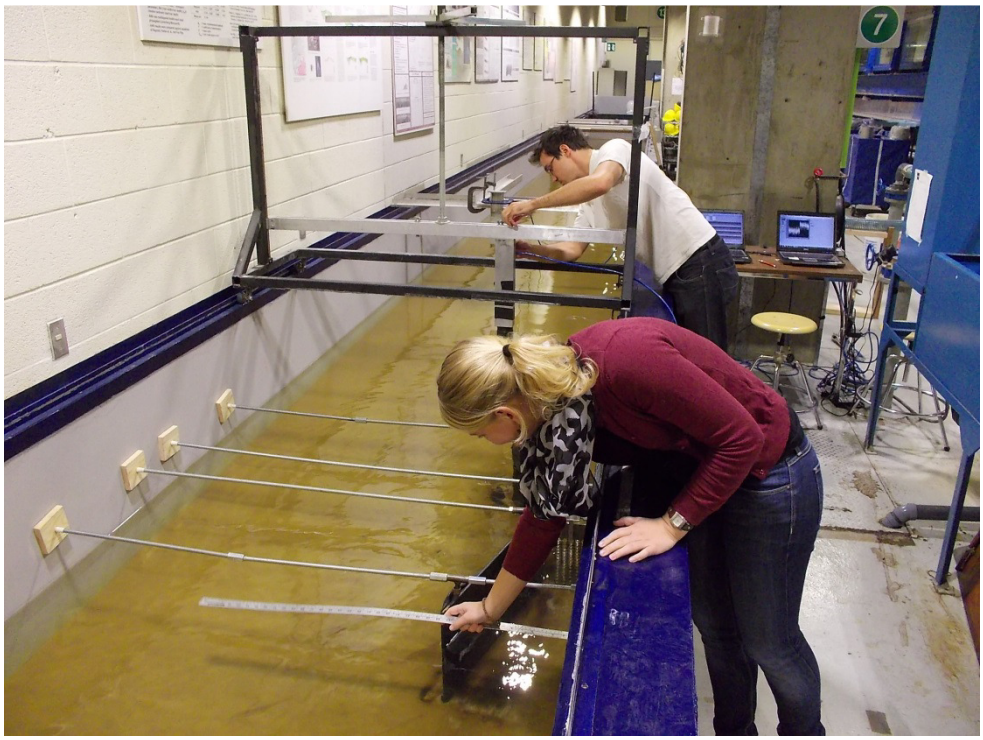

Figure 4-2: *TAS* Model Modification

4.2.4 Flume Specifications

The flume used for the experiments is located in the Civil Engineering Hydraulics Lab at the University of Ottawa and it is a concrete walled flume that was refinished with a concrete-polymer lining in the winter of 2014 just prior to the experiments being conducted. The flume is 30 m long and has a width of 1.5 m. The flow rate is controlled using a pump pressure control panel and an opening valve which can be set to a precise level for flow rate replicability from day to day. The water level in the flume is controlled

using a crank-operated gate at the downstream end and the water is recycled in an underground reservoir located underneath the floor of the lab. Three turbulence dissipating baffle gates were installed at the upstream end of the flume to reduce the variation in free-stream velocity at the location of the *TAS* model testing. These baffle gates are shown in Figure 4-3 below:

Figure 4-3: Turbulence Dissipating Baffles

4.3. Instrumentation

The main phenomenon of interest in testing the scaled Tidal Acceleration Structure was the velocity field in and around the structure. For its measurement, several options such as tracer tracking and a propeller meter were considered however, to ensure the required accuracy of the measurements, two Acoustic Doppler Velocimeters were used. For the second stage of testing, the turbine was simulated using porous plates attached to a load cell to measure the drag force of flow on the plates. Using analytical drag calculations, the initial drag force was estimated to be less than 10 Newtons, thus the load cell was chosen for forces in this magnitude range.

4.3.1 Acoustic Doppler Velocimeter

The Acoustic Doppler Velocimeter (ADV) model which was used was Nortek's Vectrino. The following table lists some of its specifications (Nortek 2009):

Table 4-2: Nortek Vectrino Specifications

Sampling volume: Distance from probe	5 cm
Sampling volume: Diameter	6 mm
Sampling volume: Height	1-9.1 mm (user selectable)
Acoustic frequency	10 MHz
Data collection software	Vectrino Plus

The device functions by using the Doppler effect or the change in pitch that is heard when either the source of a sound or the receiver is in motion. The Doppler effect is easily observed by the difference an ambulance or police siren makes when it is coming towards you (condensed sound waves) or away from you (elongated sound waves). The Vectrino ADV functions by transmitting a pulse from a centre transducer to the sampling volume, which is then reflected by small particles suspended in the water and returned to four ADV receivers which then relay the Doppler shift to the Vectrino Plus software. This is illustrated below:

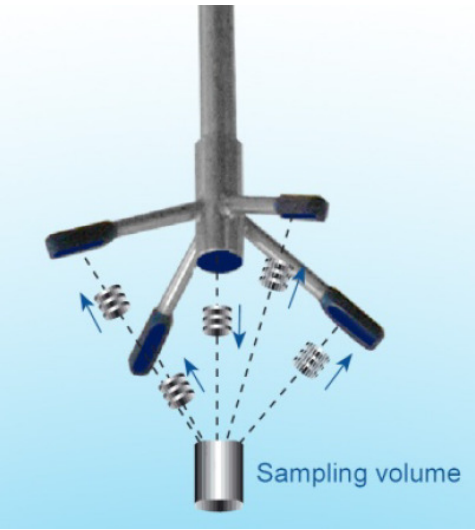

Figure 4-4: Vectrino ADV operation pictorial (Nortek 2009)

The most important ADV parameters to get consistent results with a strong correlation percentage were the SNR (signal to noise ratio) value and the nominal velocity range. The nominal velocity range of 30 cm/s gave good correlation values and was therefore used for most tests (10 cm/s used for some tests). The sampling volume height was kept at the default 7 mm with transmit length of 1.8 mm. After the data was collected by the Vectrino Plus software, the results were processed using an in-house MATLAB code developed by University of Ottawa professor Dr. Colin Rennie which returned the time-averaged, de-spiked, filtered results for velocity and relative turbulence intensity amongst others (see Appendix II:). Two ADVs were used during data collection, one was permanently mounted 3 m upstream of the *TAS* at the centre of the flume at a height of 12.5 cm above the bed (determined to be the elevation above the bed corresponding to the depth-averaged flow velocity). The purpose of this first ADV was to monitor the in-stream water velocity and filter all other results appropriately for changes in the flow-rate from test to test. The second ADV was mounted on a structure that was capable of rolling up and down the length of the flume (accuracy on the order of centimeters) and also move up and down using a threaded support (accuracy on the order of millimeters). In this manner, time-averaged ADV velocity points could be collected at any location around the structure.

4.3.2 Load Cell – Porous Plate Arrangement

The first stage of testing did not include any device for simulating the presence of a turbine. However, the second stage of *TAS* testing was done with a Load Cell – Porous Plate arrangement to simulate the energy taken out by a turbine in real flow conditions. This method had previously been employed by several other researchers (Whelan et al. 2007; Sun 2008; Myers and Bahaj 2010) and functions according to Actuator Disc Theory. The holes in the porous plate produce turbulence which in turn produces a drag force on the plate (or thrust exerted by the flow on the plate). This drag force is what was measured by the Load Cell – Porous Plate Arrangement. The load cell was a 100 Newton Artech® model and was connected to an aluminium support structure which could pivot around a pin to measure

the drag force being applied to the porous plate due to flow in the *TAS* contraction. The measured force then had to be modified using the moment arm length difference between plate-pin and pin-load cell and this calculation is shown in Appendix IV. The design for this support structure was based on a similar design used in (Sun 2008). The hole arrangement of the rectangular porous aluminium plates were influenced by the research of (Whelan et al. 2007) who found that the optimum open-area ratio or porosity should be 58% to achieve close to the best possible power extraction efficiency (Betz limit, see Section 2.4.2). A porosity of 58% was therefore chosen for the plate design and was implemented by distributing the holes evenly across the face of the plate. The plates were designed in AutoCAD (see Appendix III) and machine milled in the University of Ottawa's Mechanical Engineering machine shop along with the rest of the Load Cell – Porous Plate support apparatus. The finished product, as installed in the flume and connected to the load cell, is shown in Figure 4-5 below.

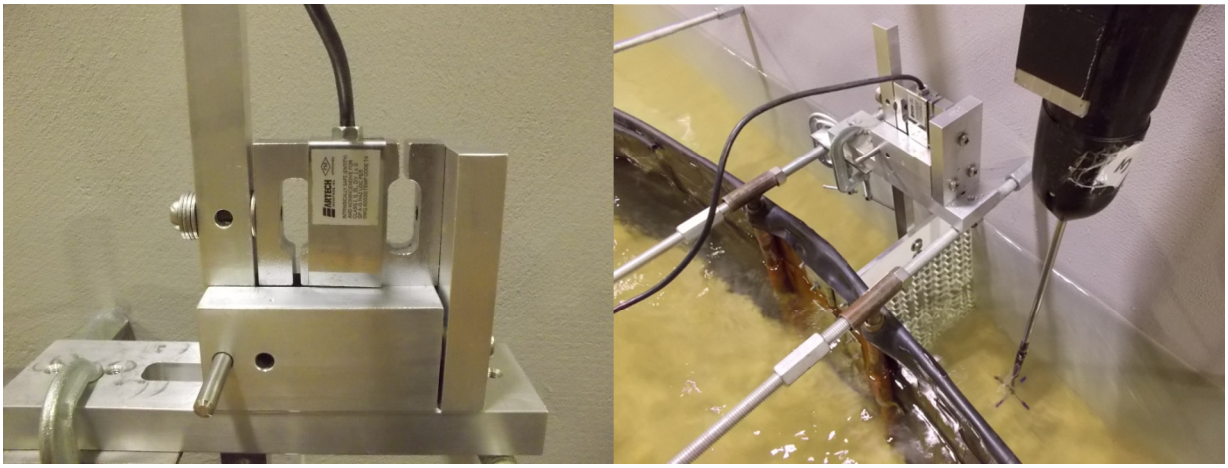

Figure 4-5: Load Cell – Porous Plate Arrangement

As one can see from Figure 4-5 above, the porous plate occupies the whole width of the centre contraction of the structure. The whole turbine simulation structure was supported by the threaded rods used to hold the walls of the structure in place which as mentioned were pressure fitted between the two walls of the flume.

4.3.3 Data Recording

Two types of data were being collected during the flume experiments: ADV velocity readings and forces on the porous plates using a load cell. The velocity data was collected during both the tests with and without the plates whereas the load cell readings were only collected during the second stage of testing. Two Dell Latitude D630 laptops were used during both stages and were positioned at a data collection desk beside the 1.5 m wide flume. The overall setup allowed for easy movement between the *TAS* model and recording station and was also useful in it allowed for frequent verification of the flume's water level to ensure that a constant 30 cm depth was being maintained. As mentioned earlier, the ADV data was collected using the Vectrino Plus software and the Load Cell force data was collected using National Instrument's LabVIEW software and a program created to measure the average force over a 5-minute period. Figure 4-6 below shows the overall flume test setup.

Figure 4-6: Overall Flume Testing Setup

4.4. Experimental Procedure

4.4.1 Stage I: Without Plates

As mentioned, the first stage of testing was done without the presence of porous plates to simulate the energy extracted by a turbine. For Stage 1 therefore the only objective was to measure the velocity field around different *TAS* configurations with the goal of optimising the structure for maximum velocity through the structure centre. The following lists the steps taken during the testing of each of the structure configurations in Stage 1.

1) The *TAS* model was placed at the correct location in the flume: 6.5 m from the end, alongside the wall facing the interior of the lab (henceforth known as the near side).
2) The *TAS* wall opening and contraction distances were arranged for the configuration specified and it was ensured that the walls were vertical using a level.
3) The flume pump was started and the valve opened to the calibrated position giving an average upstream velocity of 14.14 +/- 0.5 cm/s (for first test of day).
4) A 5-minute time series of upstream velocity measurements was performed to ensure that the average velocity was within 14.14 +/- 0.5 cm/s. Water depth was checked at several locations around the structure to ensure an exact depth of 30.0 cm.
5) ADV data collection was performed at several locations in the flume for 5 minutes per sample to ensure a reliable velocity average. The ADV test point locations were chosen based on the need to capture the main velocity features that were observed in preliminary Fluent numerical simulations including:
    - Acceleration of flow at structure centre
    - Velocity reduction at structure opening
    - Velocity increase between structure and far wall of flume

Based on these criteria, data was collected during Stage 1 at the locations as shown in Figure 4-7 and Figure 4-8 below (note for Figure 4-8, cross section described by T-T section in Figure 4-7).

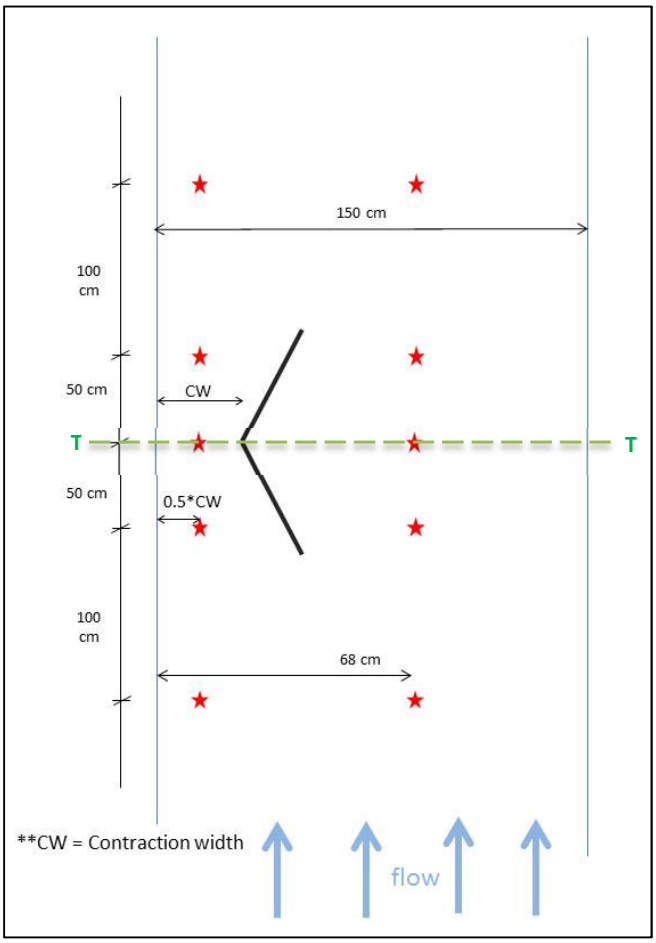

Figure 4-7: ADV Test Points for Stage 1 - Plan View 12.5 cm above Flume Bed

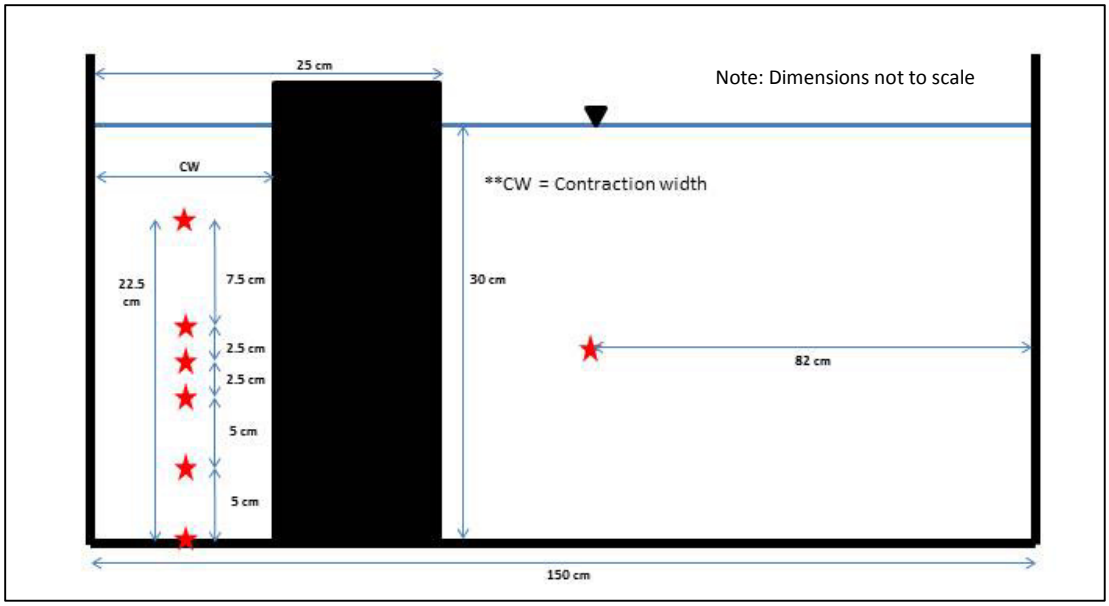

Figure 4-8: ADV Test Points for Stage 1 - Transversal Cross Section (T-T) at *TAS* Centre Location

4.4.2 Stage II: With Plates

During the second stage of testing, some of the structure configurations were re-tested in conjunction with the porous plate system. Both ADV velocity readings around the structure and force readings using the load cell were measure during this stage with the final goal of estimating the power that could be attained with each *TAS* configuration. The following lists the steps in Stage 2 testing:

1) The *TAS* model was placed at the correct location in the flume: 6.5 m from the end, alongside the wall facing the interior of the lab (henceforth known as the near side).
2) The wall opening and contraction distances were arranged for the configuration specified and it was ensured that the walls were vertical using a level.
3) The appropriate Load Cell – Porous Plate arrangement was installed and the plate set up such that distances to the flume and structure walls were minimised while ensuring that the plate could swing freely if not for the load cell.
4) The wall opening and contraction distances were re-measured and leveled.

5) The flume pump was started and the valve opened to the calibrated position giving an average upstream velocity of 14.14 +/- 0.5 cm/s (for first test of day).

6) A 5-minute time series of upstream velocity measurements was performed to ensure that the average velocity was within 14.14 +/- 0.5 cm/s. Water depth was checked at several locations around the structure to ensure an exact depth of 30.0 cm.

7) ADV data collection was performed at several locations in the flume for 5 minutes per sample to ensure a reliable velocity average. The ADV test point locations were chosen based on the desire to capture the main velocity features that were measured in Stage 1 and also to record some additional flow features to be used for power estimation including:

    - Velocity field around the porous plates
    - More detailed longitudinal velocity profiles

Based on these criteria, data was collected at the following locations during Stage 2.

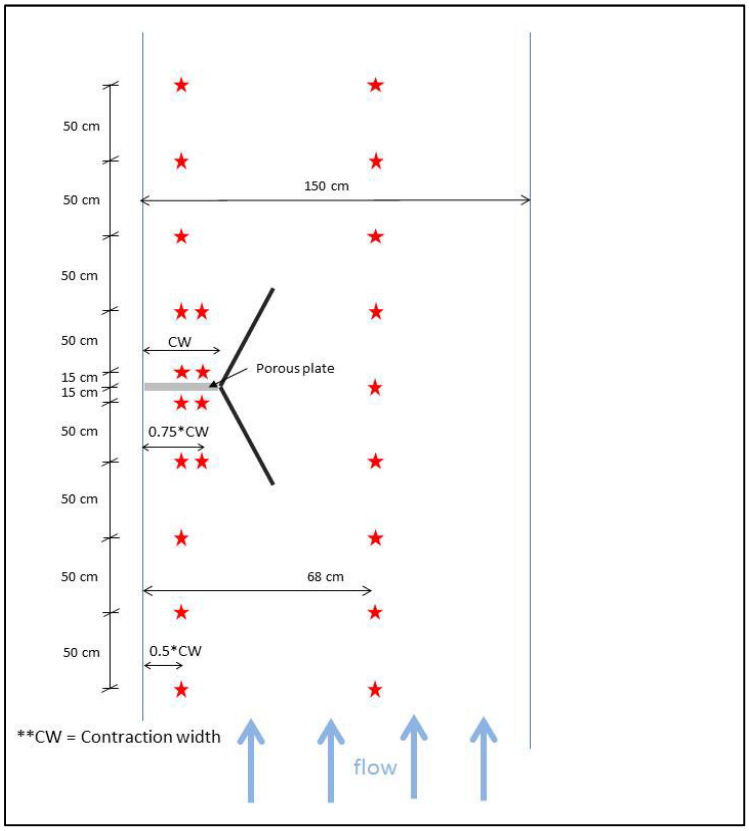

Figure 4-9: ADV Test Points for Stage 2 - Plan View 12.5 cm above Flume Bed

In addition, the three porous plates were tested in their same positions along the side of the flume but with no structure present to be able to compare the estimated power with and with the *TAS*.

4.4.3 Stage III: Detailed Tests

During the third stage of testing, a structure configuration, consisting of straight walls with a 25 cm opening and 10 cm contraction, was re-tested both without and with the 10 cm wide porous plate. Both ADV velocity readings around the structure and force readings using the load cell were measured during this stage with the final goal being the validation of the two corresponding tests in stages 1 and 2. The steps taken were the same as the corresponding ones in stages 1 and 2 except with more ADV velocity readings and more load cell readings. An additional test was also performed to see the effect of placing the 10 cm wide porous plate in a 17.5 cm contraction with 35 cm openings. This test was done out of curiosity to see if the estimated power would be larger than for the tests where the plates spanned the whole width of the contraction. The ADV readings for this test (10 cm plate – 17.5 cm x 35 cm) were the same as for the other tests of Stage 2. The additional ADV velocity readings for the two tests with 25 cm openings and 10 cm contractions (with and without 10 cm wide plate) are shown in Figure 4-10 below (note cross section described by T-T section in Figure 4-12).

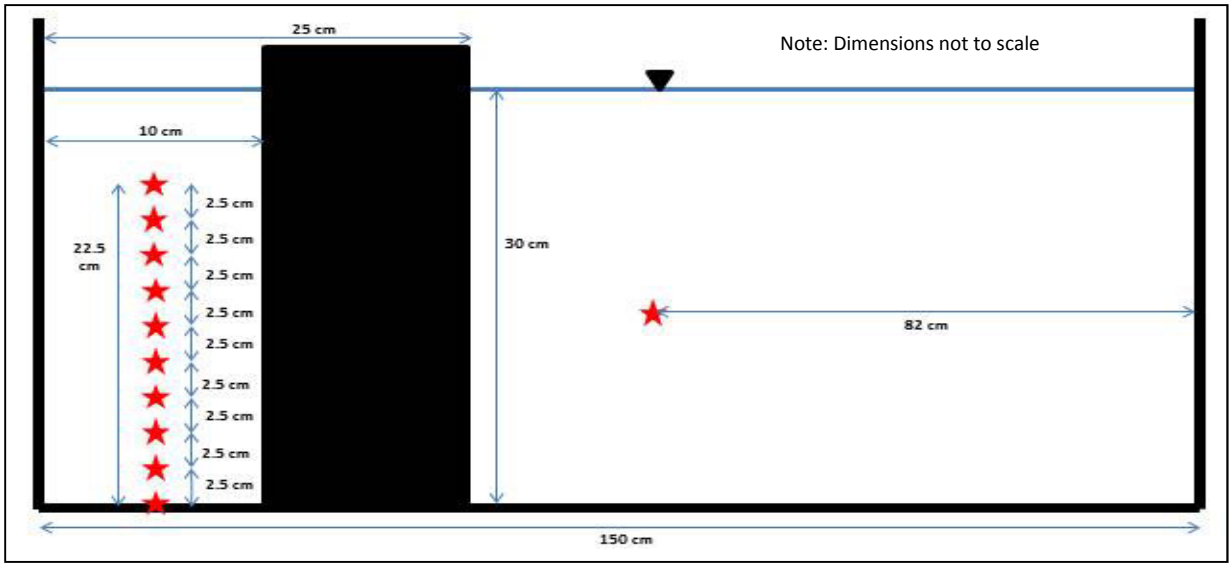

Figure 4-10: ADV Test Points for Stage 3 - Transversal Cross Section (T-T) at *TAS* Centre Location

4.5. Sensitivity Analysis

Because the *TAS* model was expected to have a blockage effect on the flow passing the section of the structure, the scale of the *TAS* simulated within the 1.5 m wide flume was important. An initial assumption was made that larger scales of the structure would produce more of a blockage effect as they'd occupy more of the flume cross-section. This blockage would not be found in wide natural channels and therefore the scale of the structure had to be limited in order to minimise the effect (not to be confused with the blockage effect of the porous plates described in Section 2.4.2). The expected outcome was that at a certain scale the side walls would not be significantly impacting flow conditions and the scale could be deemed satisfactory.

A preliminary sensitivity analysis using numerical modeling with Fluent was performed to determine the appropriate scale of the *TAS* for experimental and subsequent numerical testing. An initial scale of 1:50 for the Fluent *TAS* numerical model was assumed and then the width of the flume was varied to investigate its impact on flow hydrodynamics. A significantly wide flume would not induce an artificial blockage effect and therefore velocity magnitudes would be unaffected by flume width blockage. Because the main parameter of interest in testing the *TAS* was the velocity at the centre of the structure, a numerical "surface velocity monitor" was used at this location to compare velocity results of simulation runs. Using a 1:50th scale *TAS*, flume widths of 0.75, 1 and 1.5 m were tested. The results of the three simulations are shown in Table 4-3 below.

Table 4-3: Sensitivity Analysis Results

Simulation – Flume width (m)	Inlet stream velocity (m/s)	Average velocity at structure centre (m/s)	Max velocity at structure centre (m/s)	Min velocity at structure centre (m/s)
0.75	0.141421	0.29002	0.41913	0.23119
1.5	0.141421	0.21446	0.25930	0.17442
3	0.141421	0.18319	0.22563	0.14752

Notes:

1. The *TAS* that was tested had wall lengths of 31.78 cm with a contraction width of 9 cm and an opening width of 30 cm. These dimensions were chosen because they were those suggested by preliminary 2D modeling as part of the Capstone Project (Foran et al. 2012).
2. Average, max and min velocities refer to the velocities at the plane in the contraction of the *TAS*.

The values in Table 4-3 can also be visualised graphically in Figure 4-11 below.

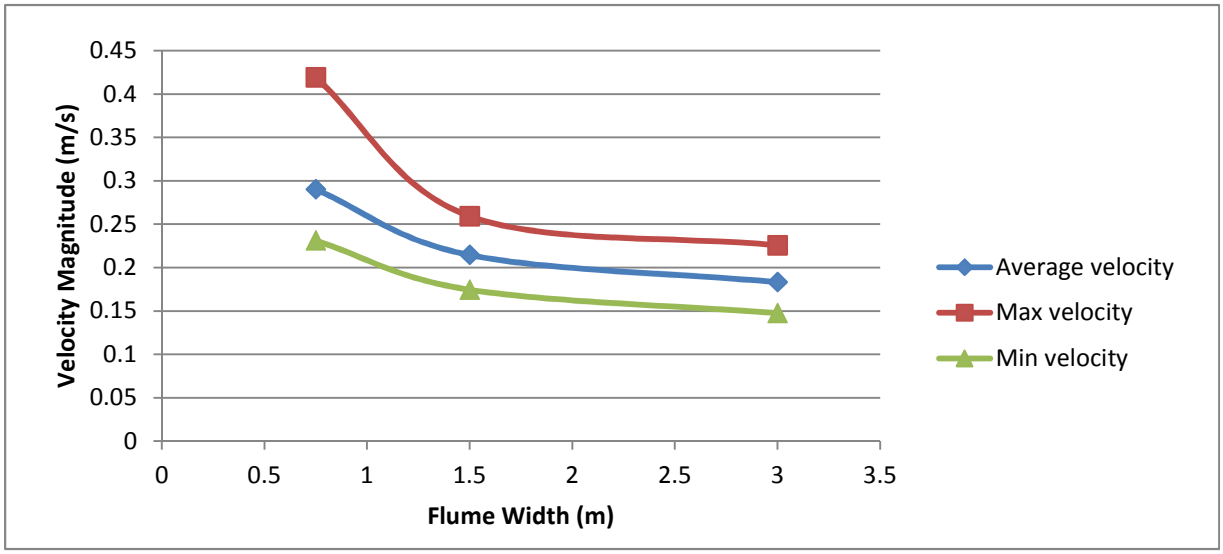

Figure 4-11: Sensitivity Analysis Results

As one can see from analysing the results in Figure 4-11 above, the flow through the centre of the *TAS* increases as the flume width is reduced. This is due to the blockage effect of the entire structure on flow, as the *TAS* represents a greater percentage of the flume width. In comparing the results for flume widths of 1.5 and 3 m, one can see that there is not a significant difference in velocities through the *TAS* contraction. It was desired to test the structure at the largest scale possible, therefore, it was concluded that the 1:50 scale *TAS* would be adequate for testing in the 1.5 m wide flume.

4.6. Results and Analysis

The following section presents the experimental testing results and their initial processing and analysis. A more broad discussion is presented in Chapter 6. While selected results are presented throughout this section, more data, including ADV turbulence measurements and additional *TAS* configuration test results, are available upon request.

As mentioned, Stage 1 consisted of measuring the velocity field around different structure configurations with the primary goal being to find an optimised Tidal Acceleration Structure (*TAS*) design. This was done by varying one structure parameter at a time and comparing the acceleration at the structure centre. The following table lists all of the tests performed in Stage 1 and their dimensions.

Table 4-4: Stage 1 Experimental Testing - Structure Configurations

Test Name	Structure Contraction Width (cm)	Structure Opening Width (cm)	Wall Curvature (cm)
10contr_20open_str	10	20	None
10contr_25open_str	10	25	None
10contr_30open_str	10	30	None
10contr_40open_str	10	40	None
10contr_50open_str	10	50	None
15contr_20open_str	15	20	None
15contr_25open_str	15	25	None
15contr_30open_str	15	30	None
15contr_40open_str	15	40	None
15contr_50open_str	15	50	None
20contr_25open_str	20	25	None
20contr_30open_str	20	30	None
20contr_40open_str	20	40	None
20contr_50open_str	20	50	None
10contr_20open_crv1	10	20	7.5 cm out of plane
10contr_25open_crv1	10	25	7.5 cm out of plane
10contr_20open_crv2	10	20	10 cm out of plane
10contr_25open_crv2	10	25	10 cm out of plane
15contr_25open_crv1	15	25	7.5 cm out of plane
15contr_30open_crv1	15	30	7.5 cm out of plane
15contr_25open_crv2	15	25	10 cm out of plane
15contr_30open_crv2	15	30	10 cm out of plane

20contr_30open_crv1	20	30	7.5 cm out of plane
20contr_40open_crv1	20	40	7.5 cm out of plane
20contr_30open_crv2	20	30	10 cm out of plane
20contr_40open_crv2	20	40	10 cm out of plane
Net_10contr_20open	10	20	None
Net_10contr_25open	10	25	None
Note: The two tests with name prefix *Net* had wire mesh attached across the opening and exit widths to simulate the reduction in flow caused by a net.			

In Stage 2 the focus shifted to selecting the best configurations from Stage 1 and testing them with the presence of a porous plate to simulate the effect that a turbine would have on flow and try to estimate the power extracted using Actuator Disc Theory. Three porous plates with porosities of 58% were constructed: 10, 15 and 20 cm wide rectangular plates. For each of these plates 2 opening widths were selected and then tested with the 3 types of wall curvature: straight-walled, moderately curved and considerably curved. The following table lists all of the tests performed in Stage 2 and their dimensions.

Table 4-5: Stage 2 Experimental Testing - Structure Configurations

Test Name	Structure Contraction Width (cm)	Structure Opening Width (cm)	Wall Curvature (cm)
10contr_20open_str	10	20	None
10contr_25open_str	10	25	None
15contr_25open_str	15	25	None
15contr_30open_str	15	30	None
20contr_30open_str	20	30	None
20contr_40open_str	20	40	None
10contr_20open_crv1	10	20	7.5 cm out of plane
10contr_25open_crv1	10	25	7.5 cm out of plane
10contr_20open_crv2	10	20	10 cm out of plane
10contr_25open_crv2	10	25	10 cm out of plane
15contr_25open_crv1	15	25	7.5 cm out of plane
15contr_30open_crv1	15	30	7.5 cm out of plane
15contr_25open_crv2	15	25	10 cm out of plane
15contr_30open_crv2	15	30	10 cm out of plane
20contr_30open_crv1	20	30	7.5 cm out of plane
20contr_40open_crv1	20	40	7.5 cm out of plane
20contr_30open_crv2	20	30	10 cm out of plane

20contr_40open_crv2	20	40	10 cm out of plane
JUST 10 cm wide disc	NA	NA	NA
JUST 15 cm wide disc	NA	NA	NA
JUST 20 cm wide disc	NA	NA	NA
Note: The last three tests listed were performed without the presence of the *TAS* model.			

Stage 3 as mentioned consisted of retesting the 10 x 25 cm straight walled *TAS* model both with and without the presence of the 10 cm wide porous plate for comparison with the results of Stages 1 and 2. These tests were performed as they offered more detailed velocity data to compare with the numerical Fluent results. Finally, the 17.5 x 35 straight-walled (with 10 cm wide plate) test was performed to estimate the power extracted when the porous plate did not cover the entire contraction width. Table 4-6 below lists all of the tests performed in Stage 3 and their dimensions.

Table 4-6: Stage 3 Experimental Testing - Structure Configurations

Test Name	Structure Contraction Width (cm)	Structure Opening Width (cm)	Wall Curvature (cm)
10contr_25open_noplate	10	25	None
10contr_25open_plate	10	25	None
17p5contr_35open_str	17.5	35	None
Note: The last test listed was performed with the 10 cm wide porous plate			

4.6.1 ADV Velocity Profiles

This section, 4.6.1, compares various velocity profiles which were recorded over the course of the experimental testing. All velocity profiles were modified based on the average upstream velocity as compared to the target upstream velocity of 14.14 cm/s. Though a 5 minute upstream velocity verification test was performed at the start of each test, the in-stream velocity was very hard to calibrate to exactly 14.14 cm/s every day due to time constraints therefore a deviation factor was used to correct the ADV readings. The Deviation Factor (DF) was calculated from the target velocity and a 15-minute average of the ADV recorded 3 m upstream from the structure during each test. This DF is calculated as:

$$DF = \frac{Target\ in-stream\ velocity}{15\ minute\ upstream\ average} = \frac{0.14142\frac{m}{s}}{15\ minute\ upstream\ average} \quad \textbf{(4-5)}$$

All velocity measurements are then multiplied by the DF of the test to get the Modified Velocity (MV):

$$MV = Initial\ Matlab\ filtered\ average\ velocity * DF \quad \textbf{(4-6)}$$

Where:

- DF is the Deviation Factor
- MV is the Modified Velocity

Although a sensitivity analysis was performed on the adequate ADV sampling time per reading, some errors were expected in the time averaged ADV readings due to flume flow-rate inconsistencies (discussed further in Section 4.7 below). There are two main types of velocity profiles compared: longitudinal velocity profiles and vertical velocity profiles. The vertical velocity profiles were all taken at the centre of the *TAS*, halfway between the flume wall and the *TAS* wall intersection. This line was chosen as the likely location for a turbine placement in a *TAS* prototype as it was thought that the highest velocities would occur at this section. This is the line connecting the red stars in the left sides of both Figure 4-8 and Figure 4-10. The second type of velocity profile, longitudinal profiles, demonstrate the velocity change for lines which are 12.5 cm above the bed and at a constant distance from the flume wall. Figure 4-12 below shows the five longitudinal velocity profiles (*Side, Plate, Edge, Middle, Far-Side*).

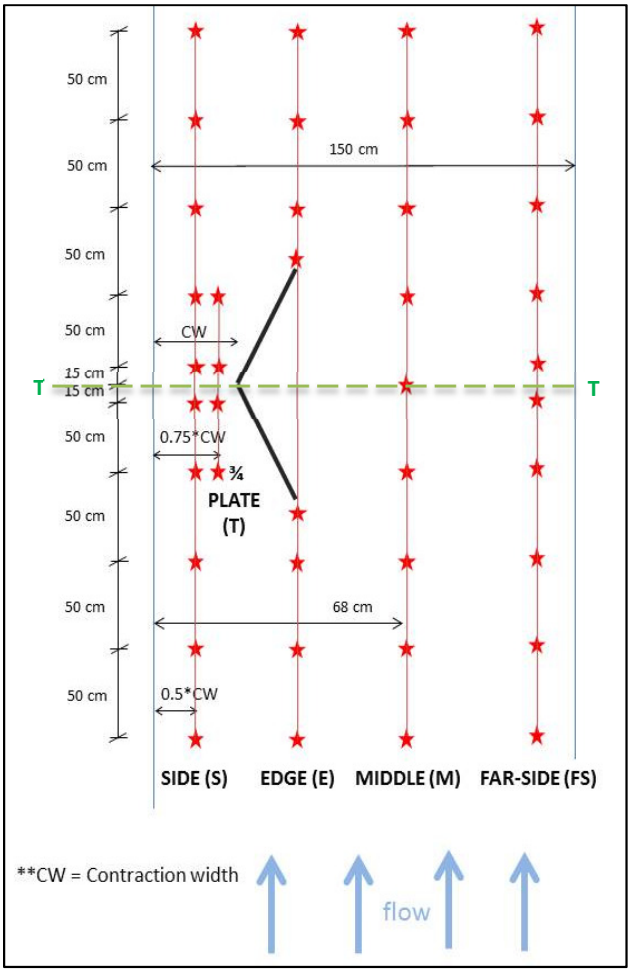

Figure 4-12: ADV Test Points for Stage 3 - Plan View 12.5 cm above Flume Bed

4.6.1.1 Comparison of Velocity Profiles for the 10 x 25 cm TAS tests

The following graph presents the vertical velocity profile at the structure centre line for the test named '*10contr_25open_str*' or the *TAS* configuration with a contraction of 10 cm, an opening of 25 cm and straight walls. The configurations with these dimensions (straight-walled, moderately curved and considerably curved versions) proved to be most effective in accelerating the current velocity and were therefore chosen for in-depth analysis.

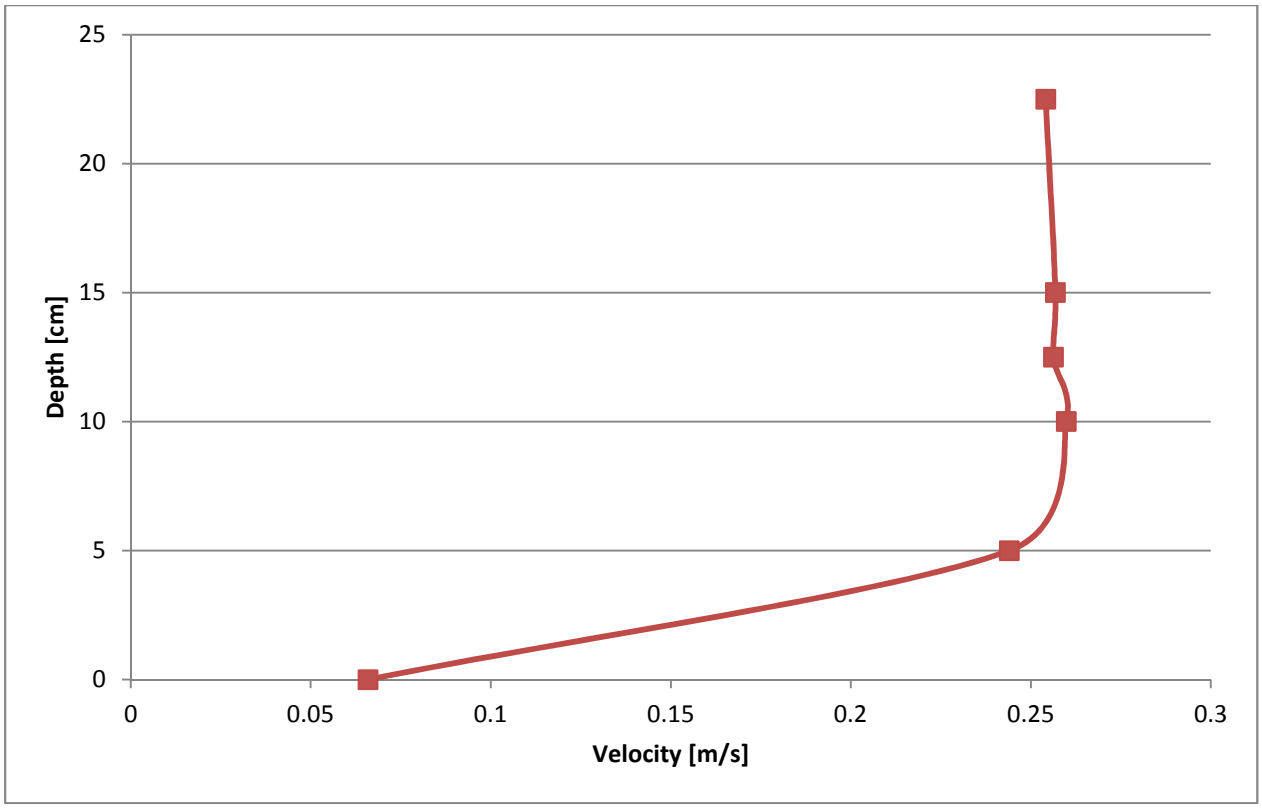

Figure 4-13: Vertical Velocity Profile Structure Centre - 10contr_25open_str Test

As shown in Figure 4-13, the water velocity at the structure centre line is above 25 cm/s, a significant increase in magnitude compared to the upstream velocity. As expected, the vertical velocity profile also seems to follow the log-law profile. It should be noted that the velocity at the bed is somewhat inaccurate as ADVs are not meant to measure the velocity in the boundary layer. A more detailed vertical velocity profile contains an ADV measurement at 2.5 cm above the bed and produces a more realistic log profile. The velocity data points at the bed were hence eliminated for some figures due to the inaccurate ADV bed velocity measurements (though they were recorded). Figure 4-14 below shows the *Side* longitudinal velocity profile at an elevation of 12.5 cm above the bed for the same test named '*10contr_25open_str*'. The location of this *Side* line is shown in Figure 4-12.

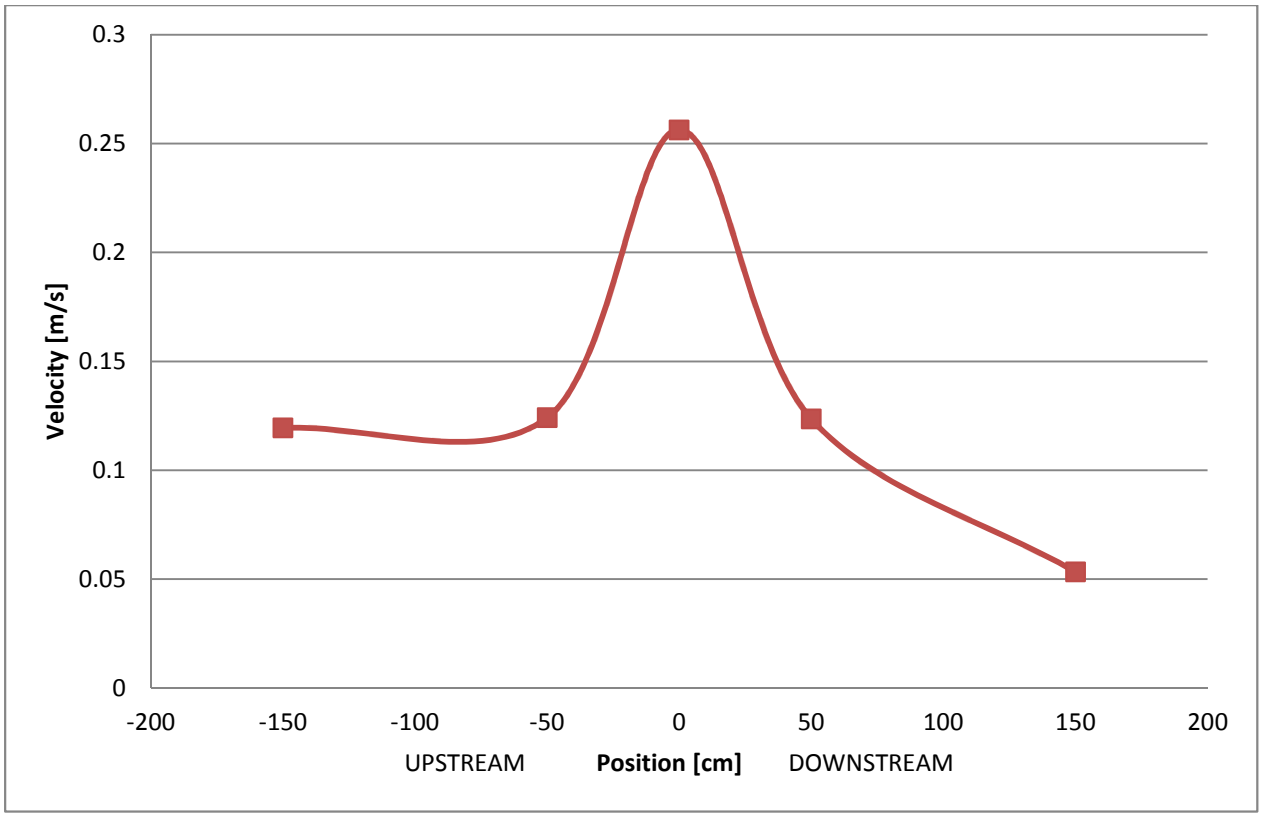

Figure 4-14: Side Longitudinal Velocity Profile - 10contr_25open_str Test

The increase in water velocity through the structure centre line is evident again in Figure 4-14 as one can observe. The velocity accelerates rapidly as it passes through the *TAS* constriction, attaining a maximum velocity of 25.6 cm/s. Figure 4-15 shows the *Middle* longitudinal velocity profile at an elevation of 12.5 cm above the flume bed for the same test named '*10contr_25open_str*'. Again, the location of this line is described in Figure 4-12.

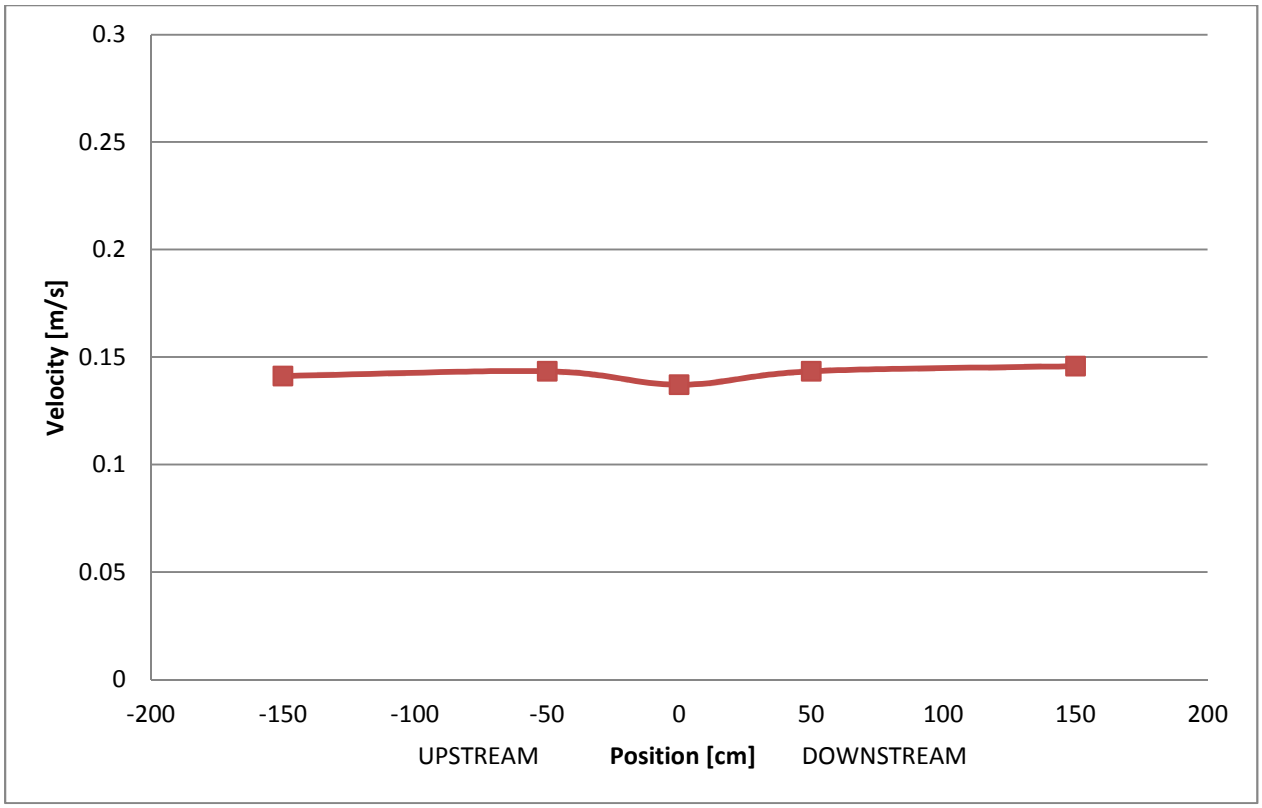

Figure 4-15: Middle Longitudinal Velocity Profile - 10contr_25open_str Test

In Figure 4-15 above, one can observe that there is no significant increase in the water velocity passing through the centre line of the flume at the longitudinal location of the structure (position = 0 cm). This indicates that the structure is not causing significant blockage of the overall flow through the flume. If the structure would have blocked the flow significantly, one would expect an increase in the velocity through the centre of the flume and also a higher acceleration of the flow passing through the structure centre. The lack of significant velocity increase in the *Middle* profile indicates therefore that the scale of 1:50 for the *TAS* model was adequate for the flume width of 1.5 m, confirming the sensitivity analysis of Section 4.5.

One can now compare the three preceding velocity profiles with their corresponding profiles from all other tests with a contraction of 10 cm and an opening of 25 cm (Stages 1, 2 and 3). The figure below presents the vertical velocity profiles.

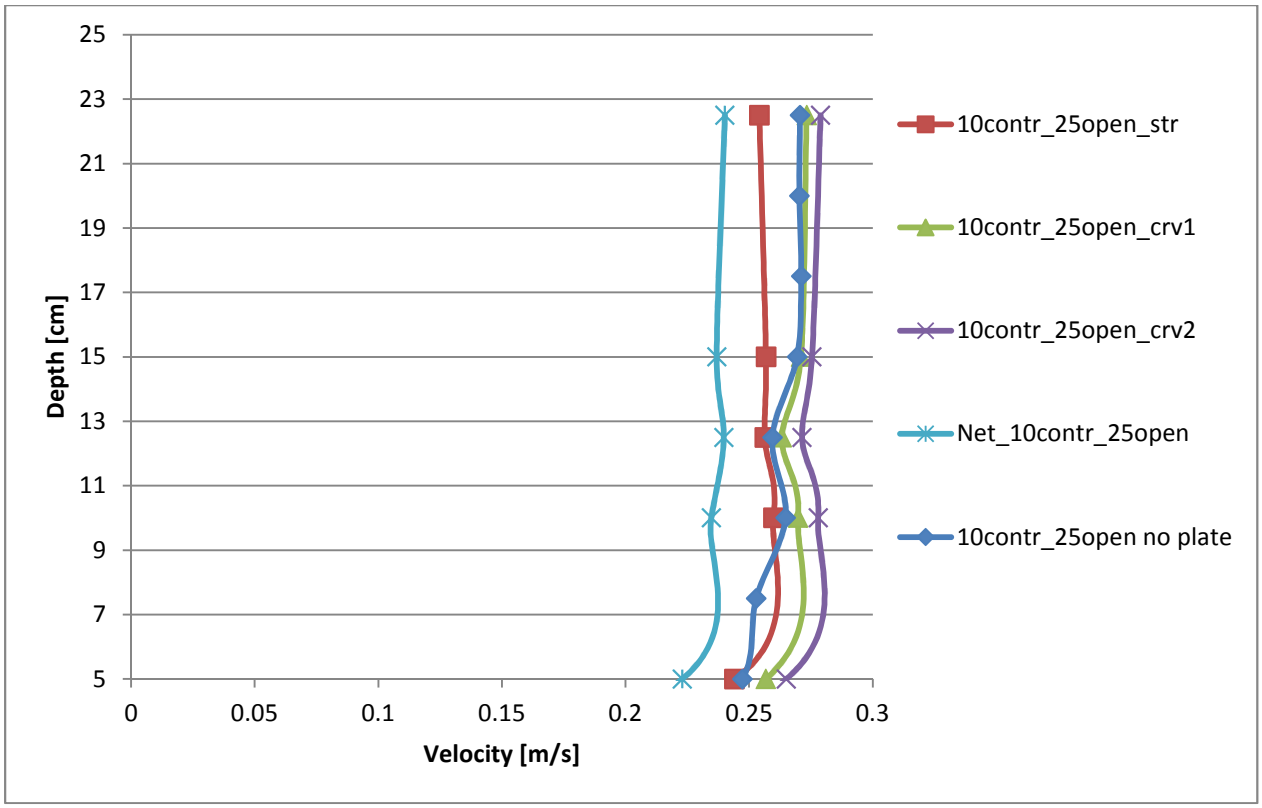

Figure 4-16: Vertical Velocity Profile Structure Centre - All 10 x 25 cm Tests

As one can see from the above vertical velocity profiles, there is not a significant difference between the different 10 x 25 cm structures. There is a reduction in the velocity profile magnitudes when nets are attached to the structure opening and exit, as can be seen in Figure 4-16 - '*Net_10contr_25open*' however, it is only marginal. The velocity magnitudes are also all quite consistent throughout the depth of flow except for a slight reduction in velocity at the point 5 cm above the bed as the shear stress from the flume floor starts to decrease the flow velocity. These vertical velocity profiles agree with the standard log-law profile as expected. The *Side* longitudinal velocity profile is also compared in Figure 4-17 below.

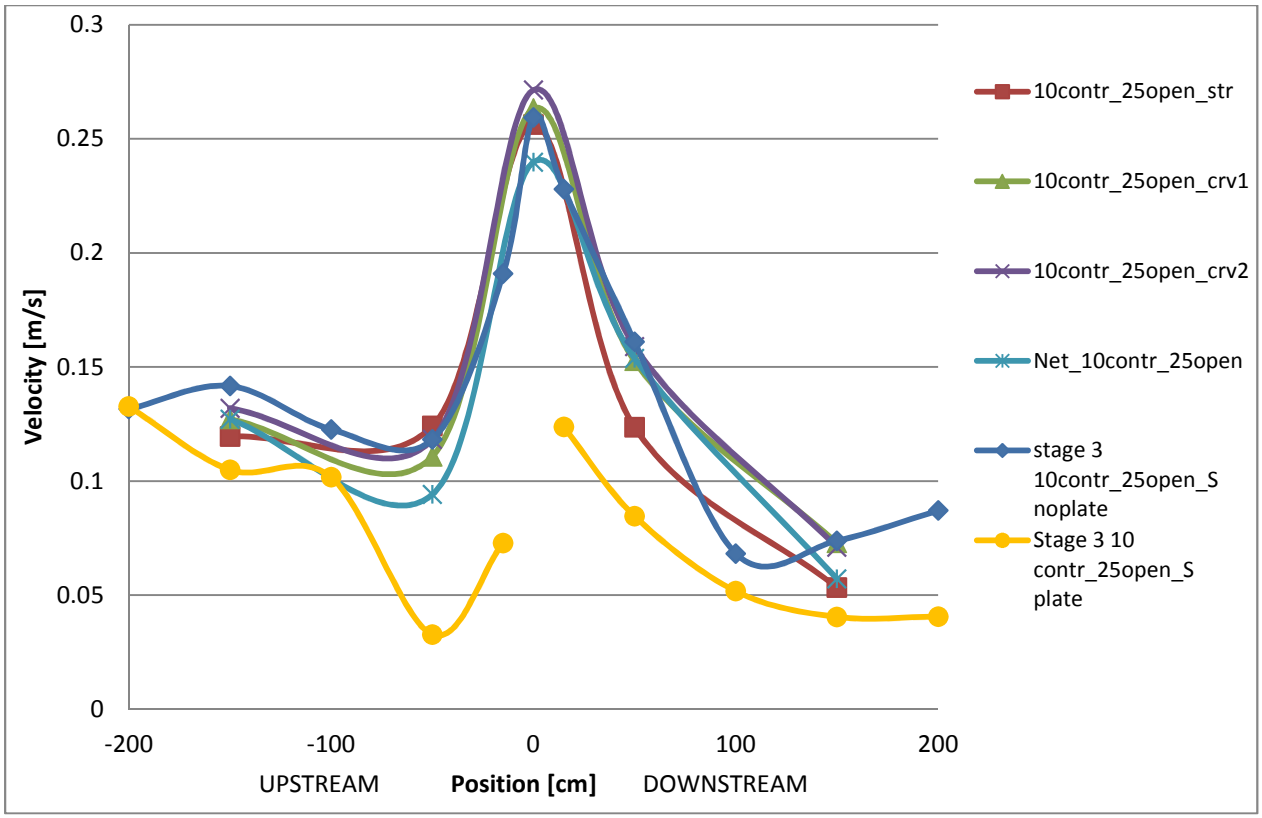

Figure 4-17: Side Longitudinal Velocity Profile - All 10 x 25 cm Tests

The *Side* longitudinal velocity profile in Figure 4-17 above illustrates the acceleration of fluid velocity as it passes through the centre of the structure (position = 0 cm). The initial deceleration of flow upstream of the structure from around 150 cm upstream to 50 cm upstream is also evident in all tests. With the exception of the test done with the plate ('*Stage 3 10 contr_25open_S* plate'), the figure shows that all variations of the 10 x 25 cm *TAS* tests yielded near 25 cm/s at the centre of the structure. The *Middle* longitudinal velocity profile is also compared in Figure 4-18 below.

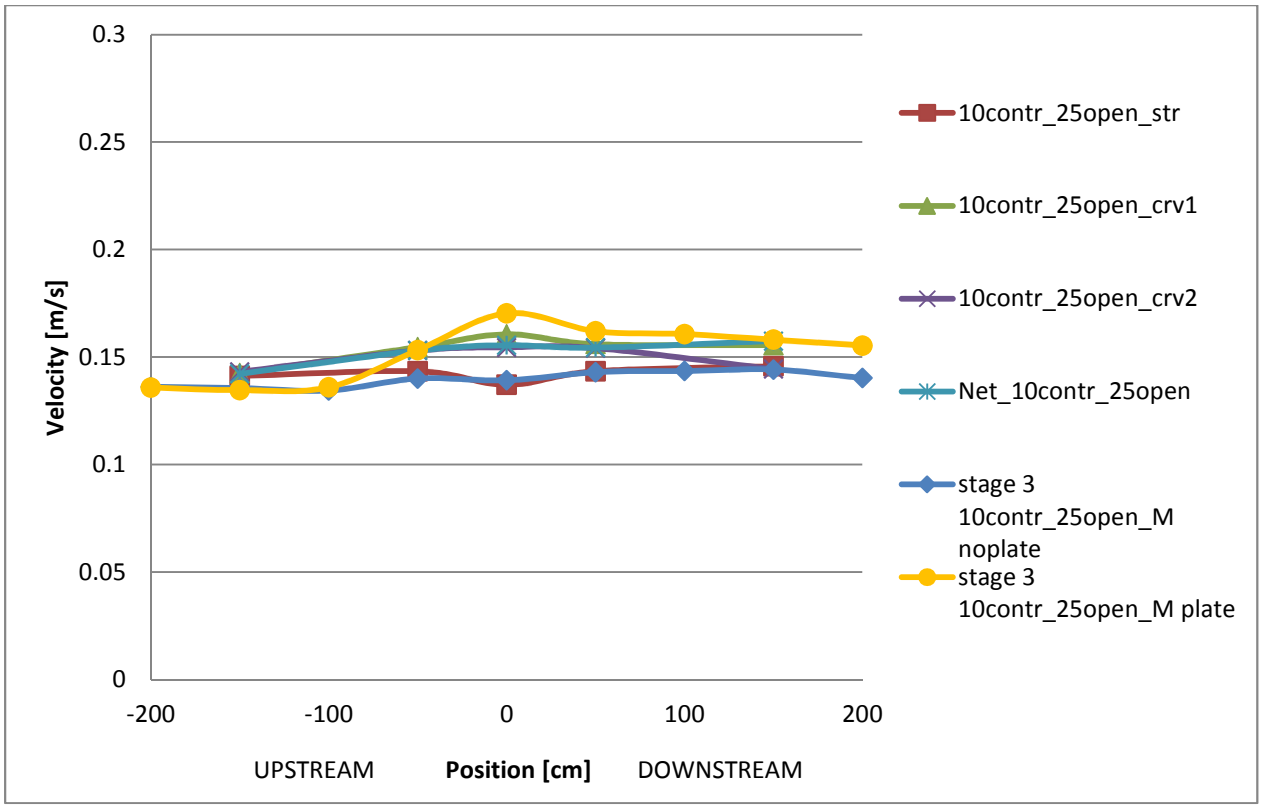

Figure 4-18: Middle Longitudinal Velocity Profile - All 10 x 25 cm Tests

In Figure 4-18, one can observe an increase in velocity magnitude through the centre line of the flume in test '*stage 3 10contr_25open_S plate*' from the far upstream to the far downstream position. This is most likely due to the increased blockage effect that the plate has on flow, forcing more water to pass around the *TAS* rather than through it. This blockage is also reflected in the decreased water speed-up through the *TAS* centre as compared to the other 10 x 25 cm tests. The tests entitled '*10contr_25open_str*' and '*stage 3 10contr_25open_S no plate*' were for the same *TAS* configuration setup dimensions therefore it is promising to observe very similar velocity profiles between the two in all three preceding figures (Figure 4-16, Figure 4-17 and Figure 4-18).

4.6.1.2 Comparison by TAS Contraction Width – All Tests

Before comparing tests with the same contraction width, the vertical velocity profiles of all Stage 1 tests are compared in Figure 4-19 below.

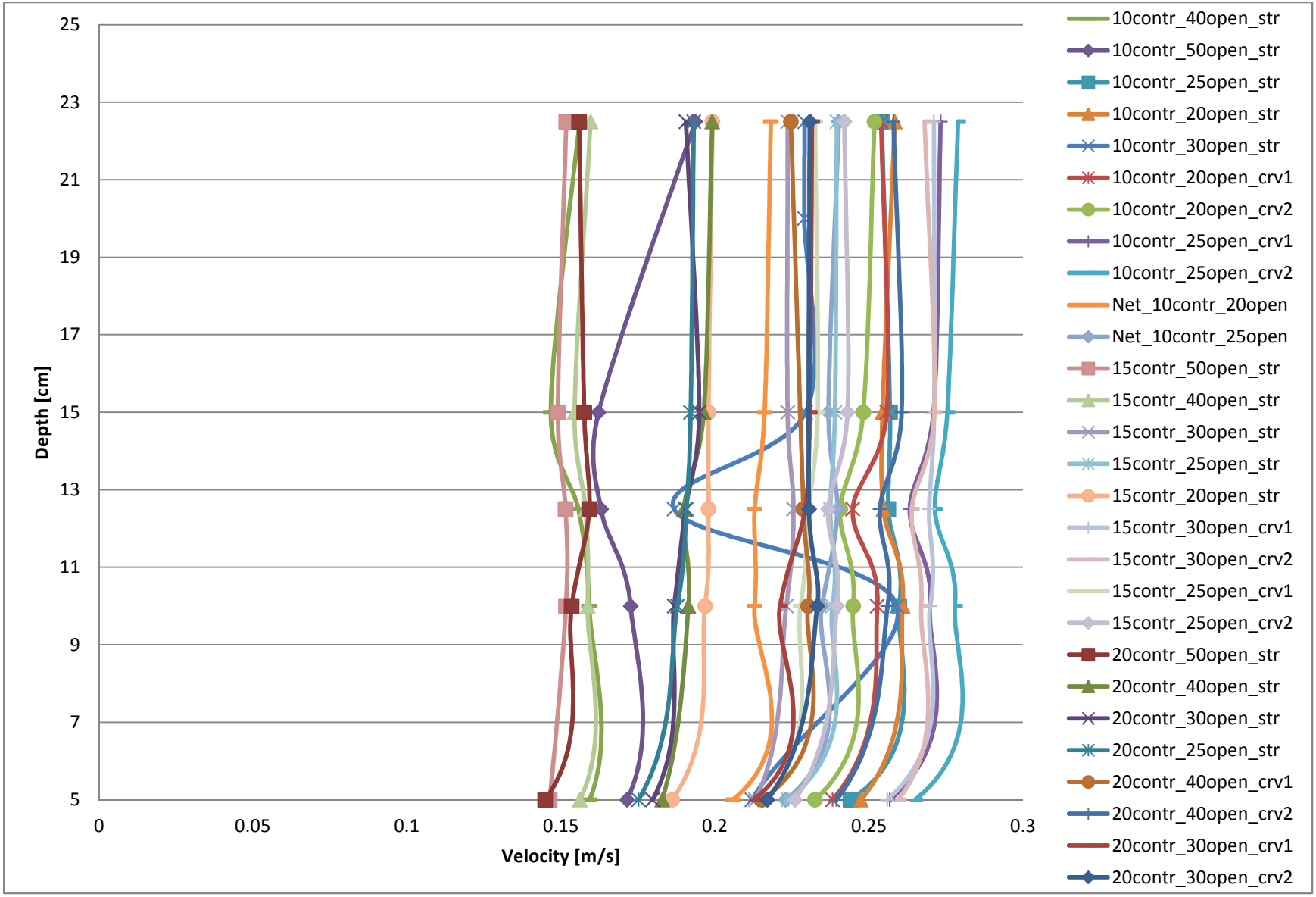

Figure 4-19: Vertical Velocity Profile Structure Centre - Stage I Tests

As one can see in Figure 4-19 above, the difference in velocities generated at the structure centre between tests can be significant. Some tests barely increase the in-stream velocity at all when compared to the upstream while others increase it significantly. The following graphs will break the information up into groups by separating the tests by contraction width.

The first series of tests that are compared are the ones with contraction widths of 10 cm. Figure 4-20 below shows the vertical velocity profiles.

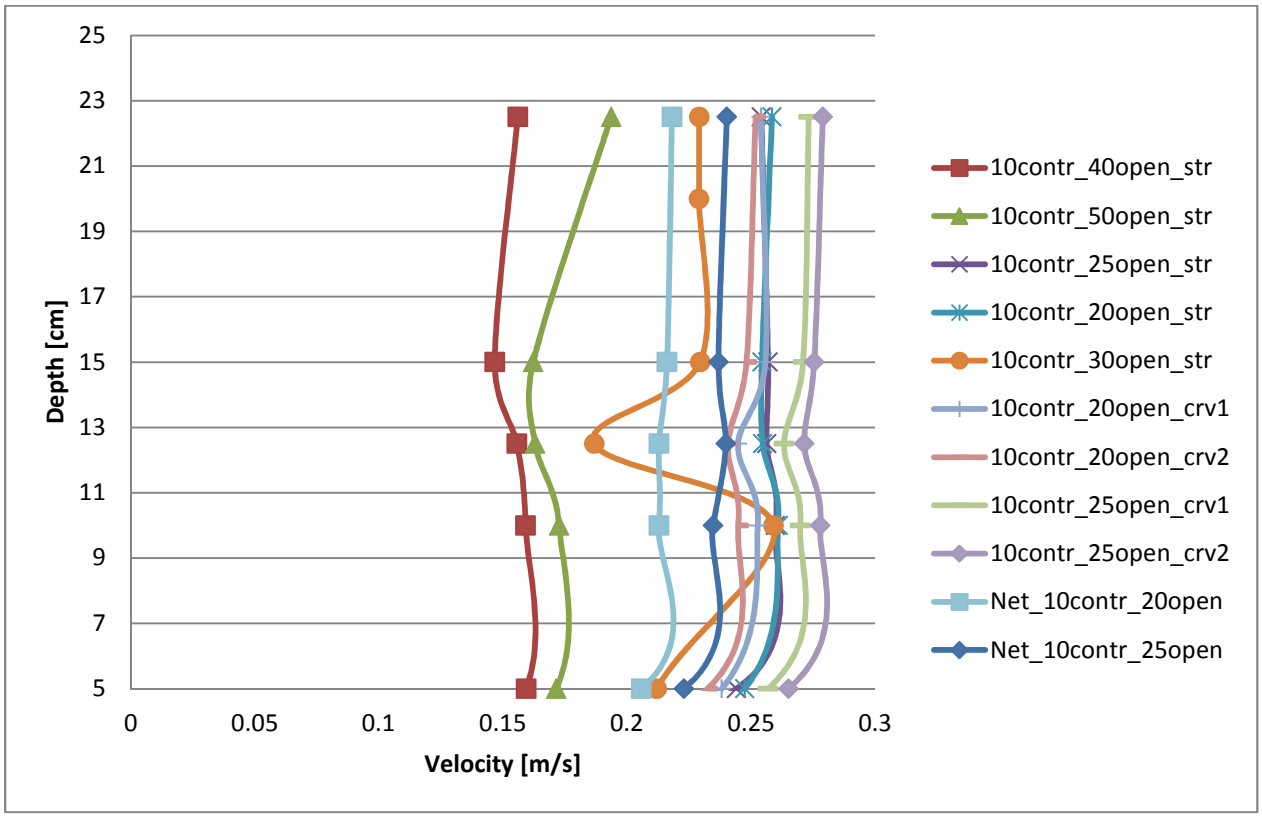

Figure 4-20: Vertical Velocity Profile Structure Centre - 10 cm Wide Contraction Tests

When looking at just the 10 cm wide contraction tests it becomes evident that the tests with large openings performed poorly compared to those with narrower openings. The configurations with 25 cm openings are accelerating flow the most while a slight drop-off in acceleration can be observed for the tests with the 20 and 30 cm openings. It should be noted that the test entitled '*10contr_30open_str*' seems to denote an error in the velocity recording as its vertical velocity profile is very irregular. This aspect is further discussed in Section 4.7.

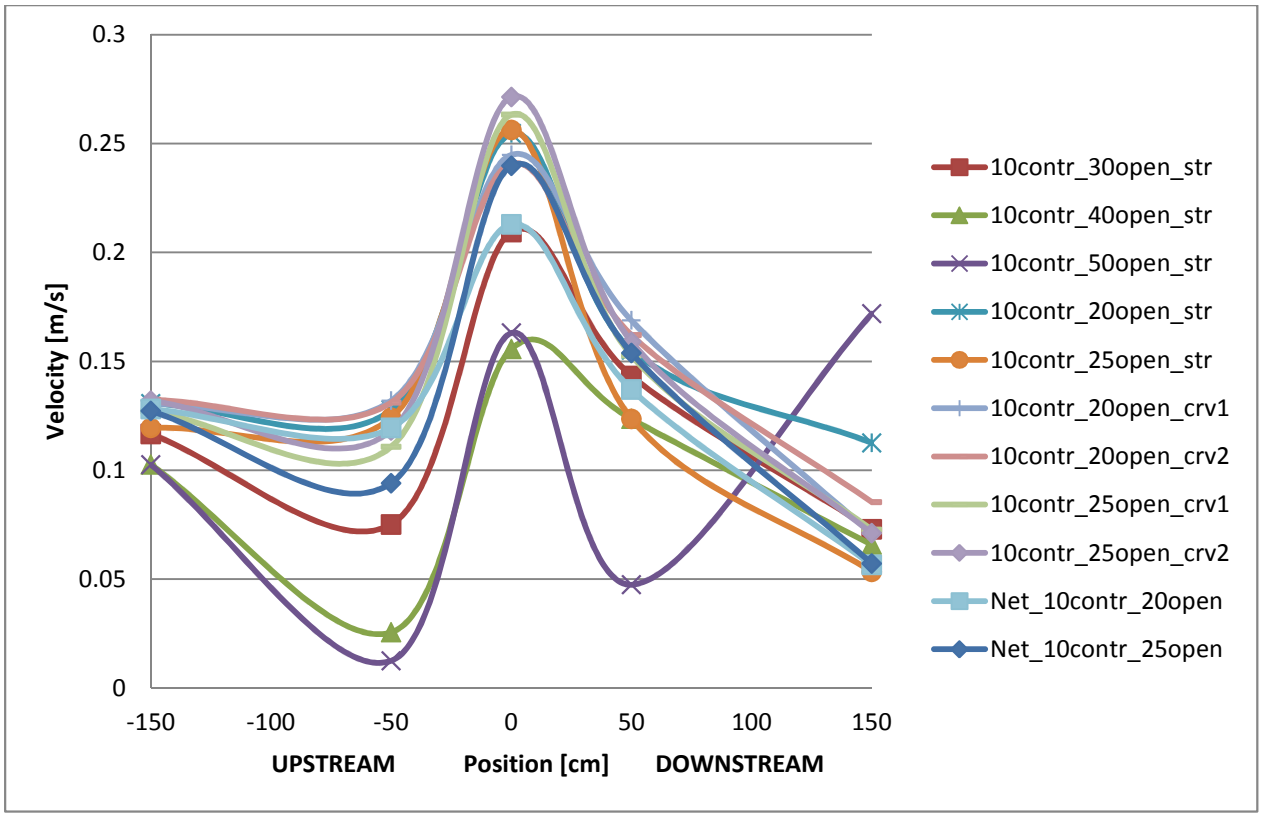

Figure 4-21: Side Longitudinal Velocity Profile - 10 cm Wide Contraction Tests

In Figure 4-21, it is again evident that the tests with large openings are performing poorly in terms of their acceleration of flow through the *TAS*. The reduction in velocity is seen even 150 cm upstream of the structure centre, with the large openings blocking flow to an extent which cannot be recuperated by the Venturi effect of the structure.

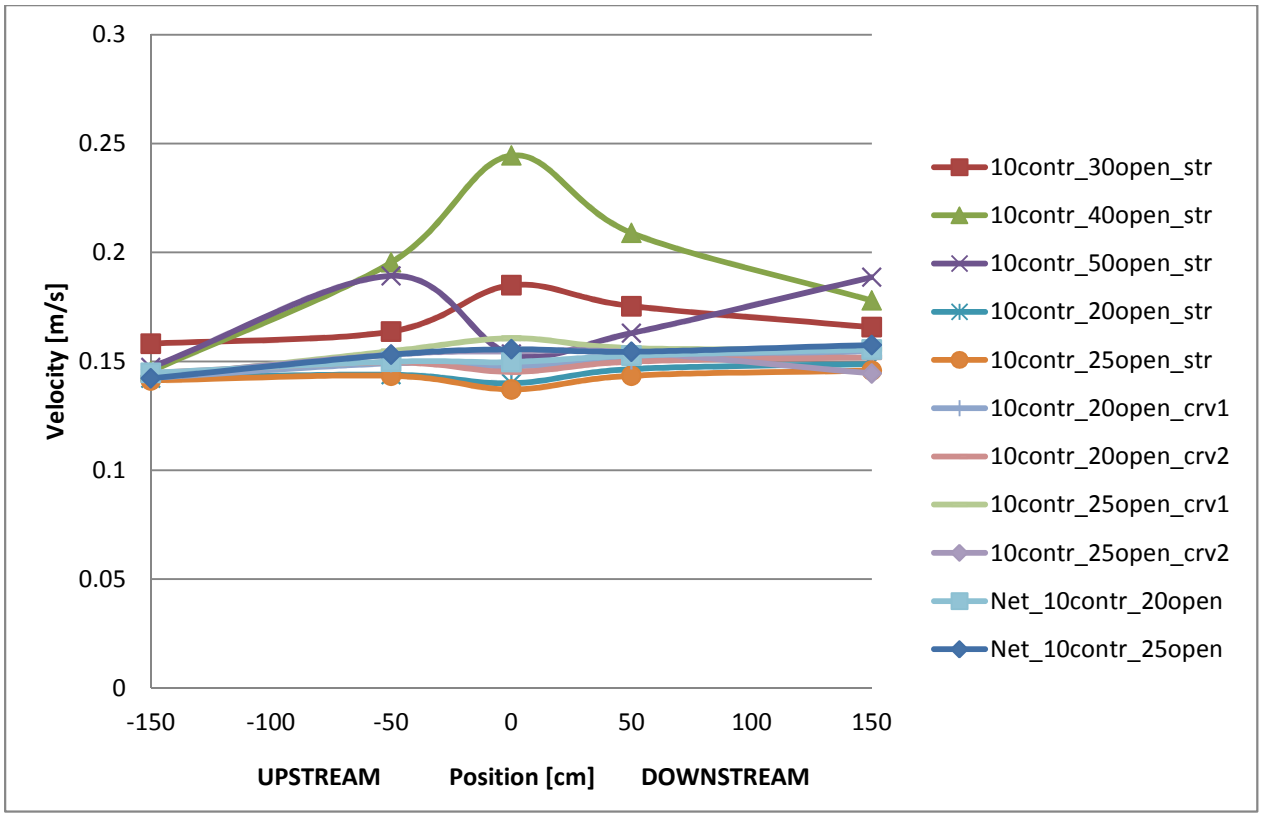

Figure 4-22: Middle Longitudinal Velocity Profile - 10 cm Wide Contraction Tests

In Figure 4-22 above, the reduced velocity through the structures with large openings resulted in the flow being forced through the centre of the flume. It should be noted that for test '*10contr_50open_str*' the sudden drop off in velocity from 50 cm upstream to position zero was probably due to the flow being forced even further away from the structure to the other side of the flume. This can be attributed to the fact that the line considered as the middle of the flume (68 cm from near wall), was close to the edge of the structure (50 cm from near wall).

One can now examine the three types of velocity profiles for the tests with 15 and 20 cm wide contractions.

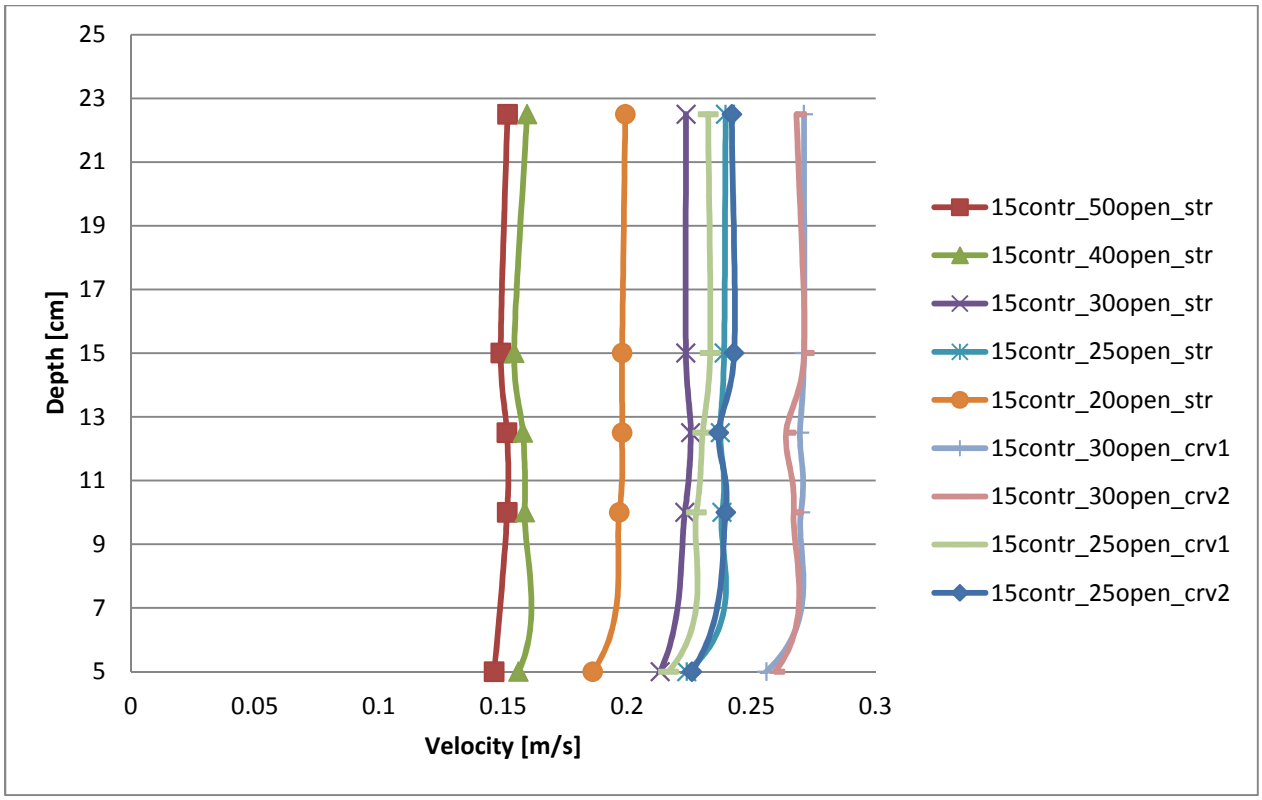

Figure 4-23: Vertical Velocity Profile Structure Centre - 15 cm Wide Contraction Tests

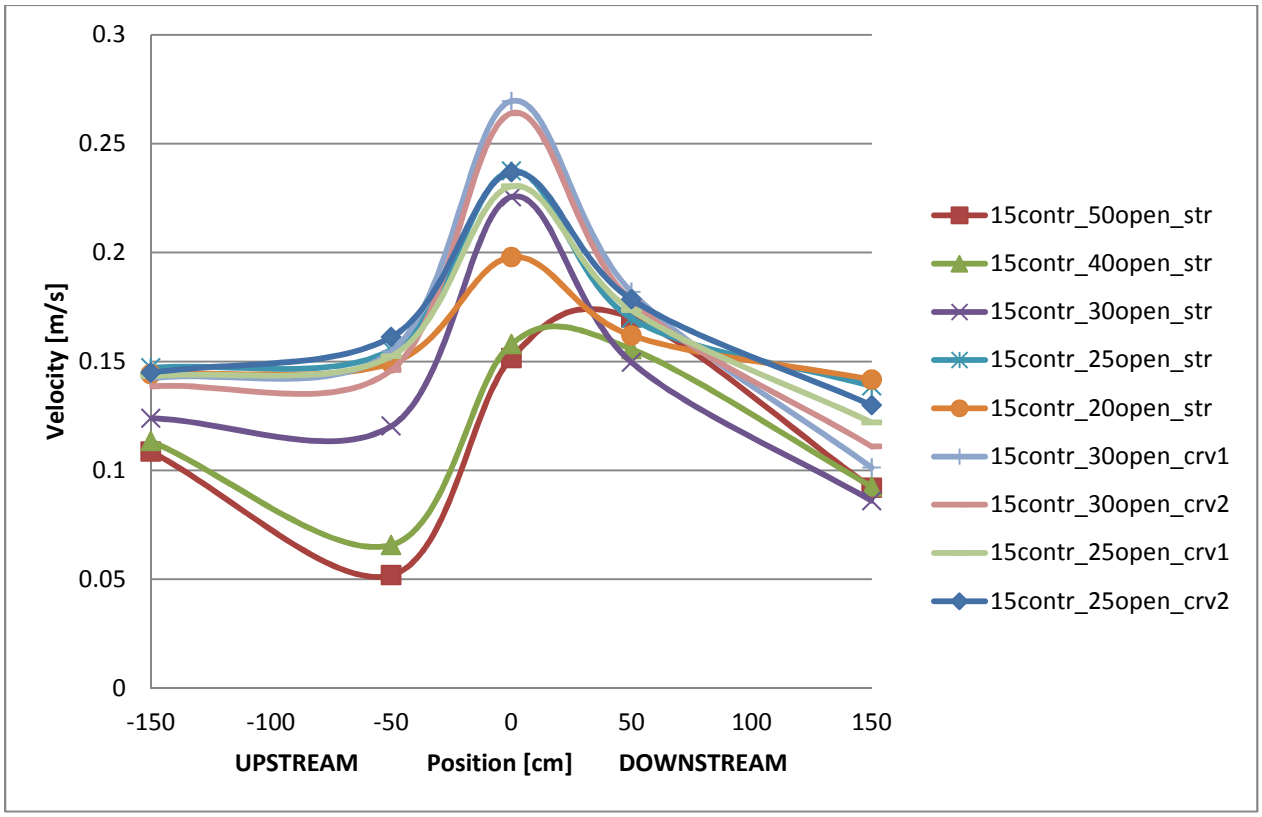

Figure 4-24: Side Longitudinal Velocity Profile - 15 cm Wide Contraction Tests

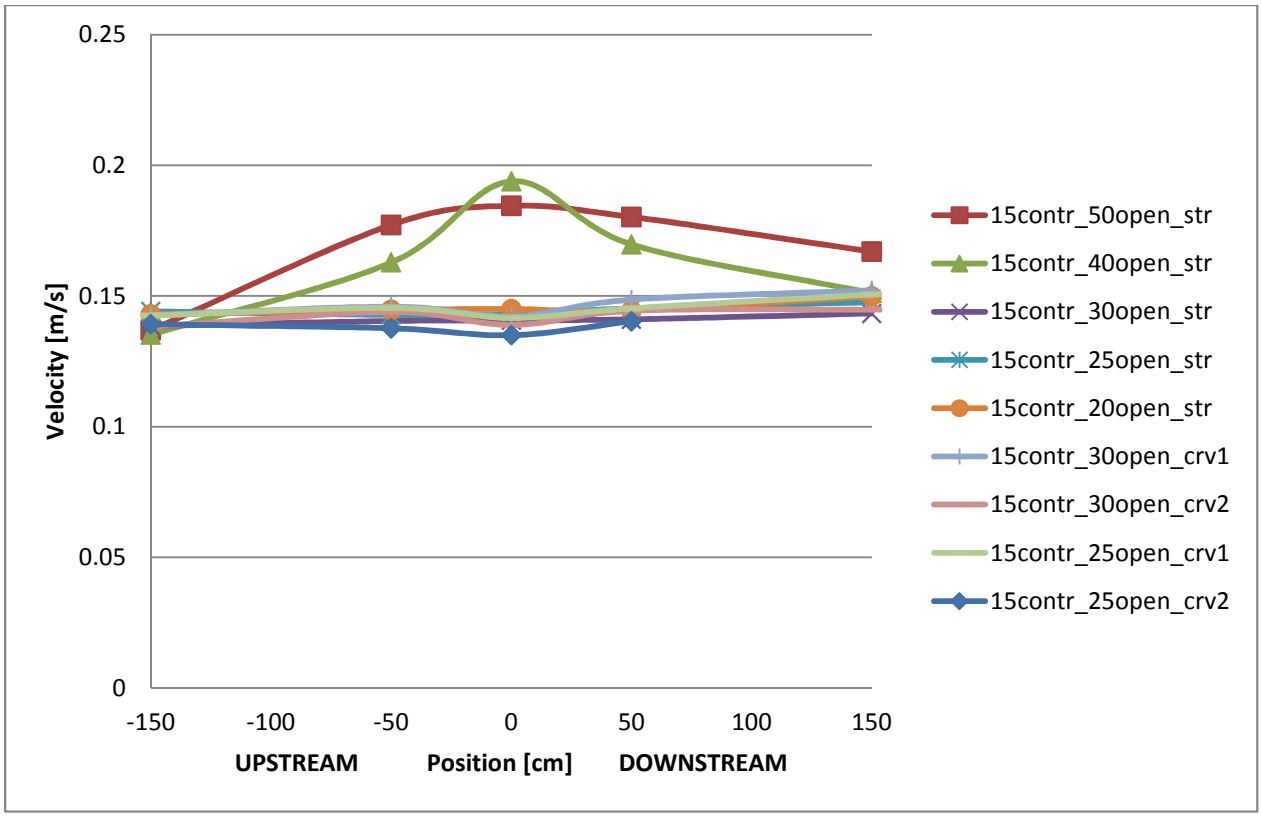

Figure 4-25: Middle Longitudinal Velocity Profile - 15 cm Wide Contraction Tests

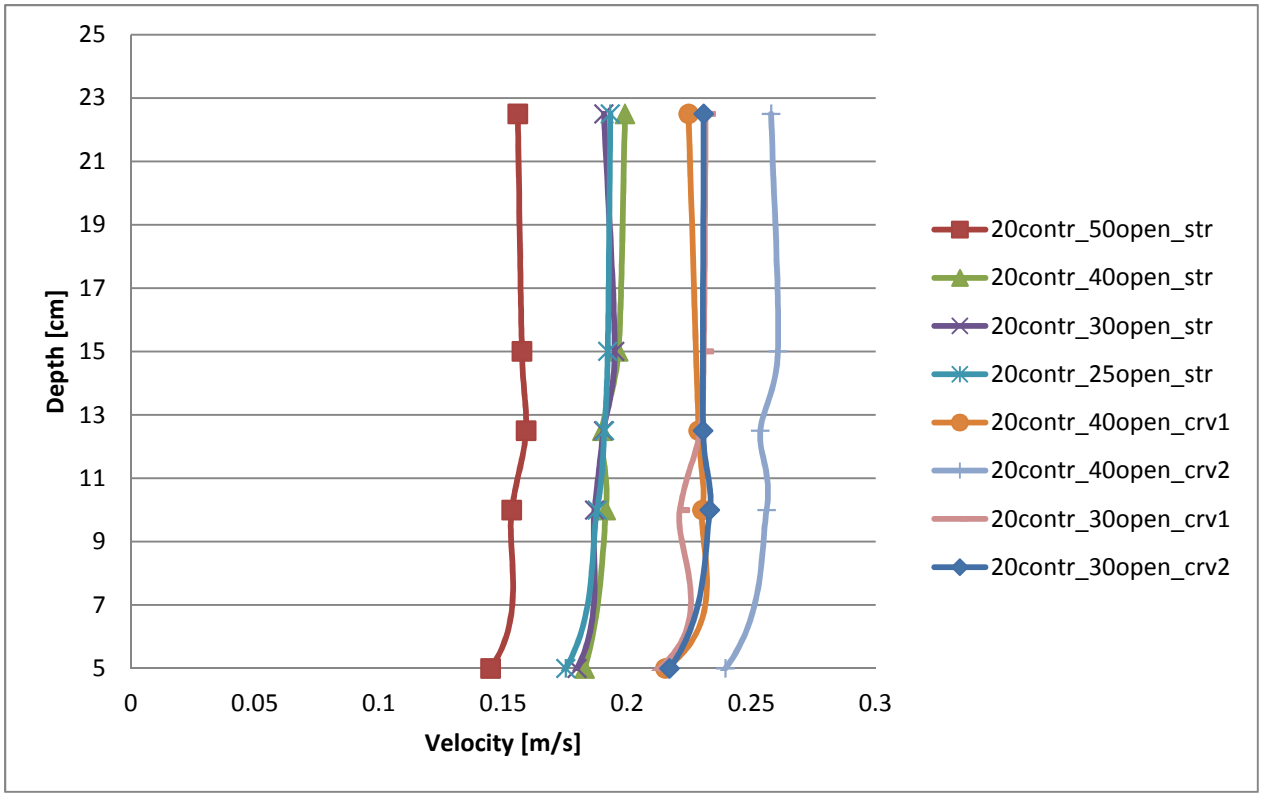

Figure 4-26: Vertical Velocity Profile Structure Centre - 20 cm Wide Contraction Tests

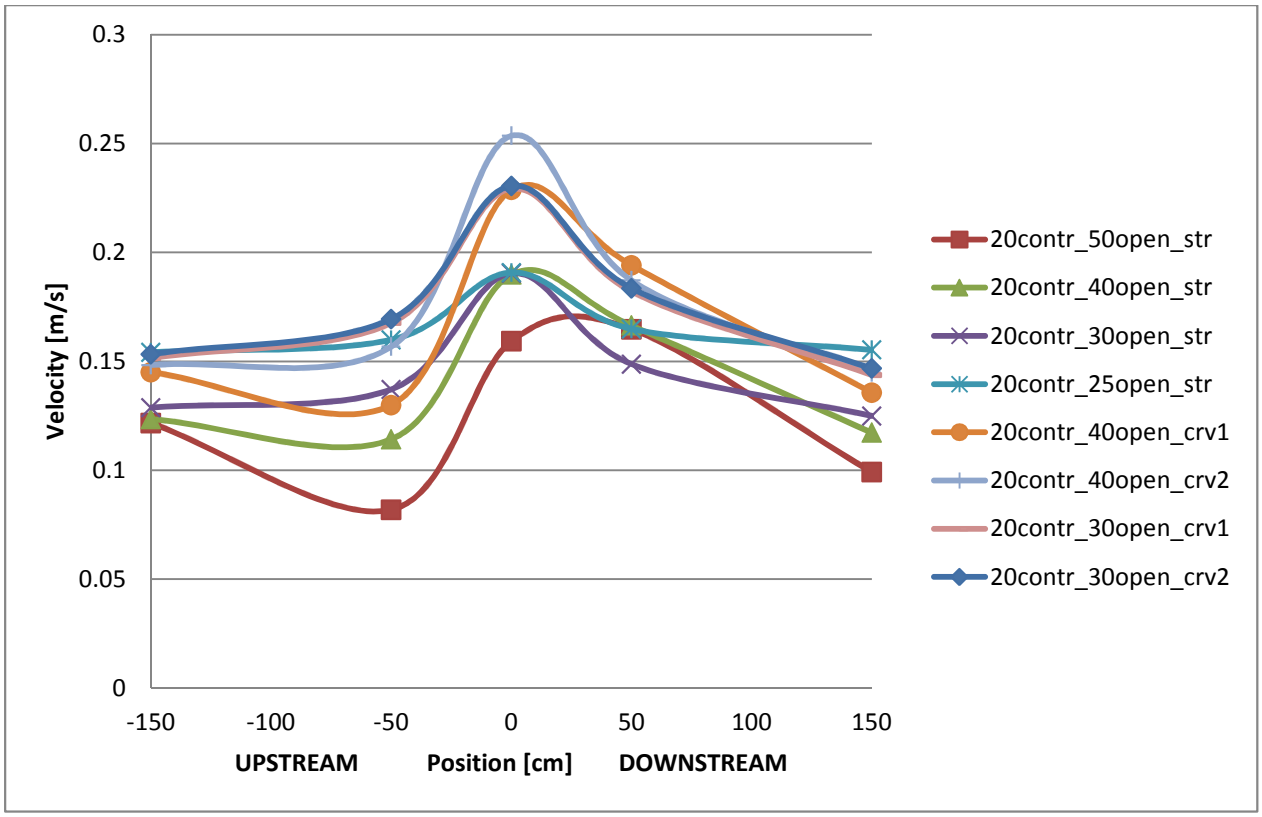

Figure 4-27: Side Longitudinal Velocity Profile - 20 cm Wide Contraction Tests

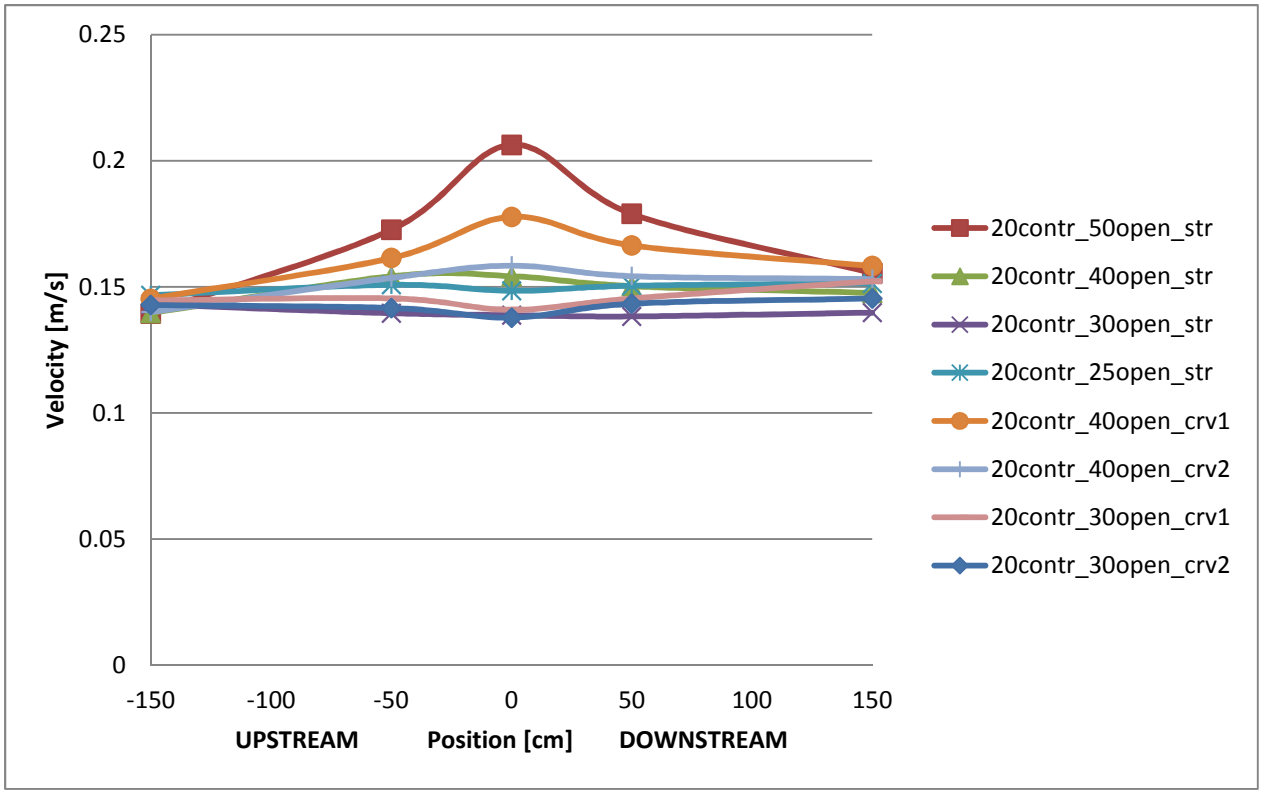

Figure 4-28: Middle Longitudinal Velocity Profile - 20 cm Wide Contraction Tests

The same observations that were made for the 10 cm wide contraction tests apply also for the tests with 15 and 20 cm wide contractions: the configurations with large openings perform poorly and result in increased velocity at the middle of the flume. These effects becomes less pronounced in the tests with 20 cm wide contractions as the increased contraction width allows for larger structure openings without increasing the blockage effect significantly. This is demonstrated by the fact that the test which performed best of the 20 cm wide contraction tests, was '2*0contr_40open_crv2*'. It would seem that the larger the contraction width, the larger the opening width must be to maximise the speed-up through the *TAS* centre.

4.6.1.3 Comparison by Velocity Speed-Up – All Tests

Another way of comparing the performance of the various *TAS* configurations is through a term called the speed-up factor. It is a method of measuring the acceleration of the fluid through the contraction centre based on its upstream velocity. This factor is measured as:

$$Speed - Up\ Factor = \frac{VC_{mean}}{V_{up}} \quad \textbf{(4-7)}$$

Where:

- VC_{mean} is the average velocity at the centre of the *TAS* in between 10 and 22.5 cm above the bed
- V_{up} is the *Side* velocity 2 m upstream of the *TAS*

Figure 4-29 below shows this factor for all Stage 1 tests.

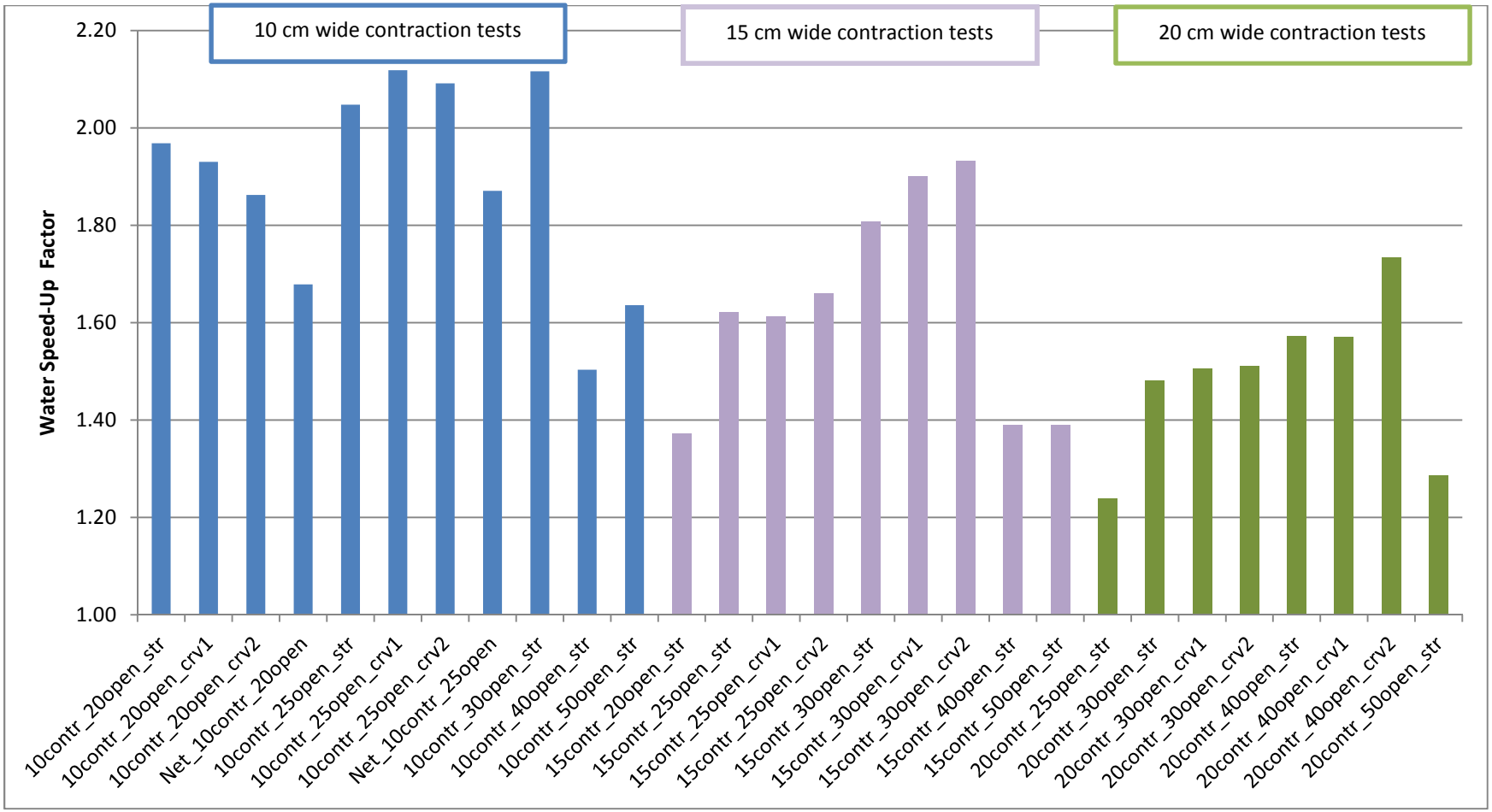

Figure 4-29: Velocity Speed-Up Factor - All Stage I Tests

As shown in Figure 4-29 above, there is a stark difference in water speed-up factors by different structure configurations. The separation of the factors by contraction width using colours highlights the fact that there is an optimal opening width for each contraction width which maximises the speed-up factor. For the 10 cm wide contraction (blue) this is a 25 cm opening, for the 15 cm wide contraction (purple) this is a 30 cm opening and for the 20 cm contraction (green) this is a 40 cm wide opening.

4.6.1.4 Detailed Stage III Recordings - 10 x 25 cm TAS Test Results

As mentioned previously, part of Stage 3 consisted of retesting the straight-walled, 25 cm opening, 10 cm contraction configuration, both without and with the 10 cm wide porous plate. This was done to verify the accuracy and reproducibility of the results from Stages 1 and 2 and also to collect additional points around the structure to create a more in-depth velocity field for use in comparing and calibrating the Fluent numerical model. Though some of the data presented in the following graphs has been presented previously, they serve to show the difference or error that is present between Stage 1 – Stage 3 and Stage 2 – Stage 3. The orientation of these profiles within the flume are shown in Figure 4-12.

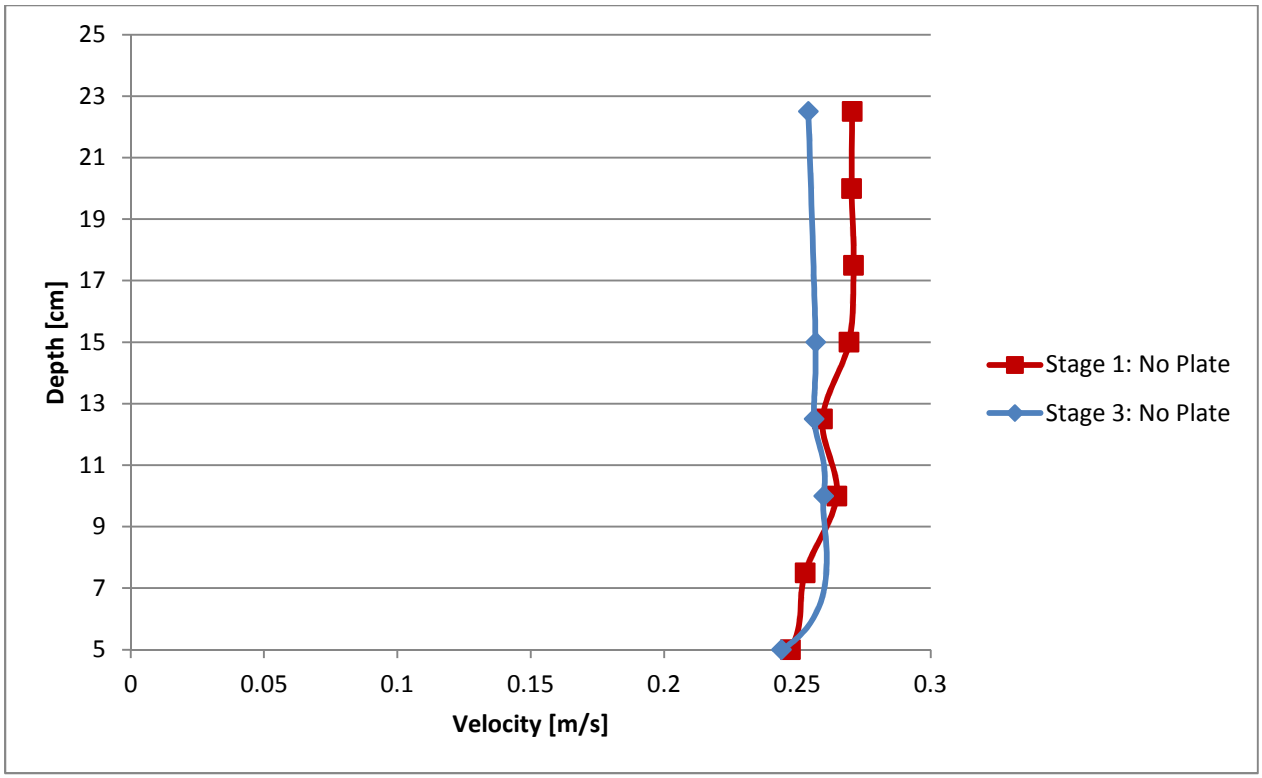

Figure 4-30: Vertical Velocity Profile Structure Centre - Straight Walled 10 x 25 cm *TAS*

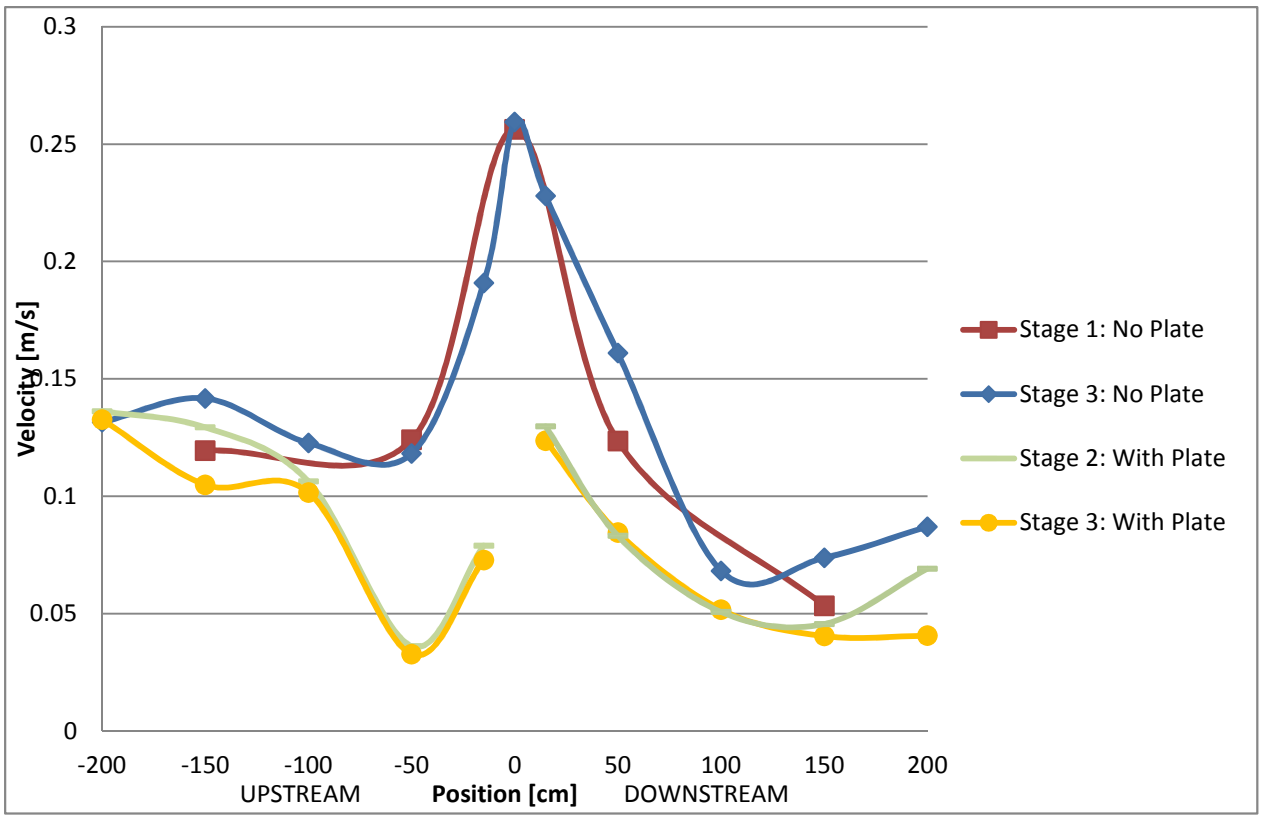

Figure 4-31: Side Longitudinal Velocity Profile - Straight Walled 10 x 25 cm *TAS*

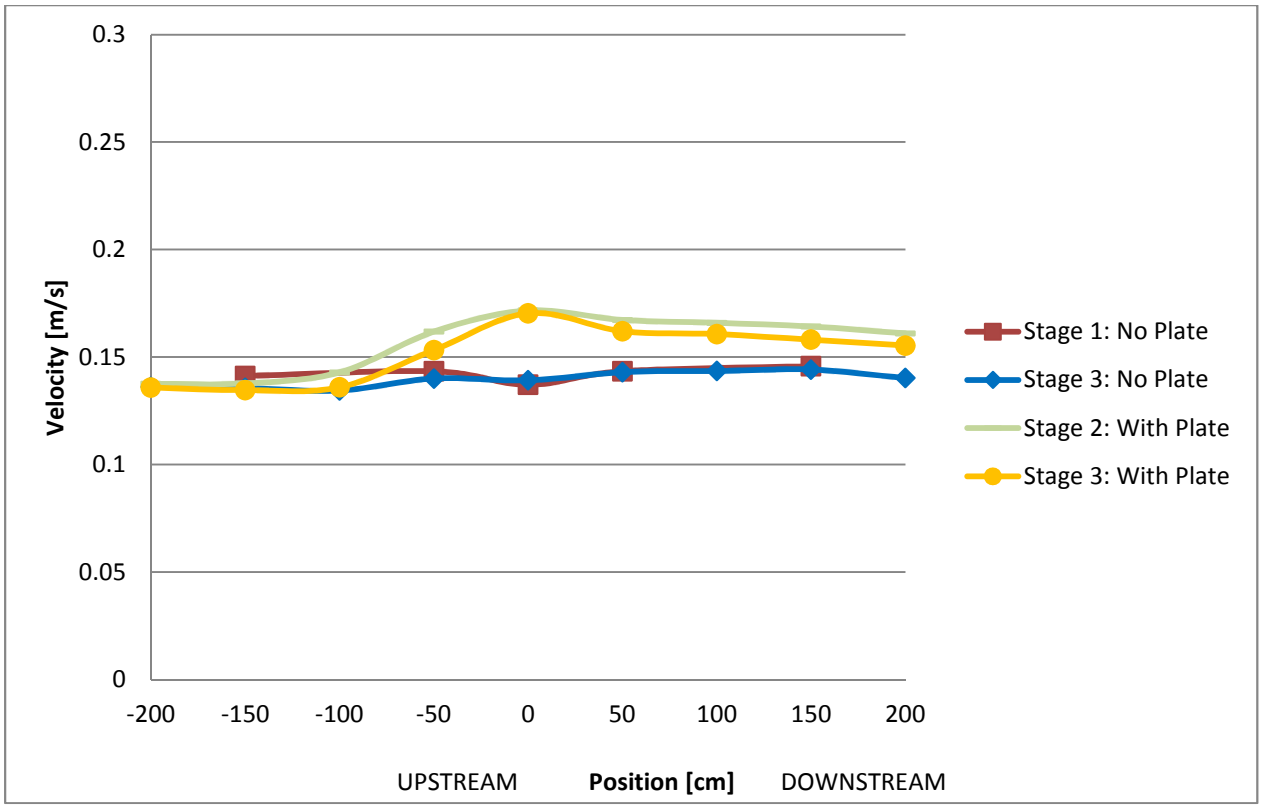

Figure 4-32: Middle Longitudinal Velocity Profile - Straight Walled 10 x 25 cm *TAS*

As one can see in Figure 4-30, Figure 4-31 and Figure 4-32, the results from Stage 3 are very similar to the first tests done in Stages 1 and 2. There are some discrepancies, but the shape and magnitude of flow velocity in the initial tests were reproduced quite well in the Stage 3 tests.

The three following graphs show the additional ADV velocity profiles unique to Stage 3.

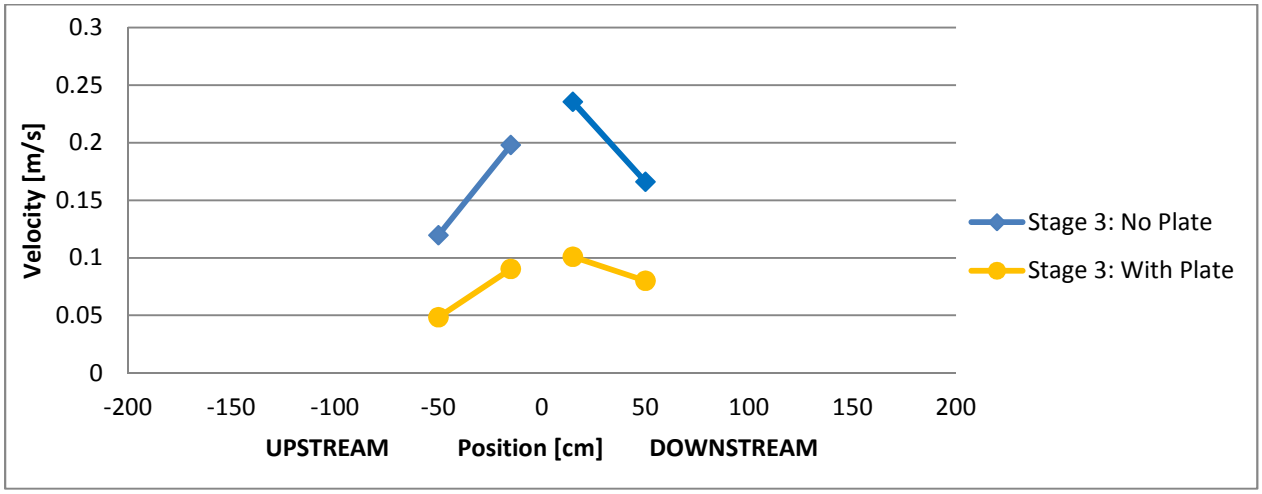

Figure 4-33: ¾ Contraction Width Longitudinal Velocity Profile - Straight Walled 10 x 25 cm *TAS*

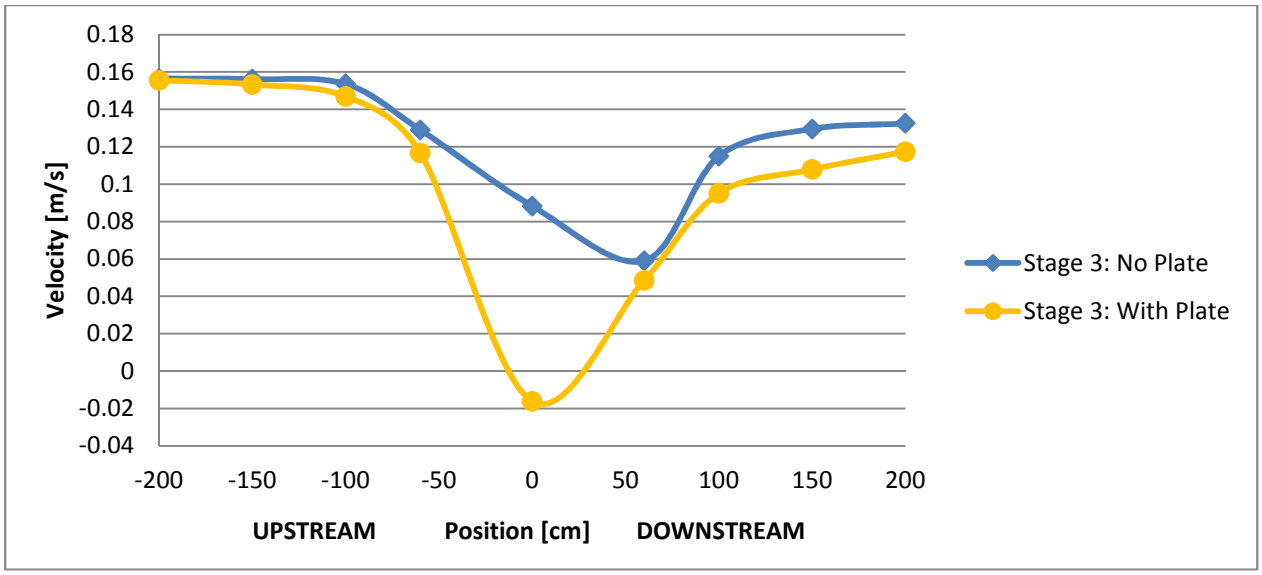

Figure 4-34: Edge Longitudinal Velocity Profile - Straight Walled 10 x 25 cm *TAS*

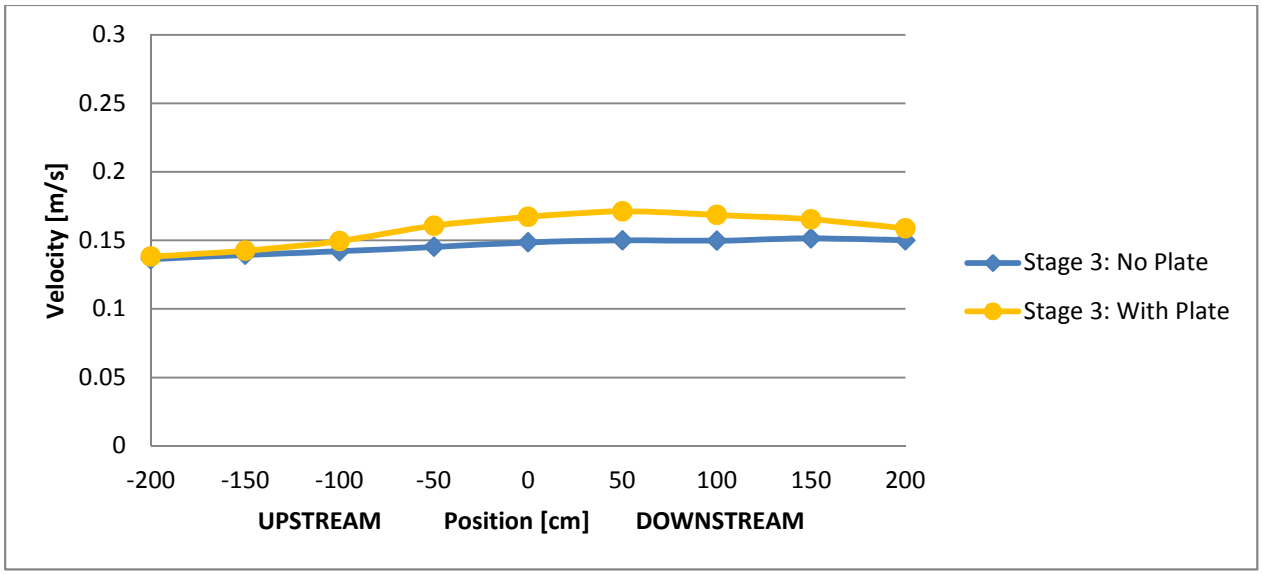

Figure 4-35: Far-Side Longitudinal Velocity Profile - Straight Walled 10 x 25 cm *TAS*

In evaluating the differences between the tests without plates and the corresponding configurations that include a porous plate, it is clear that the presence of the simulated turbine has a significant impact on the flow field surrounding the *TAS*. The blockage effect that the porous plate has on flow through the structure contraction not only decreases the velocity of the flow going through the contraction but also increases the velocity of flow through the rest of the flume as shown in Figure 4-32 and Figure 4-35.

4.6.2 Extracted In-stream Power

4.6.2.1 Velocity through Actuator Discs – 10 x 25 cm TAS Tests

In order to estimate the power extracted by the porous plates using Actuator Disc Theory and Equation **(2-7)**, it is first necessary to estimate the velocity passing through the porous plate, which will be called U_D. This is not the actual velocity passing through the holes in the plate but rather the average velocity passing through the plate section as if the plate were a uniform actuator disc. This value could not be measured physically due to the presence of the plate at the structure centre and the dimensions of the ADV. However, this velocity can be estimated by treating the fluid that passes through the porous plates as being enclosed in a stream-tube with constant flow rate at each cross-section. By estimating the flow-rate upstream, it is possible to estimate U_D. Figure 4-36 below illustrates the variables which were used in this estimation.

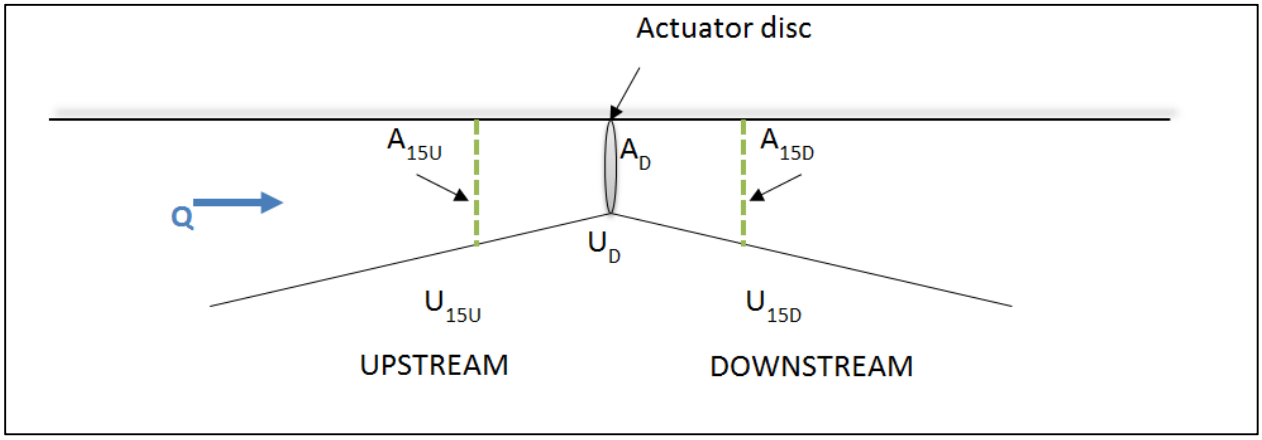

Figure 4-36: Sketch of *TAS* Stream-Tube

With the assumptions that the mass flow rate is the same everywhere along the stream-tube and that the velocity decrease due to the turbulence created by the plate is linear between A_{15U} and A_{15D} (see Figure 2-17), the following equation was created:

$$A_D U_D \rho = \frac{A_{15U} U_{15U} \rho + A_{15D} U_{15D} \rho}{2} \quad \textbf{(4-8)}$$

Where:

- A_D is the area of the disc
- U_D is the velocity through the disc
- ρ is the fluid density
- A_{15U} is the cross-sectional area 15 cm upstream of the disc
- U_{15U} is the velocity 15 cm upstream of the disc
- A_{15D} is the cross-sectional area 15 cm downstream of the disc
- U_{15D} is the velocity 15 cm downstream of the disc

It was observed that the water levels were relatively constant at both locations (verified during experiments using ruler measurements) therefore; the cross-sectional areas can be replaced by the corresponding widths. Subsequently, the above equation becomes:

$$U_D = \frac{W_{15}(U_{15D} + U_{15U})}{2W_D} \quad \textbf{(4-9)}$$

Where:

- W_{15} is the width of opening 15 cm upstream and downstream of the disc (same)
- W_D is the width of the disc

Using the above method, the velocities at the centre of the disc for all tests in Stages 2 and 3 were calculated. The following figure shows a sample result for Stage 2 test '*10contr_25open_str'.*

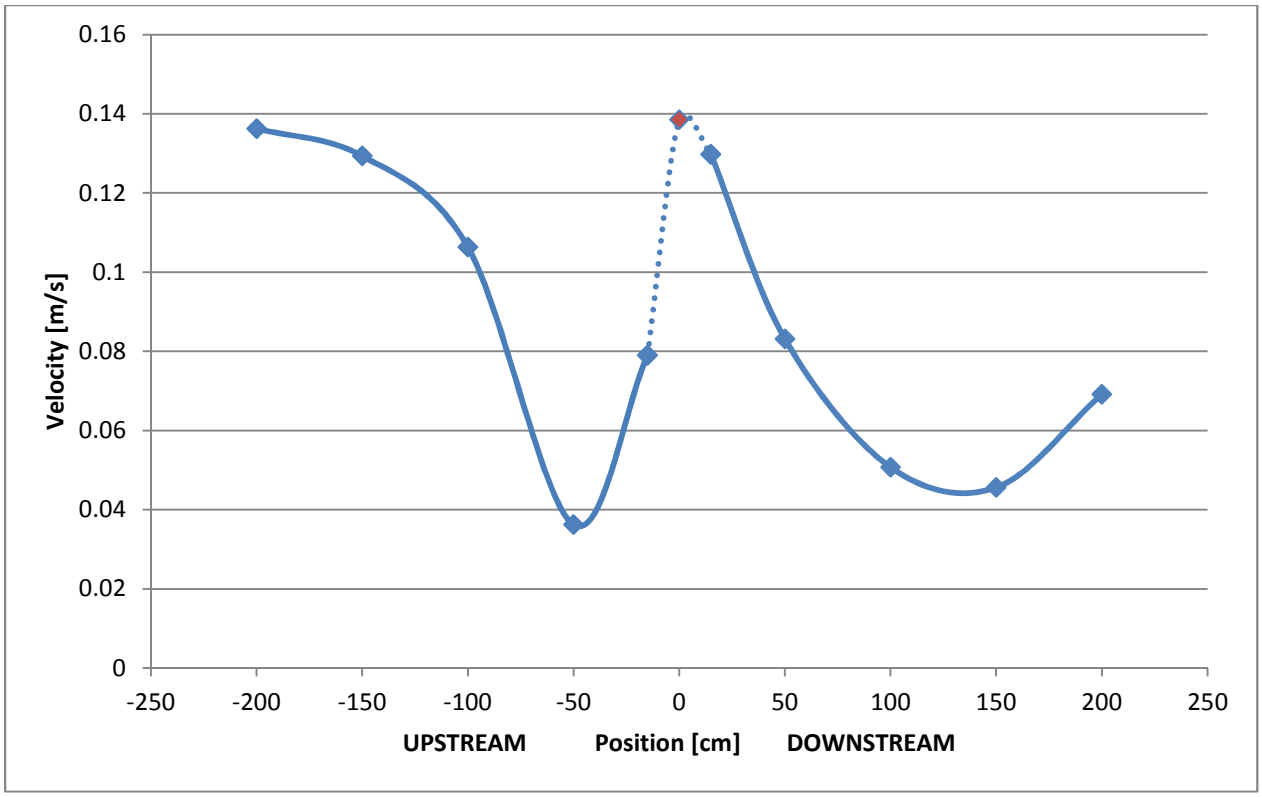

Figure 4-37: Estimated U_D for Stage 2 Test '*10contr_25open_str*'

4.6.2.2 Estimated Power Outputs using Actuator Disc Theory

With the estimated velocities calculated using the methods presented in the preceding section, it is possible to estimate the power extracted by the porous discs using **(**2-7). As mentioned in Section 4.3.2, the force on the porous plates were measured using a load cell connected to the plates via an aluminium shaft which rotated on a pin. The force which was read using the load cell was not the actual force acting on the plate but instead had to be converted using basic engineering mechanics equations and the distance from the pivot point to both the centroid of force on the disc and the load cell. The centroid of force on the disc was calculated for a number of tests and the average value of 17.63 cm above the bed was used for all tests. The calculations are shown in Appendix IV and the following figure shows the summary of forces acting on the load cell – porous plate arrangement.

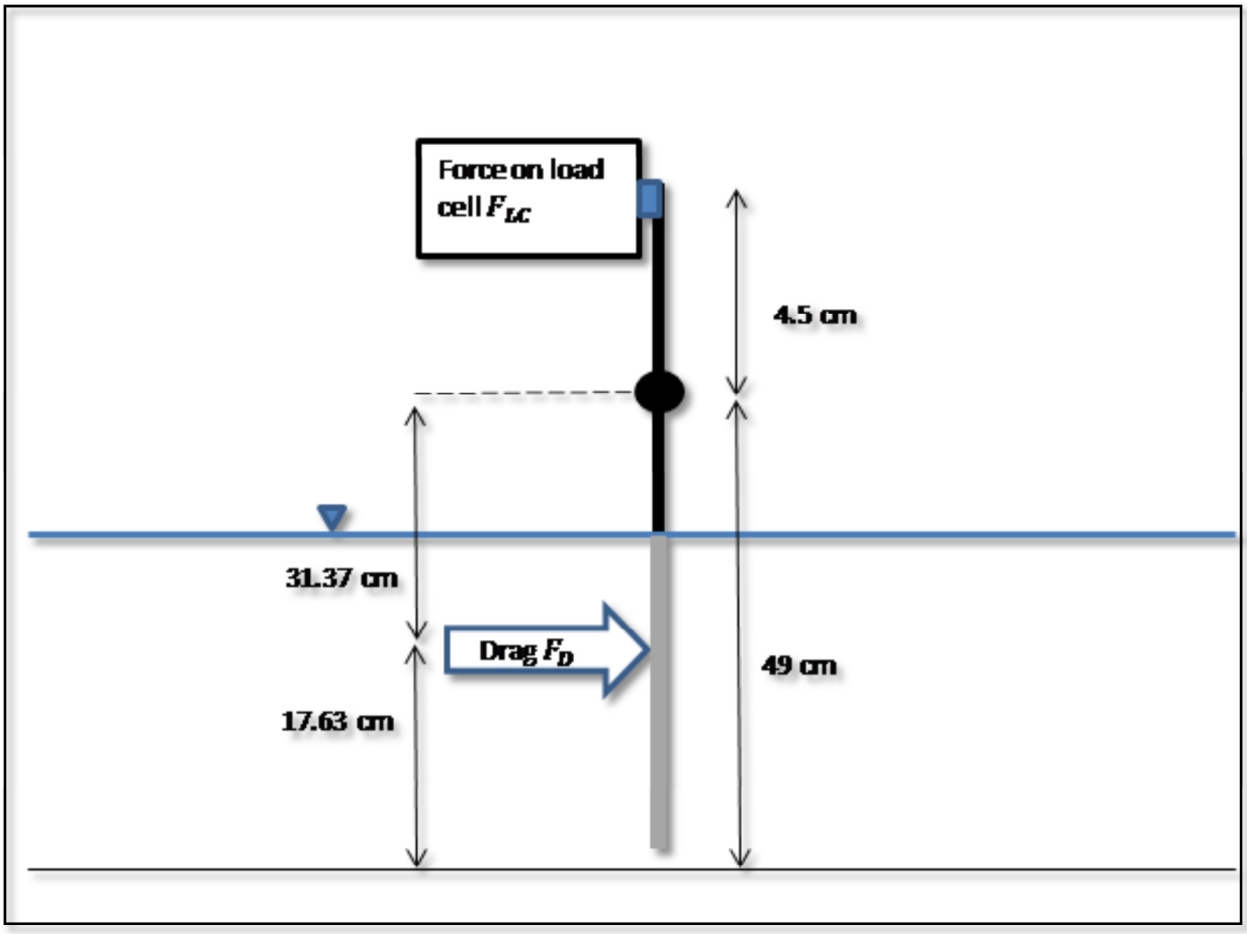

Figure 4-38: Forces on Load Cell – Porous Plate Arrangement

Using the power estimation equation of Actuator Disc Theory **(2-7)** and the figure above, one can create a new power equation:

$$P_{ext} = F_D U_D = (0.1434\, F_{LC}) U_D \qquad \textbf{(4-10)}$$

Where:

- P_{ext} is the power extracted by the actuator disc
- F_D is the drag force acting on the porous plate
- F_{LC} is the force measured by the load cell

- 0.1434 is the factor relating the distance differential between the centroid of the drag force and the load cell from the pivot point

The equation above measures the extracted power however it is also interesting to speculate on the potential power created by the *TAS* configurations. The relationship between the extracted and potential power can be related by the power efficiency or C_p value which is presented in the following equation.

$$C_p = \frac{P_{ext}}{\frac{1}{2}\rho U_\infty^3 A_D} \quad \textbf{(4-11)}$$

Where:

- P_{ext} is the power extracted by the actuator disc
- ρ is the fluid density
- U_∞ is the velocity far upstream of the disc in Actuator Disc Theory but is taken to be the velocity at the centre of the structure for the corresponding test of Stage 1 as it's the undisturbed or unblocked flow velocity
- A_D is the cross-sectional area of the *TAS* contraction

Using the above equation, the power outputs were calculated for all relevant Stage 2 and 3 tests and are presented in the following table.

Table 4-7: Power Estimates

Test	F [N]	Estimated U_D [m/s]	Extracted Power [mW]	U_∞ [m/s]	A_D [m^2]	Power Available in Flow [mW]	C_P [-]
10contr_20open	1.963	0.1293	42.52	0.2547	0.03	247.30	0.1719
10contr_20open_crv1	2.392	0.1276	42.49	0.2447	0.03	219.49	0.1936
10contr_20open_crv2	2.541	0.1363	48.79	0.2407	0.03	208.71	0.2338

10contr_25open	2.565	0.1385	59.95	0.2563	0.03	252.07	0.2378
10contr_25open_crv1	2.354	0.1263	40.25	0.2632	0.03	273.14	0.1474
10contr_25open_crv2	2.736	0.1368	51.13	0.2714	0.03	299.28	0.1709
15contr_25open	3.077	0.1314	66.53	0.2374	0.045	300.64	0.2213
15contr_25open_crv1	3.865	0.1341	74.35	0.2303	0.045	274.40	0.2709
15contr_25open_crv2	3.594	0.1304	64.50	0.2368	0.045	298.16	0.2163
15contr_30open	3.167	0.1295	56.43	0.2255	0.045	257.61	0.2191
15contr_30open_crv1	2.778	0.1416	56.40	0.2695	0.045	439.65	0.1283
15contr_30open_crv2	3.143	0.1386	58.81	0.2639	0.045	412.78	0.1425
20contr_30open	5.064	0.1271	86.81	0.1904	0.06	206.73	0.4199
20contr_30open_crv1	5.074	0.1326	89.88	0.2293	0.06	360.94	0.2490
20contr_30open_crv2	5.758	0.1330	105.68	0.2305	0.06	366.93	0.2880
20contr_40open	4.962	0.1418	97.67	0.1899	0.06	204.92	0.4766
20contr_40open_crv1	5.192	0.1444	100.94	0.2287	0.06	358.34	0.2817
20contr_40open_crv2	5.544	0.1484	113.07	0.2535	0.06	488.01	0.2317
10 cm plate: 17p5contr_35open	3.253	0.1605	71.75	0.2111	0.03	140.82	0.5095
Stage 3: 10contr_25open	2.226	0.1305	39.02	0.2594	0.03	261.33	0.1493
JUST 10 cm wide disc	1.629	0.0798[1]	17.21	0.1321[2]	0.03	34.55	0.4981
JUST 15 cm wide disc	2.053	0.0870[1]	23.99	0.1456[2]	0.045	69.37	0.3458
JUST 20 cm wide disc	3.402	0.0930[1]	41.90	0.1516[2]	0.06	104.30	0.4018

Notes:

1. [1] U_D was taken as the average of U_{15U} and U_{15D}
2. [2] Velocity 2 m upstream of structure centre was taken for U_∞ because there is no *TAS* speed-up

By observing the C_p values in the table above, one can note that the efficiency of the porous plates in capturing the power available for each *TAS* configuration was quite low. This was to be expected as the estimated velocity through the disc values (U_D) were quite low compared to the velocities observed through the centre of the configurations in Stage 1. These low U_D values were most likely due to the high blockage effect the plates had on flow. With the solid material of the plate being present in the *TAS* contraction, the effective contraction width of the configurations were drastically reduced and therefore a larger percentage of flow was forced to circumvent the structure. Despite the low C_p values, the best tests were able to extract 3.5 (10 cm wide plate), 3.1 (15 cm wide plate) and 2.7 times (20 cm wide plate) more power than their stand-alone plate equivalents. To investigate whether the porosity of the plates, or the percent of open to solid area in the contraction width, could have been the issue causing the low C_p values, an additional test was run with the 10 cm wide porous plate being placed in a larger contraction width. The 10 cm plate was placed in a 17.5 cm wide contraction with a 35 cm opening (straight-walled *TAS*). These dimensions were chosen from a quick trial and error process, modifying the *TAS* opening and contraction width, with the force on the load cell as the optimisation criteria. Due to time constraints, this method of optimisation could not be performed in depth therefore the 10 cm plate – 17.5 cm contraction with 35 cm opening should not be considered as a fully optimised design. The test was able to extract 4.2 times more power than the stand-alone 10 cm wide plate, a significant increase from the best test in which the 10 cm wide plate occupied the entire width of the contraction. The higher C_p value associated with this test demonstrates that the porous plates either should have had a higher porosity or the structure configurations should have been optimised in conjunction with the plates. The power values shown above in Table 4-7 are also shown below in Figure 4-39 to illustrate the differences between extracted power and power available in the flow.

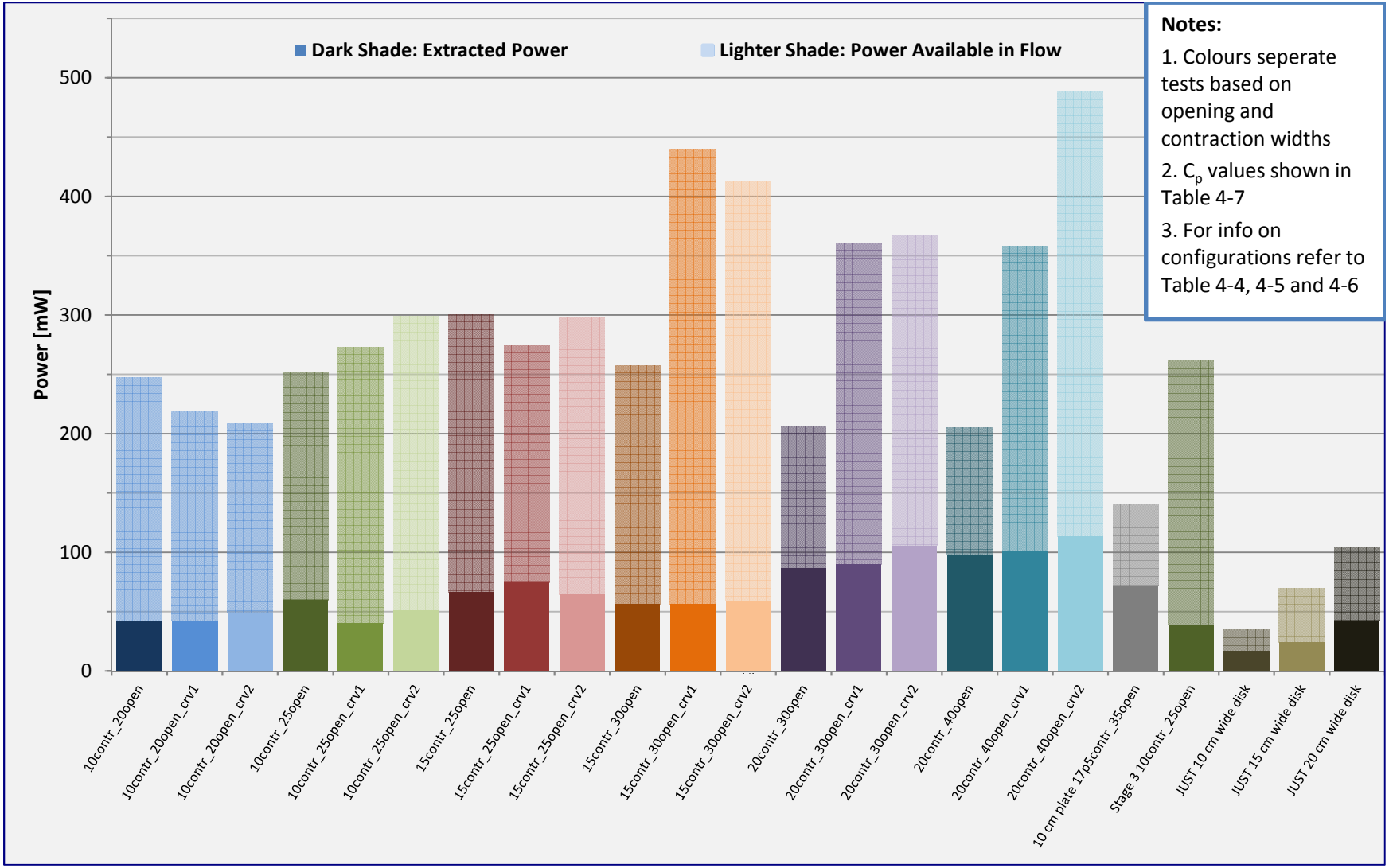

Figure 4-39: Power Extracted by the Porous Plates vs. Power Available in Flow

Figure 4-39 above clearly shows the limited efficiency of the *TAS* – Plate combination in extracting power from the flow-stream as compared to the plates on their own. Though the power extracted by the *TAS* - Plate combination always extracted more power than the corresponding plate just used on its own, the plate porosity value used with the *TAS* was probably not optimal. This is demonstrated by the fact that the *TAS* – Plate combination which performed best (in terms of C_p) was the test with a 10 cm wide plate and a 17.5 cm contraction – 30 cm opening. Though this combination performed better it is foreseeable that plates with higher porosity would have performed equally well as the blockage effect on flow through the contraction would have been lower as well.

4.7. Discussion

In this chapter, the physical modeling results for the simulation of the Tidal Acceleration Structure were presented. The main goals included the optimisation of the *TAS* shape, the observation of the velocity field around the *TAS* in the 1.5 m wide flume and the simulation of a turbine inside the *TAS* using a porous plate and Actuator Disc Theory.

In regards to optimising the *TAS* to maximise the acceleration of fluid velocity, a total of 26 structure configurations were tested and their results compared. It was found that for the specific flow conditions which were chosen (1 m/s in-stream flow and 15 m depth at full-scale) the variation of structure opening and contraction widths, as well as wall curvature, can drastically alter the performance of the *TAS*. Though it is somewhat insignificant to compare structure setups with different contraction widths, as this would directly impact the size or number of turbines in a prototype (hence cost), it was found that the 10 cm contraction x 25 cm openings structure configurations were able to increase flow velocity the most (see Figure 4-29).

In Stage 2, a total of 15 of the best performing structure configurations from Stage 1 were re-tested in conjunction with porous plates in the hopes of measuring the change to the velocity field as well as to

estimate the power extracted by the plates. Additionally, the three plates were tested on their own to find a baseline for power extraction. The tests were successful in measuring the change to the velocity field and estimates for power extracted by the plates and potential power through the *TAS* contraction were both found. Despite this, the 58% porosity plates seemed ineffective in extracting energy from the velocity field as they blocked the flow through the *TAS* too significantly. This was reflected by the low C_p values of the *TAS* – Plates combination tests when compared to simply the plates on their own (see Figure 4-39). An additional test, the 10 cm plate with a structure contraction of 17.5 cm and openings of 35 cm, reinforced the theory that the *TAS* configurations from Stage 1 would have performed better, and extracted more energy from flow, if the porosity of the plates had been higher.

Stage 3 consisted of re-testing the 10 cm contraction width x 25 cm openings structure configuration with and without the 10 cm wide plate for the purposes of verifying the results of the preceding stages and also to collect additional data points which could be compared with the Fluent numerical model. The results from these two Stage 3 tests corresponded well with those from Stages 1 and 2 (see Figures Figure 4-30, Figure 4-31 and Figure 4-32), which was a significant first step in showing that the test results are reproducible. The estimated extracted power values from the Stage 3 and corresponding Stage 2 tests also agreed quite well (see Figure 4-39) considering it was the first time the testing methodology had been employed in conjunction with an augmentation structure such as the *TAS*.

Potential sources of error in the physical modeling of the *TAS* and the subsequent data analysis include the following.

- **Temporary changes in flow velocity due to inconsistencies with the flume pump.** It was realised during the latter stages of testing that the pump pressure dropped if another flume in the hydraulics lab was turned on at the same time. This could explain some of the inconsistencies in the velocity profiles.

- **Changes in structure or testing setup parameters during a test.** Though improbable, it is possible that the structure parameters were altered during the course of a test, either by someone in the lab during a brief absence by the testing team or due to the natural movement of the structure walls due to the flow. There were often undergraduate Fluid Mechanics laboratory sessions occurring at the same time as the testing and it is conceivable that a student may have moved an instrument, such as an ADV, without the testing team realising.
- **Changes in wall shape from one test to the next.** As explained earlier, the wall curvature was implemented by heating and bending the plywood pieces. It is possible that some of the curvature was lost from one test to the next due to bounce-back in the wood. The slight change in curvature could have resulted in changes to the velocity field and or extracted power values. A more accurate bending technique or different wall type could have eliminated this risk however it would have greatly increased the cost of the testing and construction time.
- **Changes to the velocity field due to the presence of the ADV.** Though the ADV is a relatively small instrument, the presence of the ADV within the contraction of the *TAS* most likely had an impact on the flow field as its cross-section is not negligible compared to the contraction. This would have been particularly important for the 10 cm wide contraction tests as it would have represented a larger percentage of the total cross-section. This could explain some of the odd shaped vertical velocity profiles.
- **Error in the velocity field caused by the wall being used as a symmetry plane.** Though the use of one of the walls as a symmetry plane was necessary to simulate the *TAS* at 1:50 scale, there was a reduction in the velocity magnitudes near the wall due to the shear effects of the wall. This was accounted for in the Speed-Up factor calculations (see Figure 4-29) as the factor was the relationship between the velocity upstream of the *TAS* along the wall and the velocity at the contraction however, there was likely some effects to the results that were not corrected. These

could potentially be analysed in a future experimental project with both sides of the *TAS* structure simulated in a 3 m wide flume.

- **Errors in the estimation of U_D.** The velocity passing through the plates was estimated as assiduously as possible but would have been more accurate if measured with a more advanced velocity measurement system or if the ADV could have been placed closer to the plate. ADV velocity measurements were taken 15 cm upstream and downstream of the plates in order to estimate U_D however they could not be placed any closer due to physical restrictions. It may have also been beneficial to take more ADV readings close to the plates in the horizontal direction however, this was not possible as the ADV itself was approximately 5 cm wide.

4.8. Conclusions

In conclusion, most of the stated goals of the experimental testing of the *TAS* were accomplished, including:

- Successful simulation of a 1:50 scale Tidal Acceleration Structure in a 1.5 m wide flume using a versatile, easy-to-use and low-cost setup.
- Logging and analysis of the flow-field surrounding different *TAS* configurations including water speed-up at the centre of the structure and change to velocity profiles surrounding the structure. By comparing these speed-up factors, it was concluded that some structure configurations are much more effective in accelerating the flow through the *TAS*. This, along with the increased velocity magnitudes found at the centre of the flume in tests with lower speed-up factors also helped to establish the theory that the blockage effect which the structure has on flow is extremely important for structure performance. With too little blockage, the *TAS* does not capture enough upstream flow but with too much blockage the upstream flow slows down significantly and cannot recover once inside the *TAS* Venturi section.
- Successful estimation of the power extracted by porous discs meant to represent turbines placed at the centre of the *TAS* using Actuator Disc Theory and successful estimation of the power present in the flow passing through the *TAS* without the presence of porous plates. The results of these estimations exposed the ineffectiveness of the porous plates in capturing the energy present in the flow. Through analysis it was determined that this was probably due to the porosity of the plates (58%) which was too low and caused too high a level of blockage on flow. This was reinforced by the results from a test using the 10 cm wide plate with a 17.5 cm contraction and 35 cm opening. This test was able to capture much more power than other tests and had a higher C_p value which was attributed to there being more percent open-area in the contraction with space on either side of the plate, thus reducing blockage on upstream flow and increasing incoming flow velocity.

Overall, though there were some issues with the testing methodology that should be corrected in future tests, the 1:50 scale physical modeling of the *TAS* in the 1.5 m wide flume at the University of Ottawa should be considered a success.

Chapter 5. Numerical Modeling of the *TAS*

5.1. Introduction

The numerical modeling of the Tidal Acceleration Structure, alongside the physical modeling, was a primary goal of the research project. Though there are limits to the accuracy that can be attained with using CFD models to validate fluid problems, many programs exist which can help estimate fluid interactions with a reasonable degree of certainty. The accuracy of 2D and 3D fluid simulations can be program dependent but often proper meshing, and parameters such as roughness, boundary conditions and turbulence models can be the biggest factors to the success of the simulation in reproducing accurate flow interactions. The main benefit of simulating the *TAS* with a 3D numerical model was that a validated numerical could then be used for future simulations of the *TAS* at full scale. The secondary objective was to find out to what extent a numerical model can represent observed data and replace the need for the physical model in design applications. The initial 3D numerical efforts focused on calibrating a 1:50 scale model to the equivalent physical scale results. ANSYS Fluent was chosen as the 3D CFD software because of its versatility, easy to use graphic user interface and its vast variety of included models. In this chapter, an initial numerical modeling effort using the 2D software HEMAT is presented also as it was the first step in testing the *TAS*. The 3D Fluent results are subsequently analysed in detail and compared with the physical results of Chapter 4.

5.2. 2D Modeling using Hemat

The first program group which was used to test the *TAS* was the Hemat2D software. This software was created by Dr. Mohammadian of the University of Ottawa, a supervisor of the project, therefore direct knowledge of the functions used by the programs and troubleshooting advice was readily available to assure a successful simulation process. The Hemat2D program group was a good test starting point for the *TAS* because as a 2D simulation software, the computational cost was relatively low compared to 3D

simulations. Trial simulations could be done quickly, allowing for the sensitivity analysis of many simulation and structure parameters. In the following sections, the governing equations used by the Hemat2D solver program will be discussed to justify the use of the software for the testing of the tidal structure. The methodology of testing will be explored and subsequently a detailed analysis of the Hemat2D simulation findings for the disclosed tidal concept will be presented.

5.2.1 Model Description and Theoretical Background

The 2D Hemat computational fluid dynamics software was created by Drs. Mohammadian and Le Roux and was based primarily on two papers which they published (Mohammadian et al. 2005; Mohammadian and Le Roux 2006). The model uses the shallow water equations and a key improvement of their model over existing models was the utilisation of Roe's scheme with the surface gradient method as presented by (Zhou et al. 2001). Though originally developed for unstructured grids over non-constant topographies, it was thought that the scenario of the *TAS* could also be handled well by Hemat2D as it is non-complex in terms of geometry and inlet flow conditions.

In the hopes of validating the Hemat2D numerical model, (Kheradmand et al. 2015) performed a comparison of how Hemat2D simulated a real shallow flow area to data collected in the field. The location which they chose was Mooney's Bay, a popular beach area located in Ottawa, Canada on the Rideau River. The parameters which the authors wished to compare were the velocity field and topography in the bay. The field data was collected by boat with an ADCP, the boat criss-crossing the bay in the path shown in Figure 5-1 below.

Figure 5-1: Path Taken by Boat Equipped with ADCP (Kheradmand et al. 2015)

Using the field data gathered from the ADCP and an interpolation scheme, the authors were able to construct a complete picture of the bay topography. The interpolation method is explained in further detail in the referenced paper (Mohammadian and Le Roux 2006) and the results are shown in Figure 5-2. The field velocity collected was used as the initial upstream boundary condition and the downstream topography as the other boundary condition. For the meshing in MeshGenerator (the meshing program of Hemat2D) a variable size grid was used with more precision given for the regions of constrained flow or higher velocity. The simulation was initially defined to have constant water surface elevation and zero velocity and then the Hemat2D simulation was run until a steady state condition was reached.

A sensitivity analysis was conducted by the authors to see the impact of using a larger or smaller grid. This analysis was able to find the point at which a more refined grid did not alter simulation results and then this grid size was retained. Sensitivity analyses were also conducted for bottom roughness and eddy viscosity coefficients which can both be modified within Hemat2D. They found that the model in

the case of Mooney's bay was not overly sensitive to the eddy viscosity parameter within a range of 10^{-5} to 10^{-3} m^2/s, which is the typical range in such cases. The sensitivity analysis of Manning's bottom roughness was found to be more important as alterations of the roughness could have quite significant impacts on flow conditions. To try and match the simulation and field results, the authors decreased the roughness in bay areas of underestimation of flow velocity (thus increasing velocity) and increased the roughness in areas of overestimation. This was done within a reasonable range and was found to produce good results. Figure 5-2 below shows the Mooney's Bay topography and the velocity field found from Hemat2D.

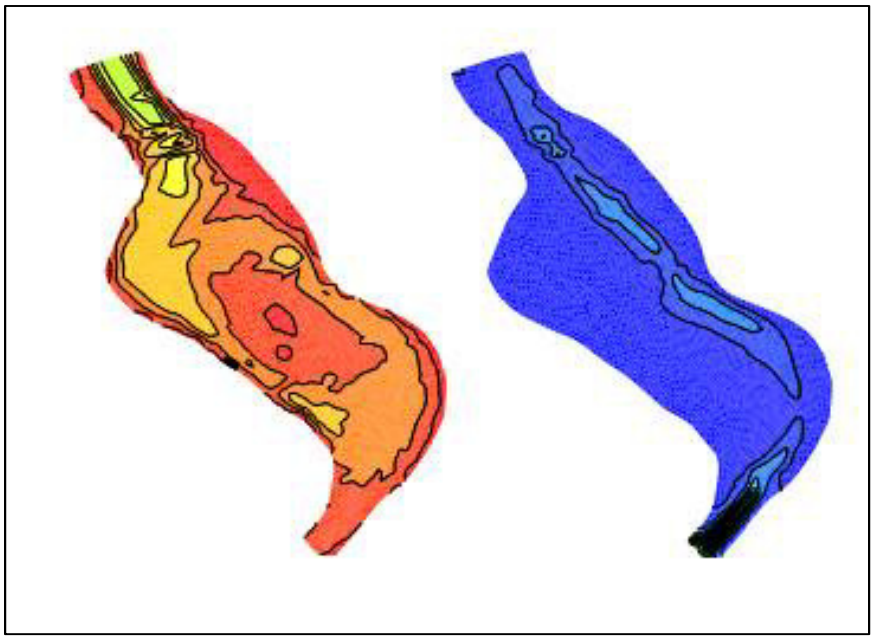

Figure 5-2: Contours of Topography and Hemat2D Simulated Velocity (Kheradmand et al. 2015)

From a comparison of the simulated and observed results concerning the velocity field within Mooney's Bay, the authors were able to conclude that Hemat2D is capable of accurately reproducing flow within shallow water areas if the right boundary and initial conditions are used. Though the above validation was performed for a river, coastal tidal regions are no more complicated in terms of topography and flow conditions thus implementation was thought to be similar. The use of Hemat2D for testing the Tidal Acceleration Structure was therefore expected to be positive.

The shallow water equations given in their conservative form as used in Hemat 2D are as follows (Mohammadian and Le Roux 2006):

$$\frac{\partial \vec{U}}{\partial t} + \nabla \vec{F} = \vec{S} + \nabla \vec{F}^{\,d} \qquad \textbf{(5-1)}$$

Where:

- $\vec{U}^t = (h, uh, vh)$
- $\vec{F} = (\vec{E}, \vec{G})$

and E and G are flux vectors described by,

$$\vec{E} = \begin{pmatrix} uh \\ u^2 h + 0.5\, gh^2 \\ uvh \end{pmatrix} \quad , \quad \vec{G} = \begin{pmatrix} vh \\ uvh \\ v^2 h + 0.5\, gh^2 \end{pmatrix} \qquad \textbf{(5-2)}$$

Where:

- *h* is the water depth
- *g* is the gravitational acceleration
- *u* and *v* are velocity components

The physical interaction of the elements is described by:

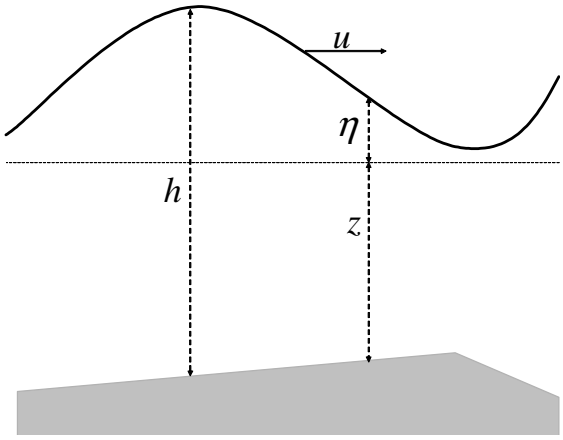

Figure 5-3: Variables in Shallow Water Flow over Irregular Topography (Mohammadian and Le Roux 2006)

Also, the equation for diffusive flux in which the superscript ^{d} refers to the diffusion is as follows:

$$\vec{F}^{d} = (\vec{E}^{d}, \vec{G}^{d}) \tag{5-3}$$

For which:

$$\vec{E}^{d} = \begin{pmatrix} 0 \\ (\nu + \nu_t) h \partial u / \partial x \\ (\nu + \nu_t) h \partial v / \partial x \end{pmatrix} \quad , \quad \vec{G}^{d} = \begin{pmatrix} 0 \\ (\nu + \nu_t) h \partial u / \partial y \\ (\nu + \nu_t) h \partial v / \partial y \end{pmatrix} \tag{5-4}$$

Where:

- ν and ν_t are the water and eddy coefficients respectively

The source term $\vec{S}$ is:

$$\vec{S} = \begin{pmatrix} 0 \\ c_f u \sqrt{u^2 + v^2} + gh \partial z \ / \partial x \\ c_f \nu \sqrt{u^2 + v^2} + gh \partial z \ / \partial y \end{pmatrix} \tag{5-5}$$

Where:

- Z is the distance between the bed surface and the reference level (see Figure 5-3)
- c_f is the friction coefficient based on the Manning or Chézy coefficients

For reference to the non-conservative form of the shallow water equations, the numerical scheme and other model specifications for Hemat2D please see (Mohammadian and Le Roux 2006).

5.2.2 Methodology

As discussed earlier, the raison-d'être of the Tidal Acceleration Structure is to accelerate tidal or river currents by exploiting the Venturi effect. To evaluate the effectiveness of the concept at a preliminary level, the initial testing objective using the Hemat2D software was to find the flow acceleration that the structure induces. This acceleration is quantified using the *Acceleration Ratio* as described below:

$$Acceleration\ Ratio = \frac{Maximum\ Velocity\ at\ Centre\ of\ Structure\ (\frac{m}{s})}{Mean\ Incoming\ Current\ Velocity(\frac{m}{s})} \quad \textbf{(5-6)}$$

Where:

- The *Acceleration Ratio* (*AR*) is analogous to the *Speed-Up Factor* as described in Equation **(4-7)**

Though the above relation does not fully describe the benefits of the *TAS* design, as the structure was thought as also being capable of reducing flow turbulence, it was chosen as the main optimization goal for the Hemat2D testing for its simplicity both in measuring and optimizing. The main method which was used during the 2D numerical test runs was to change one parameter of the *TAS* at a time and observe the impact it had on the *Acceleration Ratio* (*AR*). The different *AR*s were plotted for each parameter and the one yielding the largest was chosen to use moving forward for testing subsequent parameters. Though this method was somewhat flawed because the parameters are interdependent, the testing methodology was still able to yield a more optimised structure design in terms of its *AR* than that of the original. Because the amount of parameters which could influence the *TAS* performance are numerous there were some that were not explored during the initial Hemat2D testing due to the high computational costs which would have been incurred. The parameters which were thought to be most important in terms of their effect on the *AR* were given priority and their testing forms the base of the 2D optimised *TAS* design. The parameters tested and whose results will be presented are: simulation pad area, length-width ratio, inflow factor, structural scale and contraction ratio.

With the testing goals established, the above parameters were tested using the two Hemat2D programs *MeshGenerator* and *SolverGUI* along with a third commercial software *Tecplot*. The initial program used was *MeshGenerator* and in it the boundaries were delineated, their type specified and subsequently a grid of appropriate size generated. The general setup of the *TAS* and the boundary conditions as used in the Hemat2D software are depicted in the plan view below.

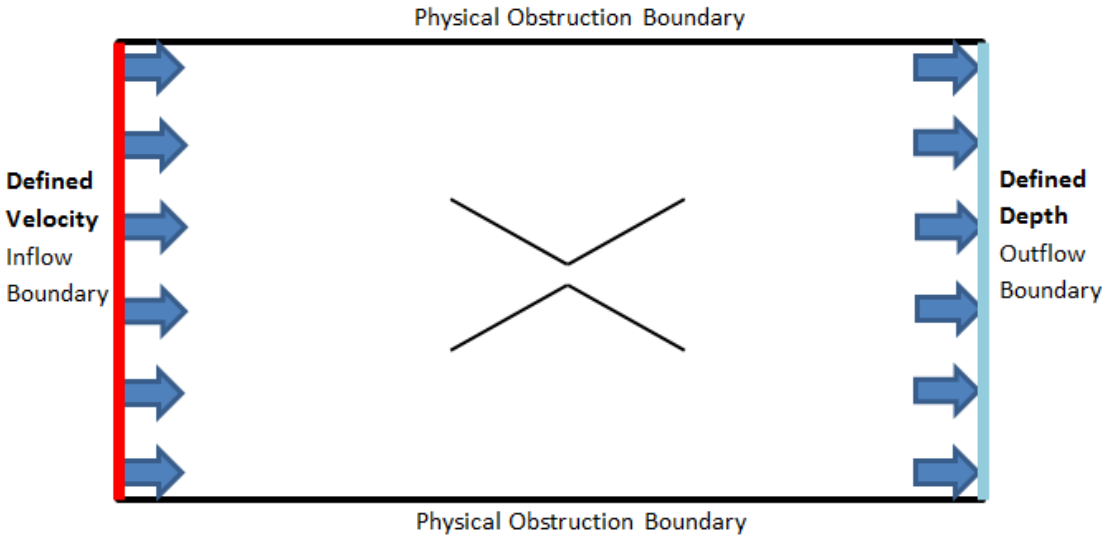

Figure 5-4: Boundary conditions used in the Hemat2D testing of the *TAS* – Plan View

After the boundary conditions were specified as shown in Figure 5-4 above, the *MeshGenerator* program was used to generate a grid for which the numerical computations would subsequently be done. Because of the higher velocities and greater turbulence that the *TAS* creates in its vicinity, a finer mesh was created around the structure as shown below.

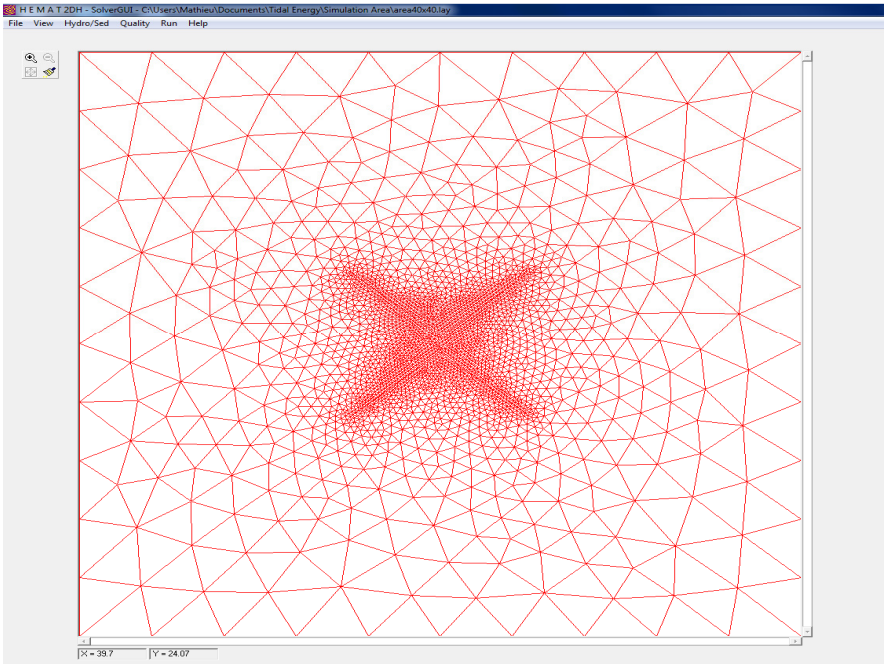

Figure 5-5: Sample Mesh grid as created in MeshGenerator and the General Interface of SolverGUI

This mesh was then imported into *SolverGUI* as in Figure 5-5 above so that the initial simulation conditions could be established. These included bed level, water surface level, initial flow velocity, bottom Roughness and eddy viscosity. A bottom roughness factor of 0.03 (corresponding to a sandy-cobble bottom) and eddy viscosity of 0.1 were used for all simulation runs. Simulation boundary conditions and various setup parameters were also specified in the second program *SolverGUI*. The program was then run with the program using the shallow-water equations described above to find a solution. The solution file generated was then brought into *Tecplot* with which the results could be animated and the *Acceleration Ratio* of the particular run extracted. Figure 5-6 below shows the relative water elevation as displayed in the program for one of the *TAS* simulations.

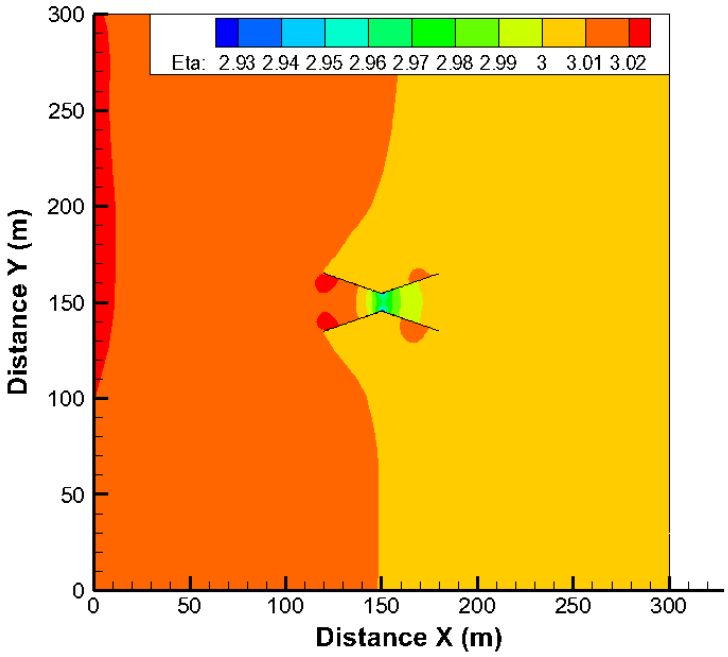

Figure 5-6: Plan View of Water Elevation Surrounding the *TAS* as Displayed in Tecplot

5.2.3 Results and Analysis

As mentioned, there were several parameters which were modified one by one to maximise the *Acceleration Ratio* and optimise the Tidal Acceleration Structure. The results of varying each of these will now be explored.

5.2.3.1 Simulation Pad Area

The first parameter which was tested was the size of the simulation pad or the area of flow within the simulation. This factor was of importance because of the way the boundary conditions were set up in *MeshGenerator*. The inflow side of the pad area was defined as a stream velocity, the outflow side a specified water height and the two parallel sides as walls, as depicted in Figure 5-4 above. For the flow to accurately represent the conditions which would be found in nature, the flow had to be able to move freely around the structure and therefore the impact of the simulation pad area had to be tested. It was desired to know the impact of varying solely the simulation pad area therefore, all other parameters were left constant and were as follows:

- Inflow flow of 0.5 m/s
- Water depth of 3 m
- Contraction ratio (structure opening divided by structure contraction at centre) of 0.1
- Structure size 10 m (total length) by 10 m (width of opening)

With the above conditions set, nine simulations were run. The impact of pad area on the *Acceleration Ratio* is presented below.

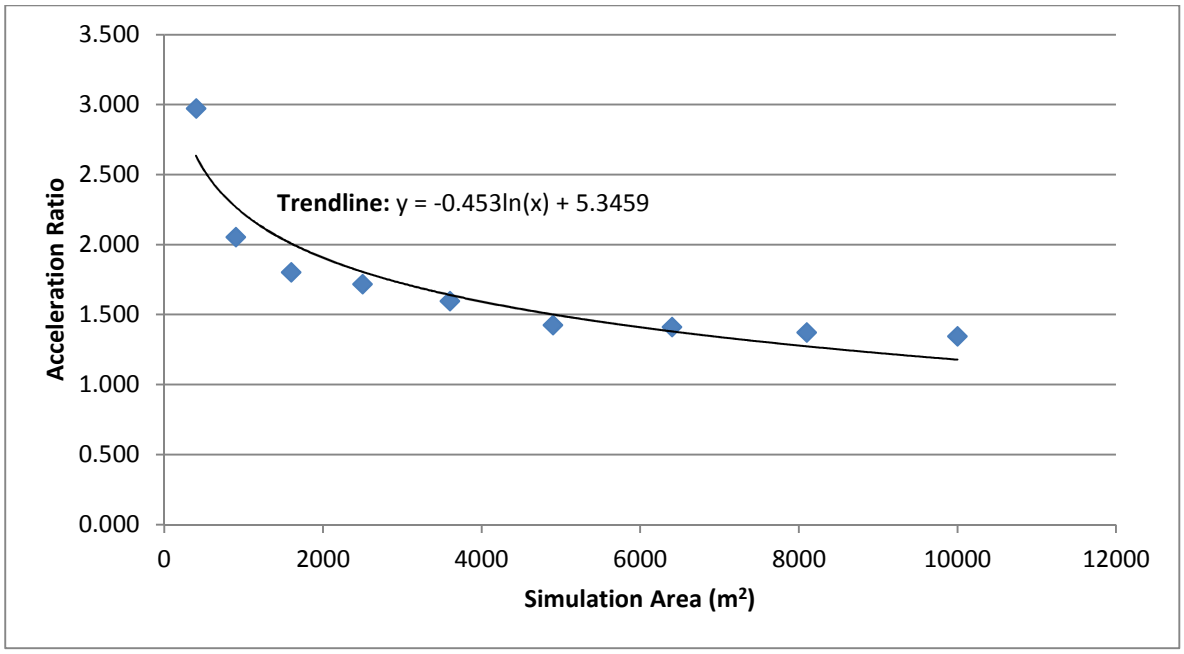

Figure 5-7: Change in *Acceleration Ratio* as Simulation Pad Area Increases

As shown in the figure above, the *Acceleration Ratio* is higher with a small simulation area. This is explained by the fact that the water is bottlenecked behind the structure and thus the increased water elevation creates a larger AR. This does not represent a realistic scenario as the water at the upstream side of the structure would not be blocked in a wide tidal channel. The simulation area at which bottlenecking seems to disappear in the graph above is 10 000 m^2 and therefore a simulation pad with dimensions greater than 100 m by 100 m was used for subsequent tests.

5.2.3.2 Inflow Velocity

The next parameter which was chosen for study was the incoming water velocity or ambient stream velocity. It was expected that changing velocity would have an impact on the resulting *AR* but it was also initially theorized that the dimensions of the structure would highly influence the resulting *AR* for particular velocities. For the test, the same initial structure dimensions as in the above described test were used along with the same flow conditions. The only difference between the two test trials was the size of the simulation pad, which was taken as 500 x 500 m to be on the side of caution for the higher

velocity runs. A total of 5 simulations were done with the result of varying velocity on the *AR* presented in the following graph.

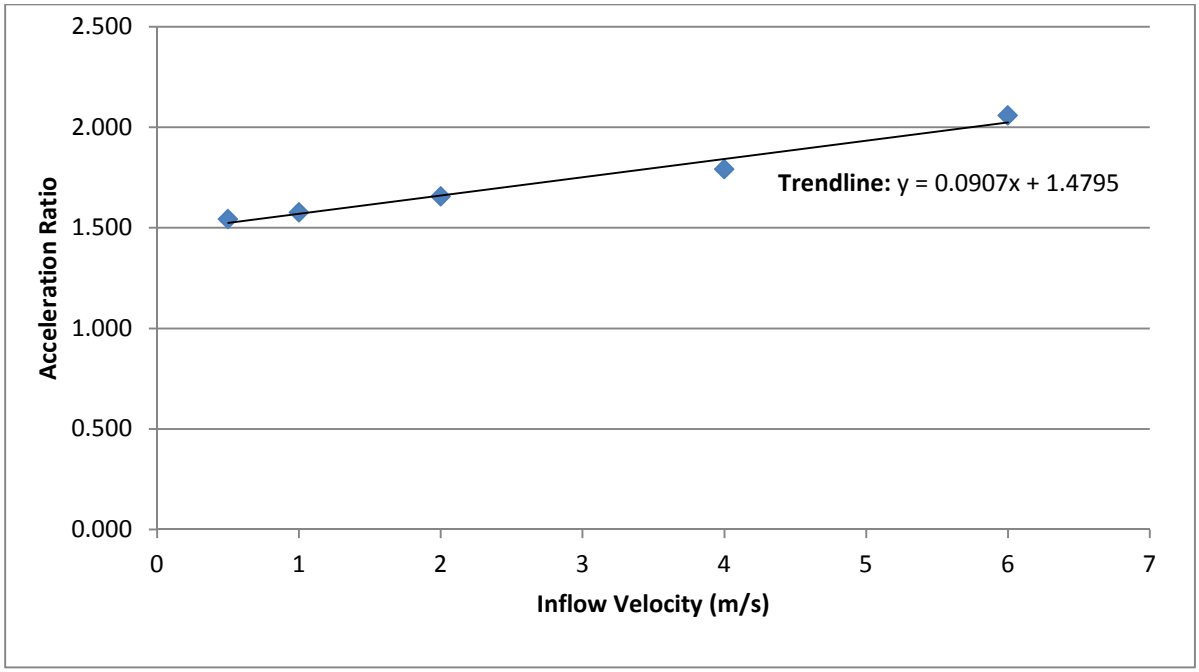

Figure 5-8: Change in *Acceleration Ratio* as Inflow Velocity Increases

If one observes Figure 5-8 above, it appears as though the *Acceleration Ratio* increases by increasing the inflow velocity. Though this may be true for the chosen structure dimensions, the test is misleading as the results would be completely different for a structure of different dimensions. The linear relationship for the change in acceleration ratio based on inflow velocity is therefore of little meaning. For this reason, the particular test was not taken into account moving forward and instead a tidal stream velocity of 0.5 m/s was instead taken for use in further optimizations. Another reason for this choice was that 0.5 m/s is a very conservative velocity magnitude therefore the resulting optimised *TAS* would be appropriate for many tidal locations.

5.2.3.3 Depth

Like water velocity, testing the variation of the *AR* as a result of changing depth was done mostly to see the general trend that it would have on flow properties. Water depth is a fixed value in nature similarly

to incoming stream velocity therefore the design must be adapted to these conditions and not vice-versa. Despite this, seven simulation runs were done with varying depths and the structure dimensions and flow conditions as set in the previous tests. The results of the depth tests are presented in the following table.

Table 5-1: Impact of Changing Water Depth on Flow Properties around the Structure

Depth (m)	**Max Eta (m)**	**Min Eta (m)**	**ΔEta (m)**	**Max u (m/s)**	***Acceleration Ratio***
1.0	1.036	0.972	0.064	0.946	1.892
2.0	2.026	1.973	0.053	0.838	1.676
4.0	4.021	3.974	0.047	0.765	1.530
6.0	6.021	5.974	0.047	0.743	1.486
8.0	8.021	7.974	0.047	0.727	1.454
10	10.020	9.974	0.046	0.702	1.404
12	12.021	11.975	0.046	0.685	1.370

By analysing the above data, one can see that the *Acceleration Ratio* decreases with greater water depths for the particular *TAS* dimensions chosen. Like the velocity results, the above results can be deceiving if not deconstructed properly. If different structure dimensions had been chosen then the impact of increasing water depth could have been completely different. Because of this fact, no optimisation was drawn from the above data. Instead of concluding anything from the iterations, they were simply noted and a constant depth of 3 m was chosen. This was seen as a good depth as it was significant enough in scale in terms of accommodating a small turbine prototype but also would provide reduced simulation times as compared to larger depths.

5.2.3.4 Length-Width Ratio of Structure

The length to width ratio of the Tidal Acceleration Structure can probably be considered the most important design parameter as it determines the general shape. Figure 5-9 depicts the plan view relating the dimension parameters.

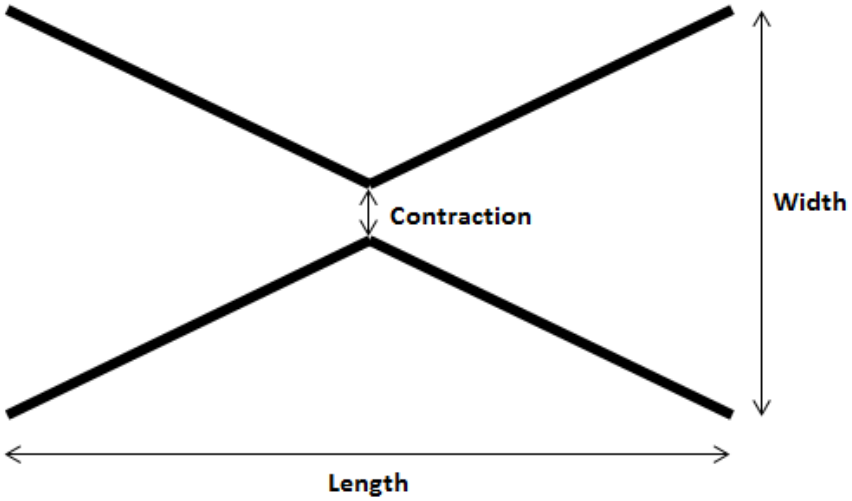

Figure 5-9: Plan view of Main Structure Parameters

From the above depiction it is plain to see that the length-width ratio is the main criteria determining the shape of the structure. To determine the length-width ratio, the flow characteristics previously mentioned were kept along with a fixed structure width of 10 m and a contraction ratio of 0.1. The only parameter that was changed was structure length. A total of 13 simulations were run with the variation to the *Acceleration Ratio* as follows.

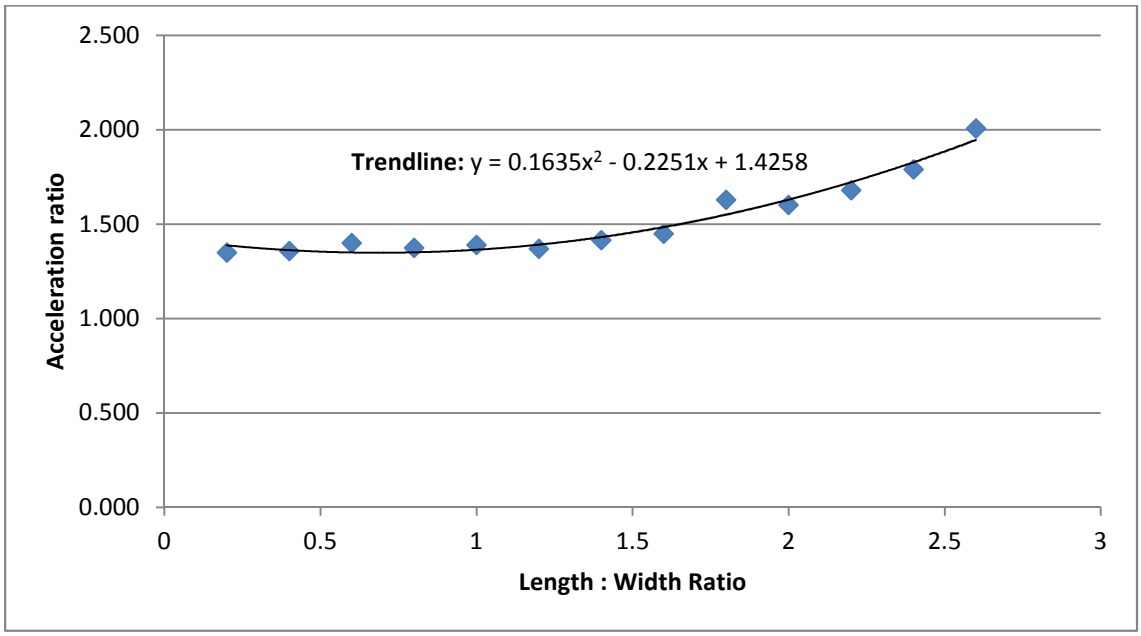

Figure 5-10: Change in *Acceleration Ratio* with Variation to Length-Width Ratio

The graph above illustrates that the *AR* gradually increases as the length-width ratio increases. This is mostly likely due to the fact that as the length of the structure increases, the opening angle of the structure decreases and the severity of the blockage effect of the walls on flow is reduced. Though the curve above was expected to eventually flatten out, the choice of optimal length-width ratio also had to factor in the elevated costs associated with increasing the structure length. Because of this limiting factor, the length-width ratio was set as 2:1 as it created a simple geometry for future tests, was reasonable in terms of size and also gave a good *AR* that could be improved with further geometry modifications.

5.2.3.5 Structural Scale

The structural scale tests were meant to determine the relative benefits of the size of the structure when keeping all other ratios and flow conditions constant. Therefore for the simulations the conditions as described above were kept along with the 2:1 length-width ratio. The main purpose of the test was to measure the change to the *AR* when increasing the size of structure while also considering the associated increased costs. It was expected that larger structure sizes would give larger ARs. It should be noted that the simulation pad sizes were increased proportionally to the structural scale to keep the blockage effect of the *TAS* on flow constant. The results of the 10 simulations are shown in the following graph.

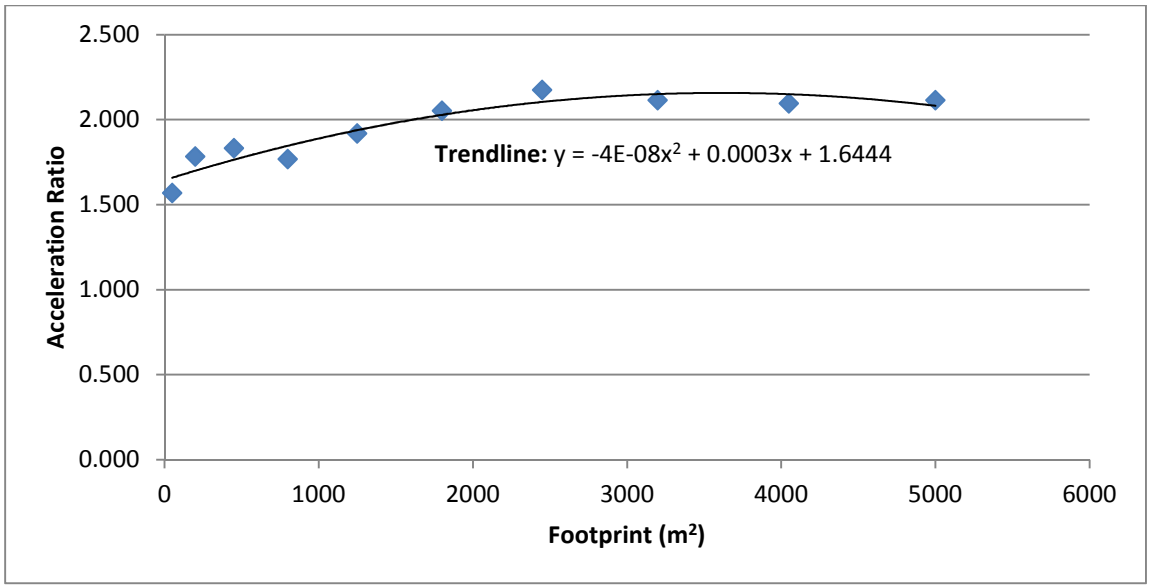

Figure 5-11: Change in *Acceleration Ratio* with Change in Structure Scale

As observed from the figure, the *AR* increases as the footprint or size of the *TAS* increases but eventually reaches a sort of plateau. Though it can be expected that modifying other parameters could yield larger *AR*s for the structures of large scale, the determination of the optimal scale also had to account for the cost benefits of the increase. Due to this, the scale which was chosen for subsequent tests was a structure of 60 m in length by 30 m in width. This scale of *TAS* was found to have a reasonable *Acceleration Ratio* (*AR*) of 2.052 as seen in Figure 5-11 above, while also being of feasible construction size thus justifying its choice.

5.2.3.6 Contraction Ratio

Before describing the simulations done for this test it should first be noted that the contraction ratio is the ratio between the contraction at the centre of the structure to the width of the structure opening as shown in Figure 5-9 above. This parameter was thought to be of large importance as it directly affects the maximum velocity passing through the structure centre according to the Venturi principle. This test was also important in the design process as it represented the last in the testing methodology and therefore the *Acceleration Ratio* which was found would represent the final preliminary design. The flow

conditions and other structure specifications which were found previously and used for this final test were as follows.

- Inflow velocity of 0.5 m/s
- Water depth of 3 m
- Structure 60 m in length by 30 m in width
- Simulation pad size of 300 m by 300 m

The results of varying the contraction ratio in 10 simulations are presented in Figure 5-12 below:

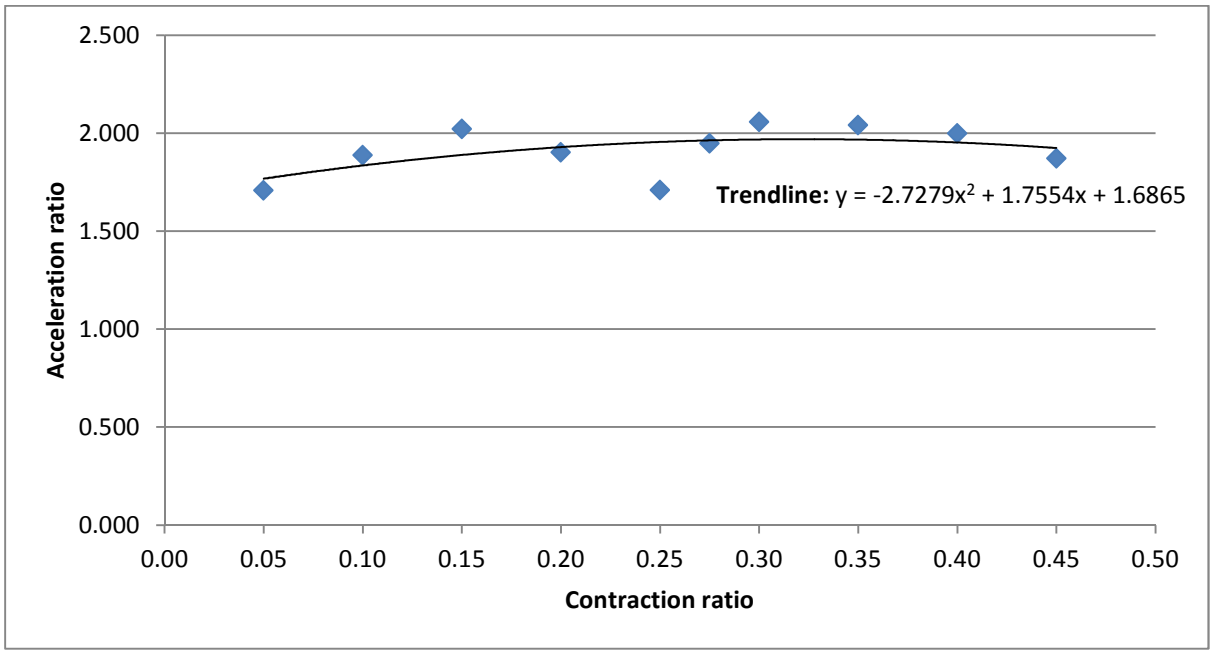

Figure 5-12: Change in *Acceleration Ratio* with Variation to the Contraction Ratio

From the graph above one can see that the maximum *Acceleration Ratio* of 2.058 occurs at a contraction ratio of 0.3. As can be observed also, the *AR* remains fairly constant implying that the *TAS* was not particularly sensitive to changes in the contraction ratio (at least for the range tested). This was most likely due to the blockage effect of the structure increasing at low contraction ratios, and thus more flow circumventing the *TAS.* The final *TAS* yielded from the 2D Hemat tests therefore had a contraction width of 9 m, a structure width of 30 m and a length of 60 m.

5.2.4 Discussion

By changing one structure parameter at a time, the simulation stages listed above were able to yield an improved Tidal Acceleration Structure design. Though some of the parameters tested did not directly lead to structure improvements, each Hemat2D test added to the understanding of how the *TAS* parameters interact in their impact on performance. The final design was tested in a water depth of 3 m and incoming tidal current velocity of 0.5 m/s. The optimisation procedure yielded a structure with the following specifications:

Table 5-2: Specifications of Improved *TAS* from Hemat2D Simulations

Parameter	Value
Structure length	60 m
Structure width	30 m
Contraction width	9 m
Acceleration ratio	2.058

Though the above described design is an improvement from the original concept it cannot be considered a fully optimised structure as there were several key aspects which were not modified. These included: wall curvature, topographical changes within the structure and alteration of ocean bottom surface roughness by use of fibreglass or other material.

Another problem with the simulation methodology of the Hemat2D work is that it did not fully take into account the interdependencies of the structure dimensions on performance. As there are innumerable combinations of *TAS* and flow parameters, not all configurations could be tested and thus the optimised *TAS* design depends largely on initial conditions. Because parameters were assumed in some way or another for each simulation test run, the final structure did not necessarily correspond to that with the largest possible acceleration ratio. If different initial structure or flow parameters were assumed it's very likely a different final *AR* would have been found.

In order to verify the above shortcoming, another sample simulation was run using different initial conditions. The flow parameters were taken from real values collected at the Minas Passage in Nova

Scotia, Canada. The water depth was taken as 15 m, the incoming flow velocity as 4.6 m/s and a pad area of 400 x 400 m was used for the simulation. The 60 x 30 m *TAS*, as yielded from the above mentioned tests, was used and only the contraction ratio was modified. From a series of five tests it was found that a contraction ratio of 0.4 gave an acceleration ratio of 2.39. Because the *AR* is higher than that found from the optimisation tests above, it can be concluded that the initial conditions chosen influence the final *AR* which will be found if the same optimisation methodology is employed.

By analysing the previously mentioned finding, it is easy to conclude that a better methodology for optimising the *TAS* design should be found. A possible solution to the problem would be the preliminary selection of a specific tidal site so that all flow conditions would be known. From there, the structure size could be decided as opposed to tested and then only a few structure parameters would need to be optimised. Fewer test parameters would reduce computational costs and allow for an iterative process to be used. The *TAS* resulting from an iterative process of tests would be closer to the optimal design and would consequently have a higher acceleration ratio. This lesson was applied to the experimental testing methodology as discussed in Chapter 4.

Overall, the testing of the *TAS* using the Hemat2D numerical model scheme can be considered a success as the Venturi effect was observed as expected. Though the structure was not optimised completely during the preliminary Hemat work, the 2D optimised *TAS* served as the basis for the experimental model design.

5.3. 3D Modeling using Fluent

Similarly to the Hemat2D software, the 3D modeling program which was needed to simulate the *TAS* had to be able to model flow in shallow waters. As demonstrated from the analysis of the governing equations of Hemat2D, a program utilising a finite-volume method was thought to be a good possibility for the 3D work. As mentioned earlier, finite-volume schemes are commonly used due to their ability to

conserve the mass and momentum in a fluid system; essential for an accurate replication of tidal current flows around the *TAS*.

ANSYS Fluent is a commercial computational fluid dynamics (CFD) software which has been widely used for a vast amount of fluid applications. It has the capability to simulate a wide range of fluid problems including laminar and turbulent, incompressible and compressible situations, both in 2D and 3D. Fluent is also popular because of its power to create detailed flow field visuals. Though the abilities of the Fluent software are diverse, the group of models that are of interest in modeling the Tidal Acceleration Structure are the free surface and multiphase flow models. The Volume of Fluid (VOF) model is of particular interest for modeling the *TAS* as it has been used in former literature for modeling tidal current applications. There are several physical models that can be used in Fluent however the software solves equations for conservation of mass and momentum in all fluid cases.

In this section, the model and its theoretical background will first be explored. After this, the results will be presented and analysed. Finally, comparisons with the experiments results will be made before final conclusions on the 3D numerical work are given.

5.3.1 Model Description and Theoretical Background

The main equations governing mass continuity and momentum balance which are used by Fluent are the Reynolds averaged Navier-Stokes equations as for unsteady incompressible flow as described in (ANSYS 2010).

The general form of the equation for conservation of mass, valid for incompressible and compressible flows, is written as:

$$\frac{\partial \rho}{\partial t} + \nabla * (\rho \vec{v}) = S_m \qquad \textbf{(5-7)}$$

Where:

- ρ is the fluid density

- t is time
- ∇ is the partial derivative with respect to all directions
- $\vec{v}$ is the velocity vector
- S_m is the mass added per unit time to the continuous phase from the dispersed second phase or any other user defined source

The equation for conservation of momentum for a non-accelerating (inertial) reference frame is as follows:

$$\frac{\partial}{\partial t}(\rho\vec{v}) + \nabla * (\rho\vec{v}\vec{v}) = -\nabla p + \nabla * (\bar{\bar{\tau}}) + \rho\vec{g} + \vec{F} \quad \textbf{(5-8)}$$

Where:

- ρ is the fluid density
- t is time
- ∇ is the partial derivative with respect to all directions
- $\vec{v}$ is the velocity vector
- p is the static pressure
- $\bar{\bar{\tau}}$ is the stress tensor (described below)
- $\rho\vec{g}$ and $\vec{F}$ are the gravitational body force and external body forces ($\vec{F}$ also can define other optional model-dependent source terms or user-defined sources)

And where $\vec{\tau}$ is the stress tensor which is given by:

$$\bar{\bar{\tau}} = \mu\left[(\nabla\vec{v} + \nabla\vec{v}^T) - \frac{2}{3}\nabla \times \vec{v}I\right] \quad \textbf{(5-9)}$$

Where:

- μ is the molecular viscosity
- I is the unit tensor

- ∇ is the partial derivative with respect to all directions
- $\vec{v}$ is the velocity vector

For all other details on the equations governing mass and momentum continuity please refer to (ANSYS 2010). The above are very general forms of the equations governing conservation of mass and momentum, the specific equations used by Fluent may change based on the models used and the fluid situation.

The VOF model in Fluent is of particular interest in application to testing the Tidal Acceleration Structure as it can model more than one fluid body. The program does this by keeping track of the volume fraction of each fluid in the scenario and solving them with a single set of momentum equations (ANSYS 2010) but with corresponding parameters for each fluid/phase. This applies directly to the *TAS* situation as the VOF model can simulate the free-surface interaction between air and water.

The VOF scheme functions by computing the volume fraction of each of the fluids in each cell. The fluids are assumed to not be interpenetrating (e.g. dilution is not possible in one fluid/phase as a result of mixing with another fluid/phase) and the volume fractions of the fluids for a particular cell must sum to 1. For open channel situations where a region of air is on top of water, as in the tidal case at hand, a steady-state calculation can be performed using the VOF model to compute the equilibrium state.

The properties or variables in any given cell during the Fluent calculations are representative of either one of the liquids or "phases" or a mixture of the phases. This is represented by the statement that for a q^{th} fluid's volume fraction in a cell is given by α_q then three conditions are possible. These are:

1. $\alpha_q = 0$, the cell does not contain the q^{th} fluid
2. $\alpha_q = 1$, the cell only contains the q^{th} fluid
3. $0 < \alpha_q < 1$, the cell contains the q^{th} fluid and at least one other fluid

By calculating α_q, Fluent is able to assign the right variables and properties to the areas within the computation domain.

A continuity equation in respect to the volume fraction of the phases is used to track the interface or free surface between the different fluids. For the q^{th} phase or fluid this continuity equation is given by:

$$\frac{1}{\rho_q}\left[\frac{\partial}{\partial t}\left(\alpha_q\rho_q\right)+\nabla*\left(\alpha_q\rho_q\vec{V}_q\right)=S_{\alpha_q}+\sum_{p=1}^{n}\left(\dot{m}_{pq}-\dot{m}_{qp}\right)\right] \quad \textbf{(5-10)}$$

Where:

- $\dot{m}_{qp}$ represents the mass transfer phase *q* to phase *p*
- $\dot{m}_{pq}$ the mass transfer from phase *p* to phase *q*
- ∇ is the partial derivative with respect to all directions
- $\vec{v}$ is the velocity vector
- S_{α_q} can be used to introduce a mass source term by the user but is otherwise ignored for the default case

The volume fraction equation can be chosen in Fluent to be either solved implicitly or through explicit discretization. For the purposes of the *TAS* the implicit scheme is adequate and the equation governing the finite-difference interpolation scheme is:

$$\frac{\alpha_q^{n+1}\rho_q^{n+1}-\alpha_q^n\rho_q^n}{\Delta t}V+\sum\ f\left(\rho_q^{n+1}U_f^{n+1}\alpha_{qf}^{n+1}\right)=\left[S_{\alpha_q}+\sum_{p=1}^{n}\left(\dot{m}_{pq}-\dot{m}_{qp}\right)\right]V \quad \textbf{(5-11)}$$

For details on notations please refer to (ANSYS 2010). The above equation uses the volume fraction at the current or n^{th} time step therefore a standard scalar transport equation is solved for each of the secondary-phase defined volume fractions at each time step in an iterative manner. Also, the spatial discretization scheme is optimised to keep sharp interfaces without mixing. The VOF model uses a single

momentum equation throughout the computational domain. The above equation is dependent on the volume fractions of each fluid and the velocity field generated is shared amongst the phases.

The Volume of Fluid model is also capable of simulating open channel flow conditions. This is a pertinent option for the *TAS* as the boundary conditions can be set to reproduce marine conditions. Other equations governing open channel flow as applied in Fluent, including options for inlet and outlet conditions, are explored in detail in (ANSYS 2010).

The following table lists some of the key model parameters which were used in the ANSYS Fluent simulations.

Table 5-3: Model Parameters Used in the 3D ANSYS Fluent Simulations

Parameter	Specific Option Used
General simulation type	*Steady-state*
Multiphase modeling	*Volume of fluid (VOF) model*
Viscous model	*SST k-omega (with low-Re corrections enabled)*
Type of inlets (air and water)	*Velocity inlets specified*
Outlet type	*Outflow*
Pressure-velocity coupling scheme	*Coupled (coupled with volume fractions enabled)*
Spatial discretization: gradient	*Least squares cell based*
Spatial discretization: pressure	*Body force weighted*
Spatial discretization: momentum	*QUICK*
Spatial discretization: volume fraction	*Compressive*
Spatial discretization: turbulent kinetic energy	*Second order upwind*
Time step method	*Pseudo transient*
Initial pseudo time step	*0.0001 s*

5.3.2 Results and Analysis

As mentioned earlier, the main eventual objective of the 3D modeling efforts was the simulation of the *TAS* at full scale. To do this, the Fluent model first had to be calibrated to make sure it was accurately predicting the structure flow interactions caused by the *TAS*. This was done by comparing the Fluent model to the experimental results in terms of the velocity field around the structure. It was thought that by using the same Fluent setup in terms of solver, turbulence model, y+ values near boundaries and

inlet and outlet conditions, it would be possible to simulate the model at full scale accurately in future work.

The first step of the 3D modeling was to create the geometry of the flume with ANSYS Geometry. The entire 30 m length of the flume was not utilised during the experimental testing as the structure centre was placed 6.5 m from the end. The 23.5 m of flume upstream of the structure mostly served for turbulence dissipation as the flow was extremely turbulent upon entering the flume (see Figure 4-3). This was not the case in Fluent as the turbulence could be specified. Only 6.5 m of flume upstream of the *TAS* centre was modeled and 6.5 m downstream of the structure therefore a total length of 13 m was modeled. The modeled width of the flume was 1.5, the same as in the experimental scenario. The structure which was chosen for the numerical modeling was the *10contr_25open_str* structure which as mentioned in Table 4-4 has a contraction of 10 cm, openings of 25 cm and straight walls. The main geometries of the model created in ANSYS Geometry are shown below.

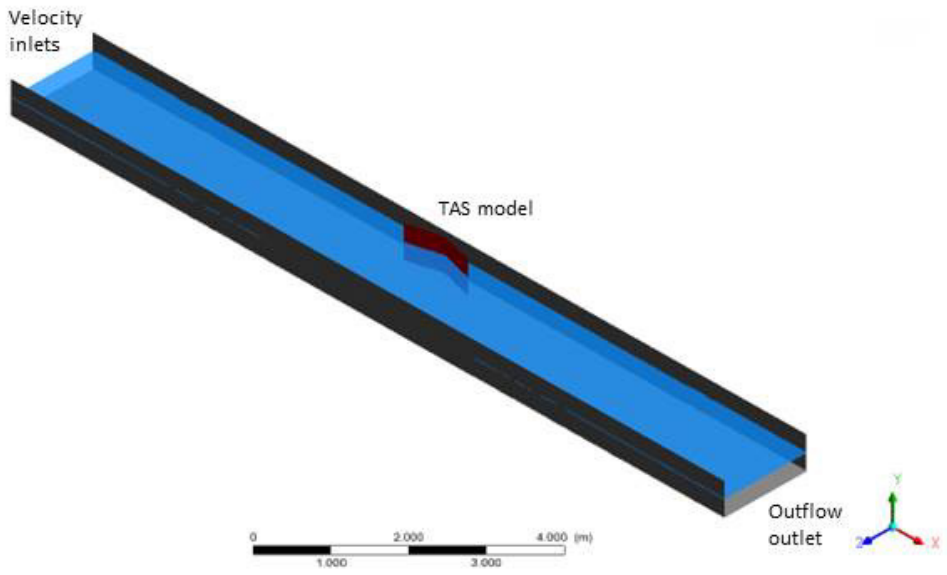

Figure 5-13: Geometry for Scaled Numerical Simulation

After the geometry was created, the next step was to mesh the model. This was done with ANSYS meshing and a mesh of 1.35 million elements was created. Significant refinement was specified around

the free surface between air and water and around the physical boundaries. The reason for the refinement around the free surface was for proper resolving of surface velocities and water surface elevation changes. The refinement of the mesh near the physical boundaries was done to ensure y+ values in the order of 1 throughout the domain for proper solving of the near wall velocities by the k-omega SST turbulence model. The refinements were done mostly using edge sizing. The mesh used in the simulation is shown below.

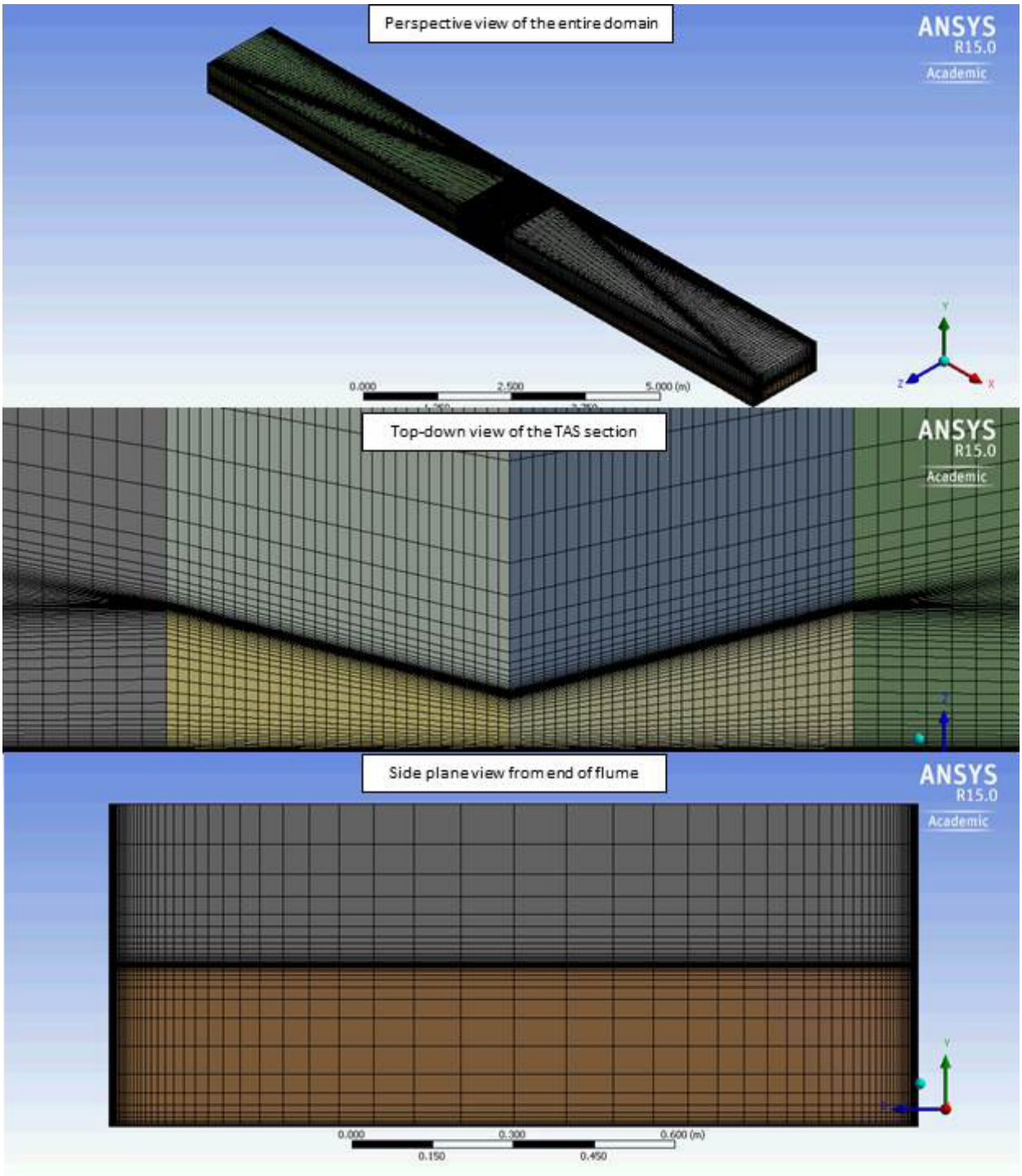

Figure 5-14: Meshing for Scaled Numerical Simulation

The simulation was run using the settings listed in Table 5-3 for a total of 75 000 iterations until all velocity monitors indicated no change in the solution and all scaled residuals reduced to below 1e-04. Using the ANSYS post-processing tool several informative graphics were created to illustrate the

converged flow parameters including: the velocity field generated around the *TAS*, water surface differentials, turbulence and velocity streamlines. The surface velocity of the converged simulation is shown below.

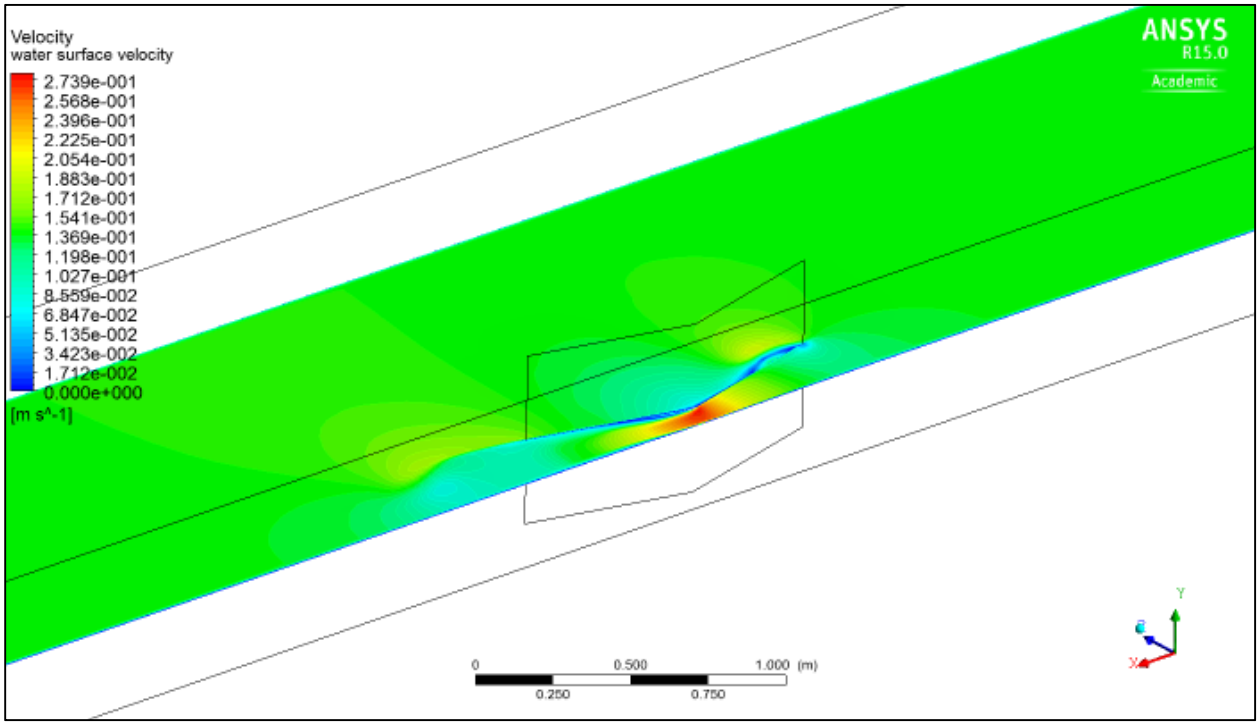

Figure 5-15: Water Surface Velocity in Fluent: *10contr_25open_str TAS*

As one can see from Figure 5-15 above, there is significant acceleration through the centre of the *TAS* and a reduction in velocity downstream of the structure. The variation of velocity can also be visualised using streamlines showing the flow through and around the structure.

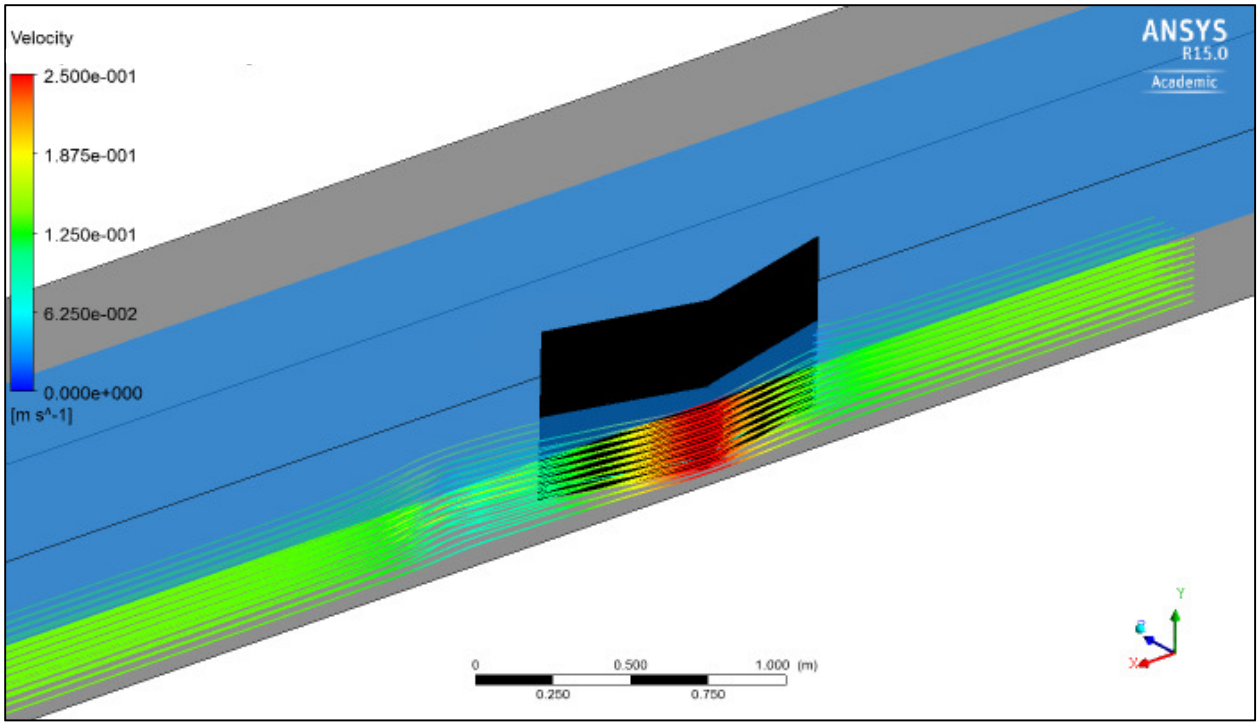

Figure 5-16: Velocity Streamlines around Structure: *10contr_25open_str TAS*

In examining Figure 5-16 above, one can see that small portion of the flow upstream of the structure opening is forced around the structure instead of through the contraction due to the blockage effect of the *TAS*. Despite this, the majority of the flow upstream of the opening is guided into the contraction and thus adds to the water flux which could be used to power a tidal in-stream turbine. Another interesting graphic which one can examine is the change to the free water surface caused by the blockage effect of the *TAS*. Though it was so minute to be immeasurable in the experimental tests, it was expected to exist and be measurable in the numerical simulation. It is shown below in Figure 5-17.

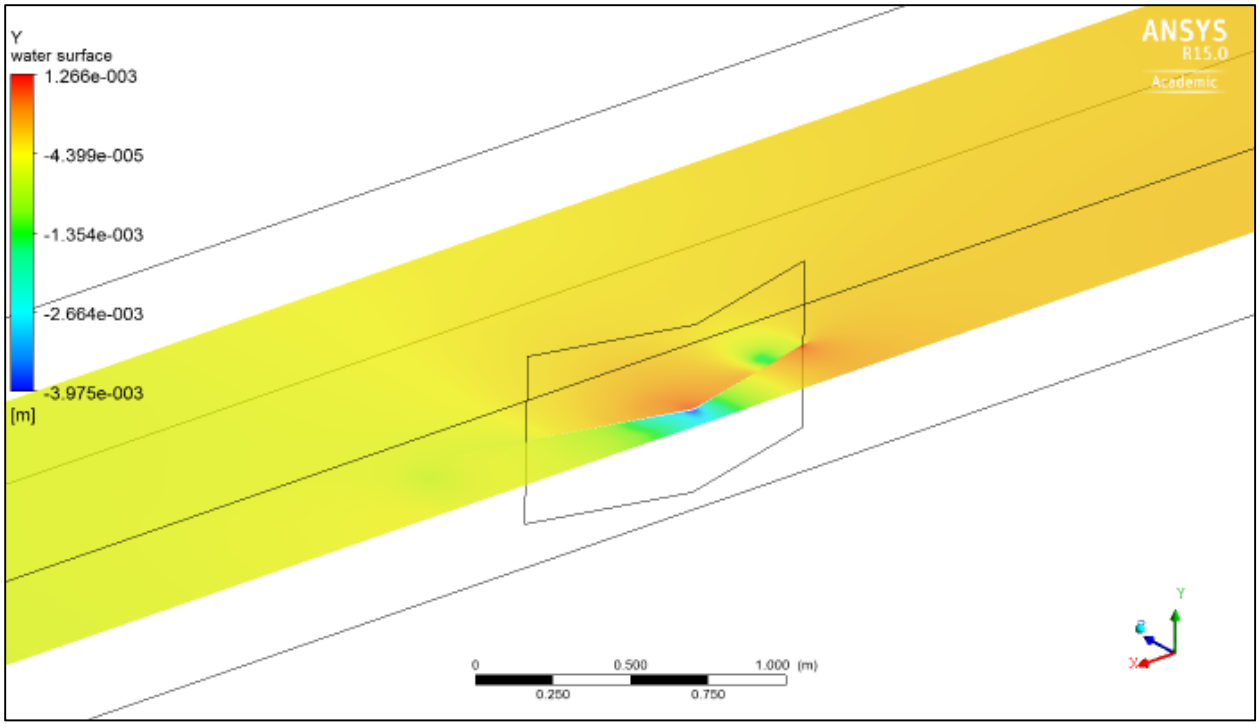

Figure 5-17: Free Surface Elevation Relative to 30 cm: *10contr_25open_str TAS*

Because the ADV velocity profiles were mostly taken at an elevation of 12.5 cm above the bed, it is relevant to illustrate the velocity and other parameters at this depth.

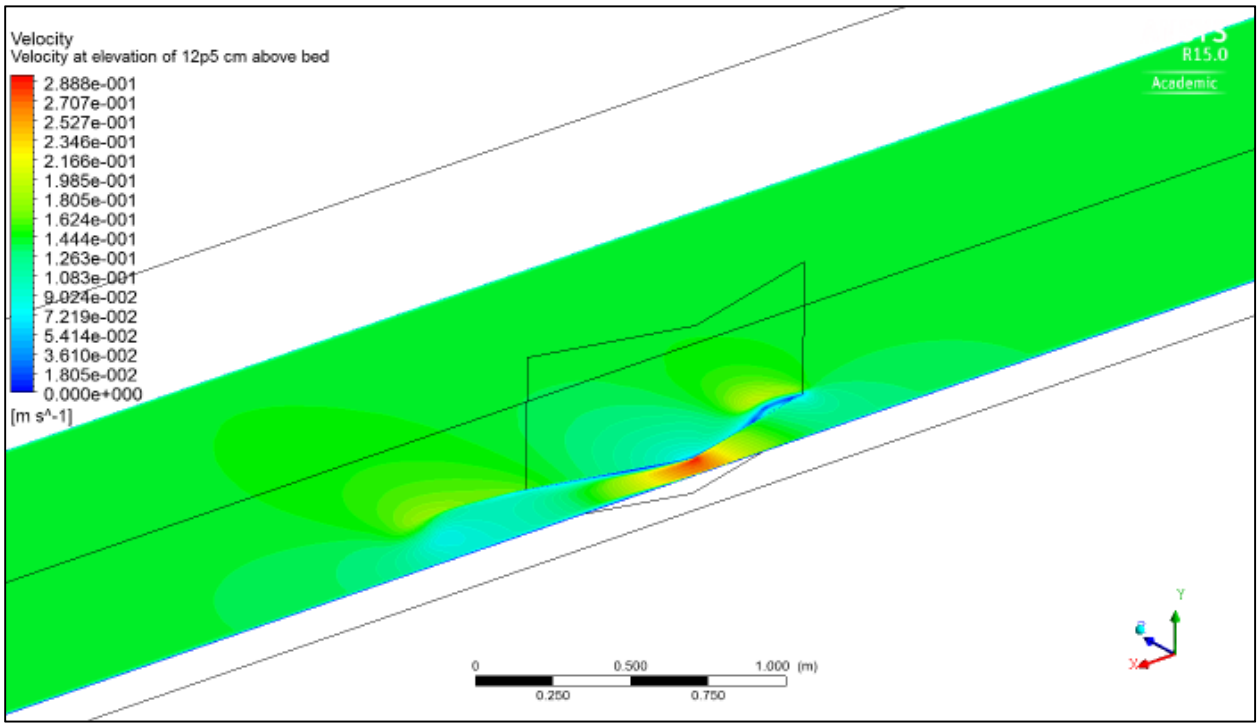

Figure 5-18: Velocity at Elevation of 12.5 cm above Bed: *10contr_25open_str TAS*

From examining Figure 5-18 above, one can see that the velocity contours are similar to those at the water surface (Figure 5-15); the flow accelerates as it passes through the structure contraction and slows downstream of the structure exit before recuperating to the in-stream velocity further downstream. As well, one can note that the velocity magnitude is significantly reduced on the outside of the *TAS* just downstream of the leading wall tip. A vortex like structure seems to be developing due to the sharp edge and this can further be viewed by illustrating the turbulent kinetic energy on the same plane.

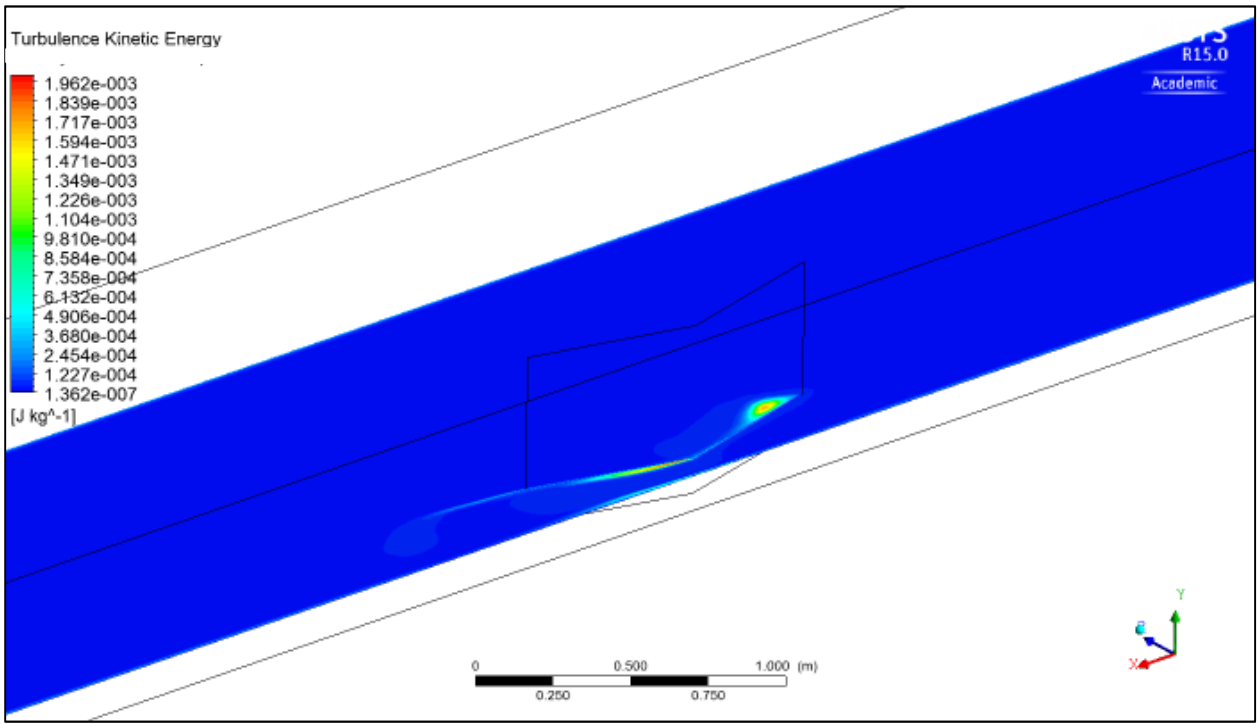

Figure 5-19: Turbulent Kinetic Energy: *10contr_25open_str TAS*

As one can see there is significant turbulence generated behind the leading edge of the structure and along the wall downstream of the structure centre on the inside of the *TAS*. Overall, the results from the Fluent simulation presented above agree with those predicted by the Venturi Effect in terms of the flow acceleration and pressure drop (manifested by a drop in water surface elevation) in the contraction of the *TAS*. The results can now be compared against the experimental results to verify the model for future simulations.

5.3.3 Comparison with Experimental Results

As the configuration which was modeled with ANSYS Fluent was the *10contr_25open_str TAS* without a plate, the main parameter which can be used to compare with the experimental results is the flow velocity. Three velocity profiles are compared below with the purpose of validating the Fluent setup for future *TAS* numerical simulations including a full scale simulation and a simulation with a actuator disc modeled at the *TAS* centre using Fluent's *Porous Jump Model*. The first profile comparison, the vertical velocity profiles at the *TAS* centre, is shown below.

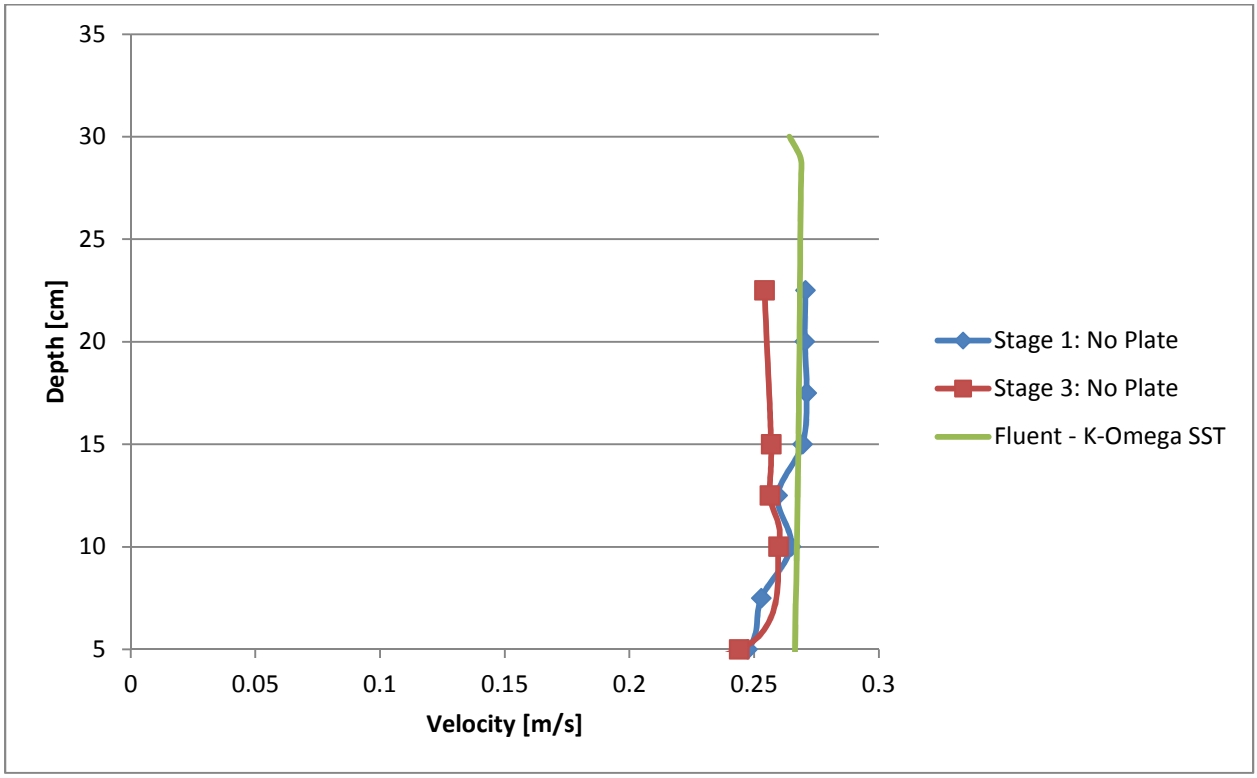

Figure 5-20: Vertical Velocity Profile Comparison: *10contr_25open_str TAS*

As one can see in evaluating Figure 5-20 above, the vertical velocity profiles of the two experimental tests (stage 1 and 3) and the Fluent – K-Omega SST simulation are all similar and follow the expected log-law profile. The profile below 5 cm above the bed was not shown as it was not accurately measured by the ADV during the experimental tests (as discussed in Section 4.6.1). Next, one can compare the longitudinal velocity profiles at the centre of the flume (*Middle* profile as shown in Figure 4-12).

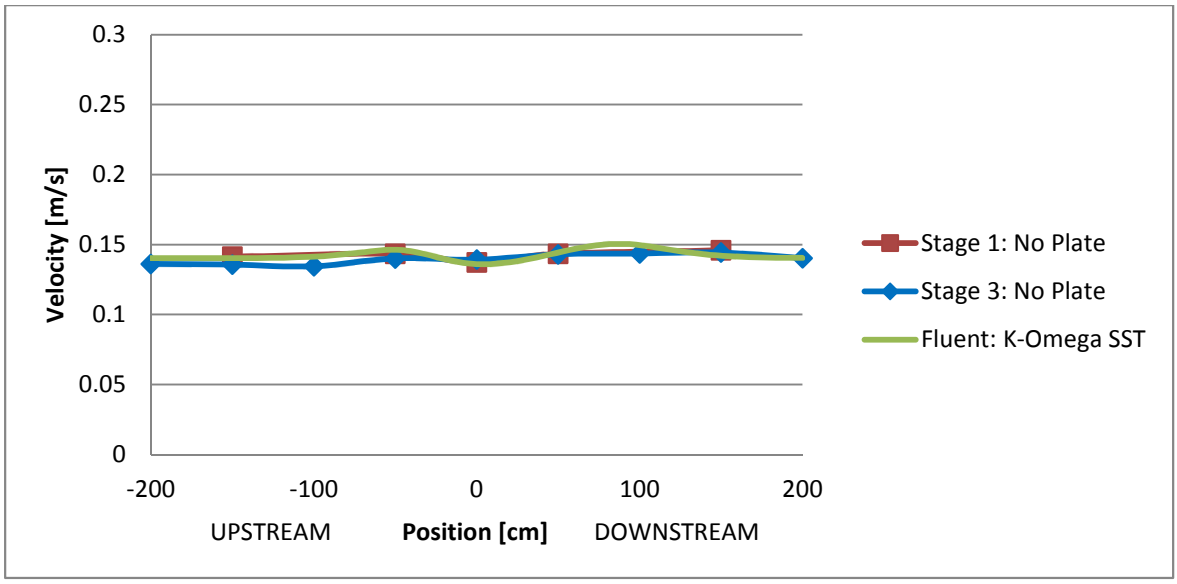

Figure 5-21: Middle Longitudinal Velocity Profile Comparison: *10contr_25open_str TAS*

As one can see from observing Figure 5-21 above, the velocity profiles of the numerical and experimental tests are very similar. This is an encouraging sign for the validity of the Fluent numerical model. Lastly, the longitudinal velocity profiles through the centre of the *TAS* can be plotted and are shown below in Figure 5-22 (*Side* profile as shown in Figure 4-12).

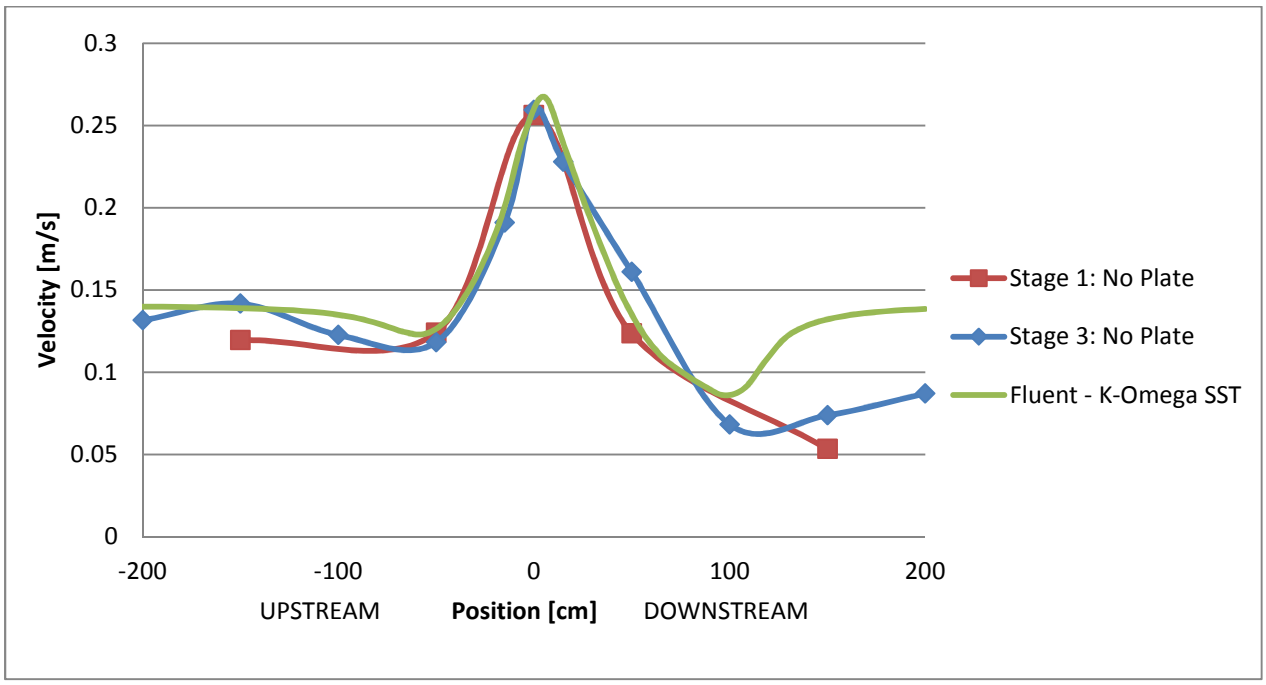

Figure 5-22: Side Longitudinal Velocity Profile Comparison: *10contr_25open_str TAS*

From examining Figure 5-22 above, it can be observed that the Fluent simulation reproduces the experimental longitudinal velocity profile fairly well, especially in terms of the velocity near the contraction or centre of the *TAS* (position = 0). The only inconsistency is the wake recovery distance. In the experimental results, one can see that the wake has not recovered 2 m downstream of the structure however in the Fluent simulation the wake is almost fully recovered. This discrepancy is probably due to the nature of the turbulence formed as flow passes through the *TAS* centre or perhaps because of the flow regime which passes outside of the *TAS*.

5.3.4 Discussion

Using the 3D CFD program ANSYS Fluent, an experimental scenario was successfully reproduced with considerable accuracy. Though some discrepancy exists between the wake structure of the numerical and experimental results, overall the velocity profiles are quite similar and it can be said that the Fluent setup is adequate for modeling the *TAS* for future test scenarios. Two additional elements which were not measured during the experimental testing were also observed: the change to the free water surface level around the structure and the turbulence kinetic energy around the *TAS* walls. As expected, the change to free water surface was small. A small increase in surface elevation was observed at the mouth of the *TAS* and a small depression in elevation at the contraction (see Figure 5-17). In terms of the turbulent kinetic energy, a turbulence feature was observed behind the leading edge of the upstream wall (see Figure 5-19). This was not noted during the experimental testing however it was most likely present regardless.

Originally, more test scenarios were planned but these unfortunately could not be completed as part of the present project because of time constraints. A full scale simulation of the same *10contr_25open_str TAS* is intended as well as a simulation of the modeled scale with the presence of an actuator disc represented by Fluent's *Porous Jump Model*. Overall, the simulation of the *10contr_25open_str TAS*

(chosen for more detailed experimental tests and numerical testing due to its high acceleration of flow) using the 3D Fluent CFD model can be considered a success. It replicated the experimental results with an adequate level of accuracy and allowed for the examination of additional flow features that could not be done in the experimental testing.

5.4. Conclusions

The numerical modeling of the *TAS* was quite broad, including both 2D and 3D simulations. To conclude, the following goals were accomplished:

- Initial 2D modeling of the *TAS* concept and observation of the expected velocity increase at the structure centre
- Successful initial optimisation of the *TAS* design using a strategy of varying structure parameters
- Sensitivity analysis of flow and boundary conditions in Hemat2D
- Successful simulation of a *TAS* configuration using ANSYS Fluent and the K-Omega SST turbulence model
- Comparison of the 3D Fluent results with the experimental test results for the *10contr_25open_str TAS* model without a plate. Similar velocity profiles observed between the 3D numerical and experimental results therefore the Fluent setup can be deemed to be validated for further *TAS* testing
- Observation of several interesting flow features around the *TAS* including slight increase in free surface elevation at the mouth and upstream of the structure, decrease in surface elevation at the *TAS* contraction and a region of high turbulence kinetic energy downstream of the leading edge of the *TAS* wall

Overall, both the 2D Hemat and 3D Fluent simulations should be considered a success. Though the *TAS* was not simulated at full scale or with the presence of an actuator disc at its centre with Fluent due to time constraints, the 3D simulation of a *TAS* model was successful and the correlation with the corresponding experimental results indicate that the Fluent model can be used for future *TAS* simulations.

Chapter 6. Discussion

As the results were discussed in detail in their respective chapters, this chapter serves to discuss the broader implications of the testing and what it means moving forward with the development of the Tidal Acceleration Structure (*TAS*) concept.

The present study was the first comprehensive evaluation of the *TAS* and had as its core purpose the optimisation of the structure design. As stated in Chapter 1, the scope of the project was mainly focused on two things: the scaled experimental testing of a *TAS* model and the validation of a numerical model using the experimental results. The specific objectives and implementation plan for the project changed somewhat over time and this was done to facilitate flexibility in the testing and also to allow for re-evaluation of testing priorities as the project progressed. Though this most likely resulted in some inefficiencies in the testing process, it also allowed for increased optimisation of the *TAS* and discovery of new aspects related to the *TAS* which were not originally envisioned including the effect of turbine (or in the experimental case a porous plate) blockage on flow.

Chapter 2 introduced the relevant literature including the physics of tides and historical and current tidal exploitation methods. Previous studies on existing tidal augmentation channels were explored in the chapter as well. It was found that though other technologies exploiting the Venturi effect exist, including channels and shrouds (Ponta and Shankar Dutt 2000; Sireli 2014), the *TAS* is unique in several ways. Differences include the fact that the structure walls extend from the seafloor to above the water surface and that the *TAS* is a large augmentation channel capable of being used for a multitude of turbine designs. One aspect that was noted while researching other tidal technologies was that information on specific turbine or augmentation devices is quite limited. Several companies employ turbines with duct enhancements but their testing and optimisation processes, or how they came to their final designs, are not available in public literature (for the most part). This makes sense however as new technologies are

generally not developed by government or not-for-profit organisations, and companies want to keep their design specifics secret. Though this issue is somewhat unavoidable, it is unfortunate that there isn't more sharing of knowledge between in-stream tidal companies. The tidal industry is still quite young and its success, as individual companies or as a whole, is by no means a guarantee. The public has other options such as wind and solar for renewable power production and tidal energy investment will eventually dwindle if economic electricity production (cf. other renewables) is not attained soon. If new ideas, such as the *TAS* concept, have the potential to make tidal energy more competitive, then it is in the interest of all turbine manufacturers to facilitate the development of these technological improvements.

The modeling of in-stream turbines, for numerical and experimental cases, was discussed in Chapter 2 also. The method of simulating the turbine was important as it was desired to find the most accurate results possible. From the review of the existing literature, it was found that Actuator Disc Theory is an adequate method of simulating the overall effects of a turbine on flow. As discussed in Section 2.4.1, the only significant irregularities with real in-stream turbines are the lack of swirl imparted on flow due to the actuator disc, vortex shedding off of disc edges instead of rotating blades and the extraction of energy by the creation of small-scale turbulence instead of mechanical motion (Bahaj et al. 2007; Roc 2013). The specific flow conditions near the rotating blades and the downstream turbulence structure were not the main parameters of concern for the project therefore, the use of porous discs to simulate the energy extraction of a turbine were considered appropriate for the experiments conducted.

The research methodology, including the initial flow parameters and fixed structure dimensions, were discussed in Chapter 3. As discussed in the chapter, the parameters which were varied were the structure opening width, contraction width and wall curvature (straight, moderately curved and considerably curved). The target flow conditions were kept constant during all tests and consisted of a flow velocity of 14.14 cm/s (1 m/s at full scale) and a flow depth of 30 cm (15 m at full scale). These flow

conditions were chosen because it was thought they would be the typical conditions for which the *TAS* would be most useful in terms of exploiting tidal sites which are not useable with current in-stream turbine technology. Though the chosen flow characteristics were thought to be reasonable, this perspective could change with time as further research is done into the actual construction of a *TAS* prototype. Potential issues include the target flow velocity of 1 m/s being too slow for economic power production or the *TAS* construction being unrealistic in the chosen flow depth. The load forces for each site, including peak breaking wave loads and potential object impacts, will have to be thoroughly investigated before a responsible prototype construction could be done. Though the main optimisation objective of the present study was to maximise the velocity at the centre of the *TAS* contraction, other optimisation objectives could become important in future optimisation schemes. The relationship between turbine and *TAS* wall cost, presently unknown, is of special concern as this would affect the ideal dimensions of a *TAS* prototype. A relatively low turbine cost (vs wall cost) would most likely result in ideal *TAS* dimensions with smaller walls whereas a relatively high turbine cost (vs wall cost) would likely advantage the ideal design having larger walls in order to produce the largest flow acceleration possible. These, and other prototype and commercial scale concerns, are unfortunately beyond the scope of the present project.

6.1. Physical Modeling of the TAS

As mentioned, the physical modeling of the *TAS* in a flume was one of the main goals of the research project and therefore the bulk of the results are contained in Chapter 4. The amount of ADV data gathered was quite exhaustive therefore not all information could be presented in this document but is available upon request.

The results of the physical modeling of the *TAS* generally fall into two categories: ADV velocity point data, forming velocity profiles, and power estimates produced using Actuator Disc Theory. In the first

stage of testing no plates were present and therefore the objective was solely the optimisation of the *TAS* shape and the measurement of the flow field surrounding the *TAS*. The velocity profiles gathered are shown in Chapter 4 and their locations are described by Figure 4-7 and Figure 4-8. The vertical velocity profiles of all tests during Stage 1 are shown in Figure 4-19 with the structure configurations showing drastically different velocities depending on their opening and contraction widths. The velocities vary from 0.15 m/s (no acceleration of flow through *TAS*) to over 0.27 m/s. Figure 4-29 illustrated the flow speed-up through the *TAS* centre, with some structures only accelerating the flow by a factor of 1.24 where as the best performing structure, the *10contr_25open_crv1,* sped-up the flow by a factor of 2.12. This proves that structure shape greatly influences the performance of the *TAS*. In terms of possible improvements for future testing schemes, the amount of ADV points collected during Stage 1 was perhaps too high as the main objective was the maximisation of the velocity at the centre of the structure. The optimisation could have been done faster if only the velocity at the centre of the *TAS* was measured but this would not have allowed for the analysis of anomalies in the velocity data, which did occur as demonstrated by some unusual velocity profiles (see Figure 4-19, *10contr_30open_str*). The irregularities in the results were most likely due to flow variations in the flume pump but might not have been noticed if less data points had been taken.

In Stage 2 several of the better performing structure configurations from Stage 1 were tested in conjunction with the three porous plates and therefore both velocity (profiles same as Stage 1) and power estimates were produced. As mentioned porous plates were mounted to a load cell, similarly to (Sun 2008), and using Equation **(2-7)** from Actuator Disc Theory (Burton et al. 2011), power estimates were produced. For this, the velocities at the discs had to be estimated using velocities upstream of the plate position and by considering the volume of water inside the *TAS* as being contained in a stream-tube of constant flowrate. This estimation of velocity has its sources of error, including the possibilities that the velocity is not constant across the width of the *TAS* interior and that the water surface elevation

changes slightly near the position of the plate. Despite this, the estimation was thought to be the most precise method possible with the equipment available. Perhaps the use of more advanced velocity instrumentation such as particle image velocimetry could have improved the estimation of the average velocity at the disc. The same Equation **(2-7)** was used for the estimation of the power available in flow; however, the free stream velocities at the centre of the *TAS* in the corresponding tests without plates were used instead of the estimation of the velocity through the disc. In comparing the estimated power extracted from the disc and the estimated power available in flow, a power efficiency value (C_p) was also computed using Equation **(4-11)**. All the Stage 2 and 3 power estimate results are shown in Table 4-7. By evaluating this table one can see that the power efficiency values (extracted power over available power) are quite low, ranging from 15% to 47%, with the average value being between 20% - 30%. This is an indication that the plate-*TAS* combinations were not very effective for the most part in capturing the energy available in flow. As discussed in Chapter 4, this was most likely due to the fact that the blockage effect of the plates was too high, in essence the porosity of the plates was too low. To test this hypothesis an additional test was performed with the 10 cm wide plate but instead of having the plate occupy the whole width of the contraction, spaces were left on each side of the plate to see if a larger extracted power value could be attained. As shown in Table 4-7, the power efficiency of this test was much higher, at 51% it was the test with the highest C_p value. Compared to the stand-alone 10 cm wide plate (plate tested without a *TAS*), the *17p5contr_35open_str TAS* with the 10 cm wide plate was estimated to be able to extract 4.2 times the power. Despite the fact that the porosity of the plates was most likely too low (resulting in low C_p values), the best tests were able to extract 3.5, 3.1 and 2.7 times more power than the 10, 15 and 20 cm wide stand-alone plate tests alone (respectively). These values are significant in that they indicate that even a non-optimised *TAS*-plate arrangement has a significant advantage over stand-alone devices (such as in typical in-stream turbines).

Figure 4-10 and Figure 4-12 show the more detailed velocity profile locations which were gathered during Stage 3, the stage conducted to verify the results of the *10contr_25open_str* configuration, both with and without the presence of the 10 cm wide, 58% porosity plate. The comparison between the results of Stage 1 – Stage 3 and Stage 2- Stage 3 showed excellent agreement as demonstrated by Figure 4-30, Figure 4-31 and Figure 4-32. This was a favourable sign for the accuracy of the results as a whole. They were further compared with the Fluent numerical results in Section 5.3.3

6.2. Numerical Modeling of the TAS and Results Comparison

As described in Chapter 5, the numerical work consisted of both 2D and 3D simulations. The 2D numerical simulations were performed using Hemat 2D, a program developed by Dr. Mohammadian, a research supervisor of the current project. As the 2D Hemat work was only a preliminary project, the optimised *TAS* was not used for comparison with the experimental or 3D Fluent results. The 2D work was important however as it did produce the rough structure dimensions which were used at the beginning of the experimental optimisation and set the precedent for the optimisation methodology which was used in the experimental testing as well.

As described in Section 5.3, Fluent was chosen for the 3D numerical work and the main objective of this aspect of the project was the calibration of a model against the experimental results which could then be used to simulate the *TAS* at full scale and with the presence of an energy sink similar to a turbine. The model was validated by comparing the velocity profiles from the *10contr_25open_str* configuration Stage 1 and 3 tests to Fluent results. The model parameters including the solver, boundary conditions and spatial discretization types, were all varied before settling on a final setup which was able to produce a converged solution similar to the experimental case. The final simulation had a mesh of 1.35 million elements and used the K-Omega SST turbulence model. As shown in Figure 5-20, Figure 5-21 and Figure 5-22, the Fluent simulation results were very similar to those of the *10contr_25open_str* no-plate

case from Stages 1 and 3. The only major discrepancy between the numerical and experimental velocity profiles was the wake downstream of the *TAS* centre. The wake recovered faster in the numerical simulation compared to the experimental case, and this was speculated to be due to the nature of the turbulence formed as flow passed through the *TAS*. Further testing of numerical parameters such as inlet turbulence intensity or the turbulence model could have perhaps improved this disagreement if time allowed. The 3D Fluent numerical model still reproduced the main parameters of interest (velocity through *TAS* centre, velocity at centre of flume) therefore the model is considered as validated for future numerical work involving the *TAS*.

6.3. Future Work

By analysing the results presented in this dissertation, it is clear that the *TAS* concept is a promising idea to help exploit tidal and river locations with flows currently too slow for economic power production. Much work remains to be done before any future site prototype can be constructed however, including a detailed analysis of all costs involved to ensure that the construction of a *TAS* is justified. As the present project yielded without a doubt the ability of the *TAS* to greatly accelerate flows, the next logical step in proving the concept would be to construct another larger model to be used in conjunction with a small-scale in-stream turbine prototype. This way the performance of the stand-alone device could be compared directly with that of a *TAS*-turbine combination for the same flow conditions or even for a full tidal cycle. To accomplish this it is obvious that a larger flume or some other sort of test facility (such as a tow-tank, channel or natural river) is needed. Though it was not verified in the current project, it is also suspected that the *TAS* is able to reduce the peak forces acting on the turbines by straightening the incoming flow and eliminating turbulence therefore this would be another benefit to test with a larger scale model. As the current project was conducted within the University of Ottawa, and the 1.5 m wide flume was the widest available, it is probable that a partner institution or company is needed to further the *TAS* concept validation. Potential partners for this work could also include a tidal turbine

manufacturer as the *TAS* can feasibly be used in conjunction with any turbine type. The testing of the turbine in conjunction with the *TAS* could expand the sites where the turbine could be deployed to slower waters, thus opening up markets that were not previously thought possible.

More immediate future work at the University of Ottawa will focus on continuing the 3D Fluent simulations, including a simulation of the *TAS* for the planned full-scale flow conditions (1 m/s, 15 m depth) and a Fluent simulation with a turbine being represented by the *Porous Jump Model*. Plans are also underway to investigate the impact of parameters such as seabed roughness, side-wall geometry, symmetry plane use and higher order turbulence schemes such as the second order LLR model. Furthermore, the depth-averaged 2D Hemat simulations will be compared in greater detail with the experimental and 3D numerical results. Beyond that, all future research avenues for the development of the *TAS* are still open.

Chapter 7. Conclusions

The existing literature on tidal energy has been explored and it was found that though several in-stream devices are in development, key challenges still remain for the tidal energy industry namely the economics of tidal power versus other renewable energies. A new concept, a channeling device entitled the Tidal Acceleration Structure or *TAS*, has been proposed as a method of enhancing the velocity of the flow entering an in-stream turbine area. Key differences between the concept and existing channeling devices include the fact that the *TAS* is a large structure, with walls extending from the seafloor to above the high water mark and the aspect that it is a non-turbine specific design meant for two-way flows.

The testing of the *TAS* concept was completed using two types of schemes, numerical (2D and 3D) and experimental. A *TAS* model was successfully tested in a 1.5 m wide flume at the University of Ottawa with the work focused on observing the Venturi Effect and other flow phenomena around the *TAS* and optimising the structure shape in the hopes of maximising velocity through its centre and the associated power which could be extracted using a porous plate. Using an analysis of previous literature regarding both tidal and wind turbines, the Actuator Disc Theory method of turbine simulation (using porous plates) was found as adequate for testing with the *TAS*. The use of porous plates was justified by analysing existing literature regarding both tidal and wind turbines. The experimental work proved successful and detailed flow fields were recorded using an ADV for numerous *TAS* configurations. This allowed for the methodological improvement of the design with the chosen scaled flow conditions (14.14 cm/s, 30 cm depth – corresponding to 1 m/s and 15 m depth at full-scale). Using this method, *TAS* designs yielding flow accelerations of as much as 2.12 times were found. Using the porous plates in conjunction with the best *TAS* designs, the power extracted by the plates was measured and some designs were found to be able to increase the power output of the plates by as much as 4.2 times compared to stand-alone plates (3.5 times in the best case where the plate occupied the full contraction

width). It was also concluded by analysing the power results that the porosity chosen for the plates (58%) was too low and resulted in too much flow blockage. It is therefore recommended that this be further investigated in future testing schemes.

The numerical work was divided into 2D modeling using the Hemat-2D program and 3D modeling using ANSYS Fluent. The 2D Hemat simulations were focused on optimising a basic *TAS* design and the configuration which was yielded formed the basis of the experimental *TAS* model. Though the results from the 2D tests were not compared with the experimental results, the work was still considered a success and was a vital first step in the validation of the *TAS* concept. The 3D Fluent work was focused on validating the model against the experimental results. The final setup utilised the VOF model in conjunction with the K-Omega SST turbulence model. Comparisons between the 3D numerical and two sets of experimental results for the *10contr_25open_str* no-plate configuration yielded excellent agreement. This validated both the replicability of the results (in comparing the two experimental data sets) and the validity of the numerical setup for use in future numerical testing.

Overall, the experimental and numerical modeling of the tidal energy channeling structure should be considered a success as significant knowledge of the concept was gained. As a whole, the present work demonstrated that the *TAS* is a promising technology with the potential to expand our use of the ocean's currents for renewable power production.

References

ANSYS. (2010). “FLUENT Theory Guide.” *Release 13.0*, ANSYS Inc.

ANSYS. (2010). “FLUENT User’s Guide.” *Release 13.0*, ANSYS Inc.

Bahaj, A., Myers, L., Thomson, M., and Jorge, N. (2007). "Characterising the wake of horizontal axis marine current turbines." *Proc.7th EWTEC*.

Bahaj, A. S. (2011). "Generating electricity from the oceans." *Renewable and Sustainable Energy Reviews,* 15(7), 3399-3416.

Batchelor, G. K. (2000). *An introduction to fluid dynamics.* Cambridge university press.

Bedard, R., Previsic, M., Siddiqui, O., Hagerman, G., and Robinson, M. (2005). "Survey and characterization tidal in stream energy conversion (TISEC) devices." *EPRI North American Tidal in Stream Power Feasibility Demonstration Project*.

Black and Veatch Consulting Ltd. (2004). "Uk, Europe and global tidal stream energy resource assessment." *Rep. No. 107799/D/2100/05/1,* Carbon Trust, London.

Burton, T., Jenkins, N., Sharpe, D., and Bossanyi, E. (2011). *Wind energy handbook.* John Wiley & Sons.

Clarke, J., Connor, G., Grant, A., and Johnstone, C. (2006). "Regulating the output characteristics of tidal current power stations to facilitate better base load matching over the lunar cycle." *Renewable Energy,* 31(2), 173-180.

Cornett, A. (2006). "Inventory of Canada's Marine Renewable Energy Resources." *Rep. No. CHC-TR-041,* National Research Coucil Canada.

Cousineau, J. (2012). *Hydrodynamic Impacts of Tidal Lagoons in the Upper Bay of Fundy*.

Cousineau, J., Nistor, I., and Cornett, A. (2012). "Hydrodynamic impacts of tidal power lagoons in the Bay of Fundy." *Coastal Engineering Proceedings,* 1(33), management. 69.

Ettema, R. (2000). *Hydraulic modeling: Concepts and practice.* ASCE Publications.

Foran, D., Infante, J., Le, S., MacKechnie, B., Mohammadian, M., Moilwa, k. G., Nistor, I., and Toupin, M. (2012). "Tidal Acceleration Generator: Final Design Report." University of Ottawa, Ottawa, Canada.

Fraenkel, P. L. (2006). "Tidal current energy technologies." *Ibis,* 148(s1), 145-151.

Froude, R. (1889). "On the part played in propulsion by differences of fluid pressure." *Transactions of the Institute of Naval Architects,* 30 390-405.

Gaden, D. L., and Bibeau, E. L. (2010). "A numerical investigation into the effect of diffusers on the performance of hydro kinetic turbines using a validated momentum source turbine model." *Renewable Energy,* 35(6), 1152-1158.

Garrett, C. (1974). "Normal modes of the Bay of Fundy and Gulf of Maine." *Canadian Journal of Earth Sciences,* 11(4), 549-556.

Harrison, M., Batten, W., Myers, L., and Bahaj, A. (2010). "Comparison between CFD simulations and experiments for predicting the far wake of horizontal axis tidal turbines." *IET Renewable Power Generation,* 4(6), 613-627.

Hicks, S. D., and Szabados, M. W. (2006). *Understanding tides.* US Department of Commerce, National Oceanic and Atmospheric Administration, National Ocean Service.

Khan, M., Bhuyan, G., Iqbal, M., and Quaicoe, J. (2009). "Hydrokinetic energy conversion systems and assessment of horizontal and vertical axis turbines for river and tidal applications: A technology status review." *Appl.Energy,* 86(10), 1823-1835.

Kheradmand, S., Mineault-Guitard, A., Mohammadian, A., Rennie, C., and Seidou, O. (2015). "Performance of a well-balanced scheme for two case studies in Canada." unpublished.

Kim, K., Ahmed, M. R., and Lee, Y. (2012). "Efficiency improvement of a tidal current turbine utilizing a larger area of channel." *Renewable Energy,* 48 557-564.

Kirke, B. (2006). "Developments in ducted water current turbines." *Tidal Paper,* (25-04).

MacQuarrie, J. A. (2011). "Aerodynamic optimization of building augmented wind turbines.

Mikkelsen, R. (2003). *Actuator Disc Methods Applied to Wind Turbines*.

Mohammadian, A., and Le Roux, D. (2006). "Simulation of shallow flows over variable topographies using unstructured grids." *Int.J.Numer.Methods Fluids,* 52(5), 473-498.

Mohammadian, A., Le Roux, D., Tajrishi, M., and Mazaheri, K. (2005). "A mass conservative scheme for simulating shallow flows over variable topographies using unstructured grid." *Adv.Water Resour.,* 28(5), 523-539.

Myers, L., and Bahaj, A. (2010). "Experimental analysis of the flow field around horizontal axis tidal turbines by use of scale mesh disk rotor simulators." *Ocean Eng.,* 37(2), 218-227.

Nortek. (2009). "Vectrino Velocimeter User Guide.

Ohya, Y., and Karasudani, T. (2010). "A shrouded wind turbine generating high output power with wind-lens technology." *Energies,* 3(4), 634-649.

Parker, B. B. (1991). *Tidal hydrodynamics.* John Wiley & Sons.

Pedlosky, J. (1987). "Inviscid shallow-water theory." *Geophysical fluid dynamics,* Springer, 57-178.

Ponta, F., and Shankar Dutt, G. (2000). "An improved vertical-axis water-current turbine incorporating a channelling device." *Renewable Energy,* 20(2), 223-241.

Ponta, F., and Jacovkis, P. (2008). "Marine-current power generation by diffuser-augmented floating hydro-turbines." *Renewable Energy,* 33(4), 665-673.

Robertson, S. (2014). "Strategic Innovation Acceleration - UK marine energy industry: pathway to commercialisation." *International Conference on Ocean Energy*.

Roc, T. (2013). "Numerical Modelling for Hydrodynamic Impact and Power Assessments of Tidal Current Turbine Arrays."

Schwartz, M. (2006). *Encyclopedia of coastal science.* Springer.

Setoguchi, T., Shiomi, N., and Kaneko, K. (2004). "Development of two-way diffuser for fluid energy conversion system." *Renewable Energy,* 29(10), 1757-1771.

Sharpe, D. (2004). "A general momentum theory applied to an energy-extracting actuator disc." *Wind Energy,* 7(3), 177-188.

Sireli, E. M. (2014). "Design Implications of Ducts on Horizontal Axis Turbines." *The Journal of Ocean Technology,* 9(2), 68-91.

Sørensen, J. N., and Myken, A. (1992). "Unsteady actuator disc model for horizontal axis wind turbines." *J.Wind Eng.Ind.Aerodyn.,* 39(1), 139-149.

Spain, R. (2002). "A possible Roman tide mill." *Kent Archaeological Society, Paper,* 5.

Sun, X. (2008). "Numerical and experimental investigation of tidal current energy extraction."

Taylor, G. I. (1971). *The Scientific Papers of Sir Geoffrey Ingram Taylor: Volume 4, Mechanics of Fluids: Miscellaneous Papers.* Cambridge University Press.

Venturi, G. B. (1799). *Experimental Enquiries Concerning the Principle of the Lateral Communication of Motion in Fluids: Applied to the Explanation of Various Hydraulic Phenomena. By Citizen JB Venturi, Prosessor of Natural Philosophy at Modena, Member of the Italian Society, of the Institute of Bologna, of the Agrarian Society of Turin, &c. Translated from the French.* J. Taylor, at the Architectural Library, High-Holborn.

Whelan, J., Thomson, M., Graham, J., and Peiro, J. (2007). "Modelling of free surface proximity and wave induced velocities around a horizontal axis tidal stream turbine." *Proceedings of the 7th European Wave and Tidal Energy Conference*.

Zhou, J. G., Causon, D. M., Mingham, C. G., and Ingram, D. M. (2001). "The surface gradient method for the treatment of source terms in the shallow-water equations." *Journal of Computational Physics,* 168(1), 1-25.

Appendix I: Froude Scale Calculations

Choosing a length ratio of 1:50, the velocity ratio is computed as follows using Equation **(4-4)**:

$$\lambda_V = \sqrt{\lambda_L} = \sqrt{\frac{1}{50}} = 0.14142$$

The model velocity is therefore:

$$V_{model} = V_{prototype} * \lambda_V = 1 * 0.14142 = \mathbf{0.14142\ m/s}$$

Appendix II: ADV Data Filtering Matlab Code

Note : Code attributed to Dr. Colin Rennie of the University of Ottawa

```
%assume water temperature in lab is 20degC, therefore

rho=998;%density of water in kg/m3, (note temp changed from 18degC to 22degC during run

writematrixall=[];

%this file will process Vectrino .dat files

%load file

%Mikes note: files must begin with alphabetic character for this script to

%work properly



filename={'C3'};

%Note you can add more file names to run several files one after the other.


% All results data for all files are stored in writematrixall (see line 95

% for what is stored)



for p=1:length(filename)

filescript = ['load ' filename{p} '.dat -ASCII'];

eval(filescript)


dummy=['tvec=' filename{p} '(:,1);'];

eval(dummy);

dummy=['vx=' filename{p} '(:,3);'];

eval(dummy);

dummy=['vy=' filename{p} '(:,4);'];%note vy follows right-hand rule with x forward and z vertical

eval(dummy);

dummy=['vz1=' filename{p} '(:,5);'];

eval(dummy);

dummy=['vz2=' filename{p} '(:,6);'];
```

```
eval(dummy);
dummy=['amp1x=' filename{p} '(:,7);'];
eval(dummy);
dummy=['amp2y=' filename{p} '(:,8);'];
eval(dummy);
dummy=['amp3z=' filename{p} '(:,9);'];
eval(dummy);
dummy=['amp4w=' filename{p} '(:,10);'];
eval(dummy);
dummy=['snr1x=' filename{p} '(:,11);'];
eval(dummy);
dummy=['snr2y=' filename{p} '(:,12);'];
eval(dummy);
dummy=['snr3z=' filename{p} '(:,13);'];
eval(dummy);
dummy=['snr4w=' filename{p} '(:,14);'];
eval(dummy);
dummy=['cor1x=' filename{p} '(:,15);'];
eval(dummy);
dummy=['cor2y=' filename{p} '(:,16);'];
eval(dummy);
dummy=['cor3z=' filename{p} '(:,17);'];
eval(dummy);
dummy=['cor4w=' filename{p} '(:,18);'];
eval(dummy);

figure
plot(snr1x)
ylabel('SNR1x')
title([filename{p} ' SNR beam 1'])
figure
plot(amp1x)
ylabel('amp1x')
```

```
title([filename{p} ' amplitude beam 1'])
figure
plot(cor1x)
title([filename{p} ' correlation beam 1'])

headerscript = ['FID = fopen( ''' filename{p} '.hdr'')'];
eval(headerscript)
for k=1:80
fgetl(FID);
end
advhead=fgetl(FID);
fclose(FID);

advheadnum=str2num(advhead(end-3:end));



%based on which adv, correct for twist of probe head.  The actual
%correction will occur after initial filtering in processVectrinocore
%Mike's note: it's not getting the 'advheadnum' value
xyrotate=0;
if advheadnum==7059
   xyrotate=2.658*pi/180;
elseif advheadnum==7047
   xyrotate=2.194*pi/180;
elseif advheadnum==7055
   xyrotate=2.497*pi/180;
end

timestep=tvec(2)-tvec(1);

if advheadnum==7857 %ie side looking ADV without duplicate vertical velocity
   processVectrinocoresidelooker
else
```

```
    processVectrinocore
end

spectralVectrinofinalfiltnoisebatch %does spectral analysis, and low pass filters data if noise observed in spectrum

Vectrinooutput%note this calculates the turbulence scales, as well as the reynstresses again in case the Vectrino data were low-pass filtered
(Vectorfiltflag=1)

writematrix=[meanxraw meanyraw meanzraw uwreynstressraw uvreynstressraw vwreynstressraw xrmsraw turbintxraw yrmsraw turbintyraw
zrmsraw turbintzraw turbkinenergyraw meanxdespike meanydespike meanzdespike uwreynstressdespike uvreynstressdespike
vwreynstressdespike xrmsdespike turbintxdespike yrmsdespike turbintydespike zrmsdespike turbintzdespike turbkinenergydespike
Vectorfiltflag noisevx meanxfilt meanyfilt meanzfilt uwreynstressfilt uvreynstressfilt vwreynstressfilt xrmsfilt turbintxfilt yrmsfilt turbintyfilt
zrmsfilt turbintzfilt turbkinenergyfilt integraltimescale microtime integrallengthscale microlengthscale taylormicrolength integraltimescaley
microtimey integrallengthscaley microlengthscaley taylormicrolengthy integraltimescalez microtimez integrallengthscalez microlengthscalez
taylormicrolengthz];

writematrixall=[writematrixall; writematrix];

save VectrinoOutput writematrixall filename rho p
clear
load VectrinoOutput

end

xlswrite('VectrinoOutput',writematrixall)
```

Appendix III: Turbine Simulator Plans - AutoCAD Drawings

Note: All dimensions in inches unless otherwise specified. Inches used due to technician familiarity with Imperial units.

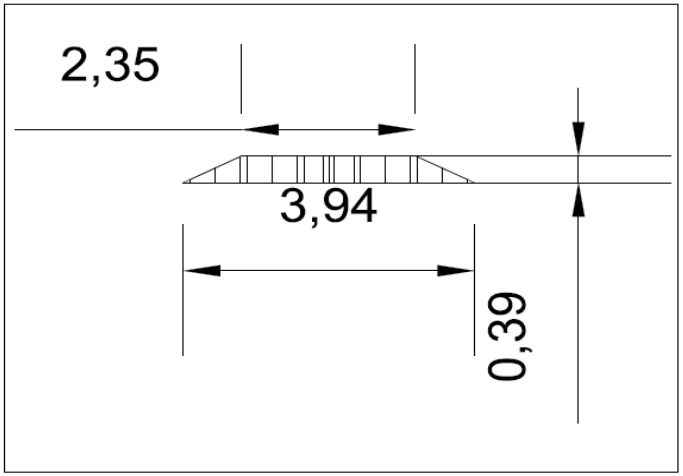

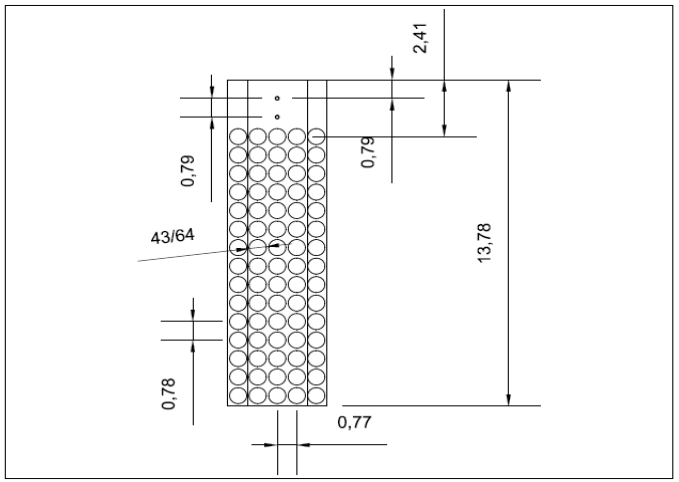

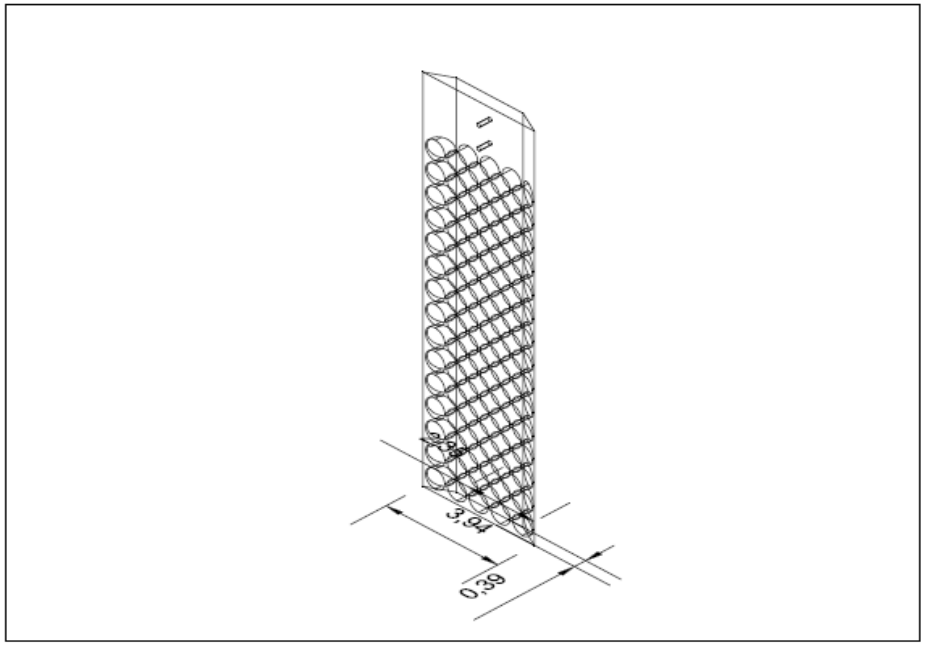

Holed test plate (100 mm width)

Top view – 3D view – Front view

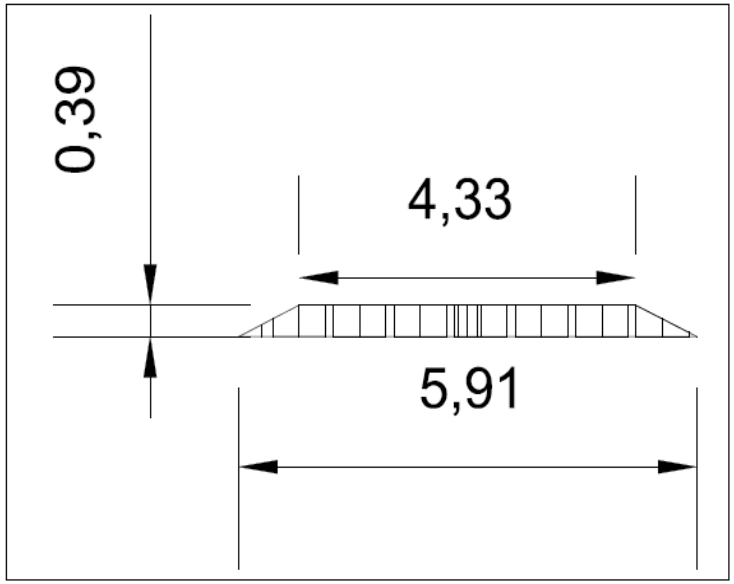

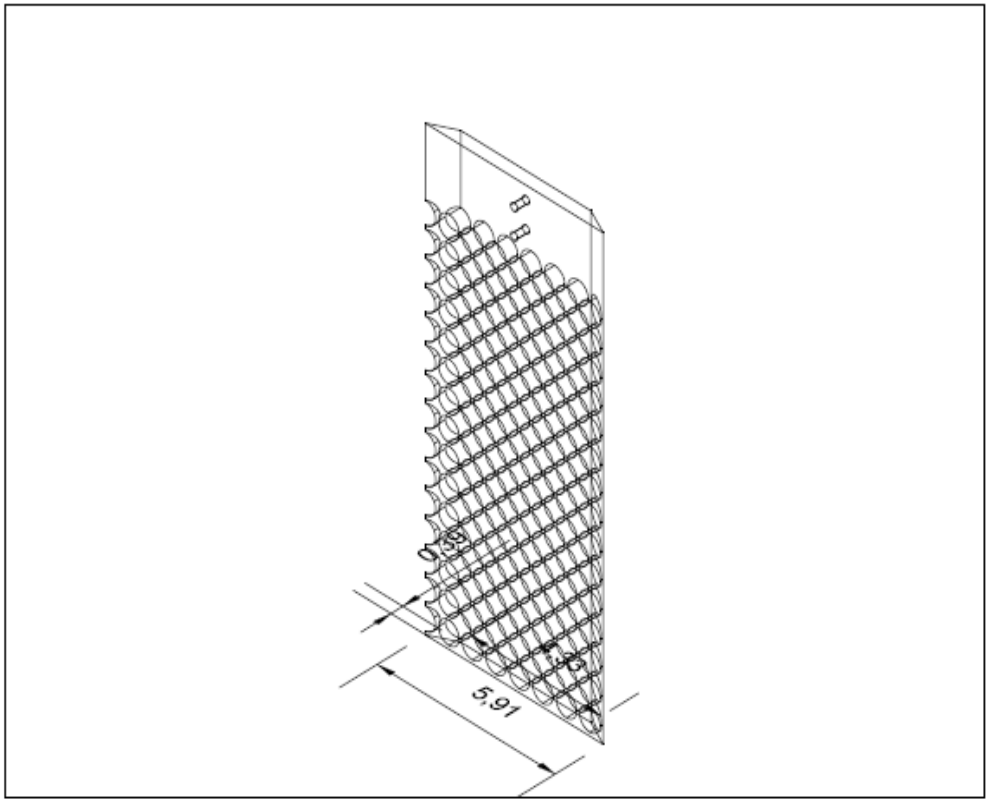

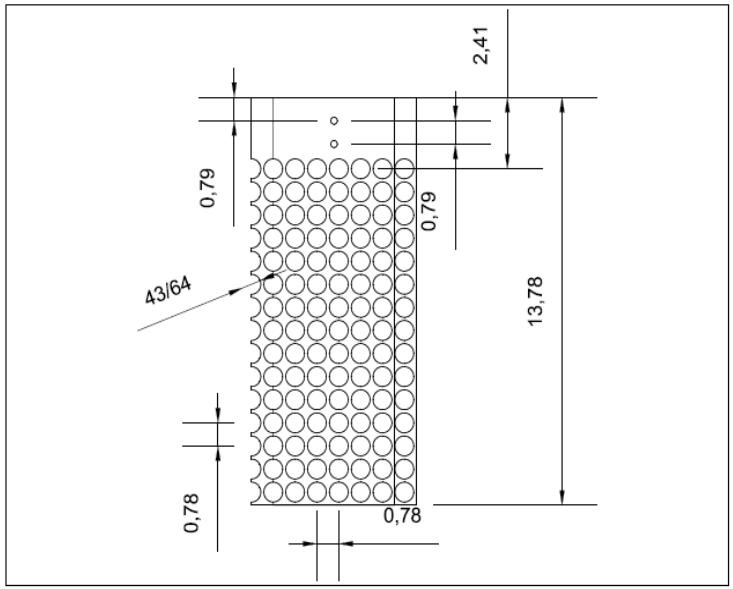

Holed test plate (150 mm width)

Top view – 3D view – Front view

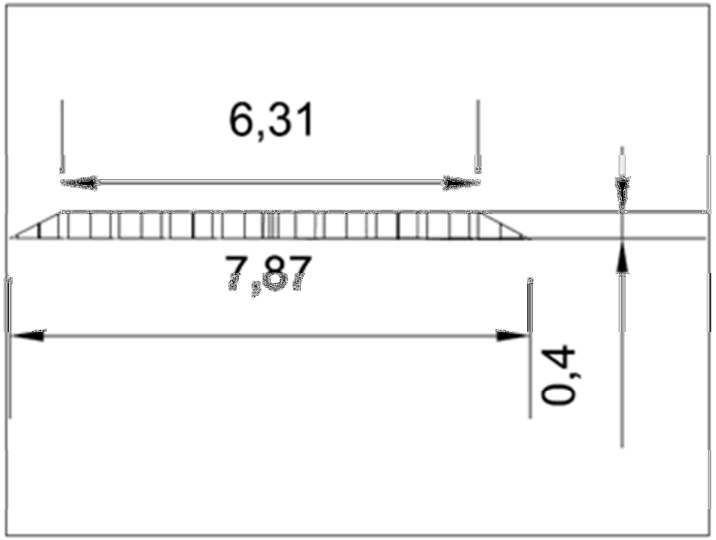

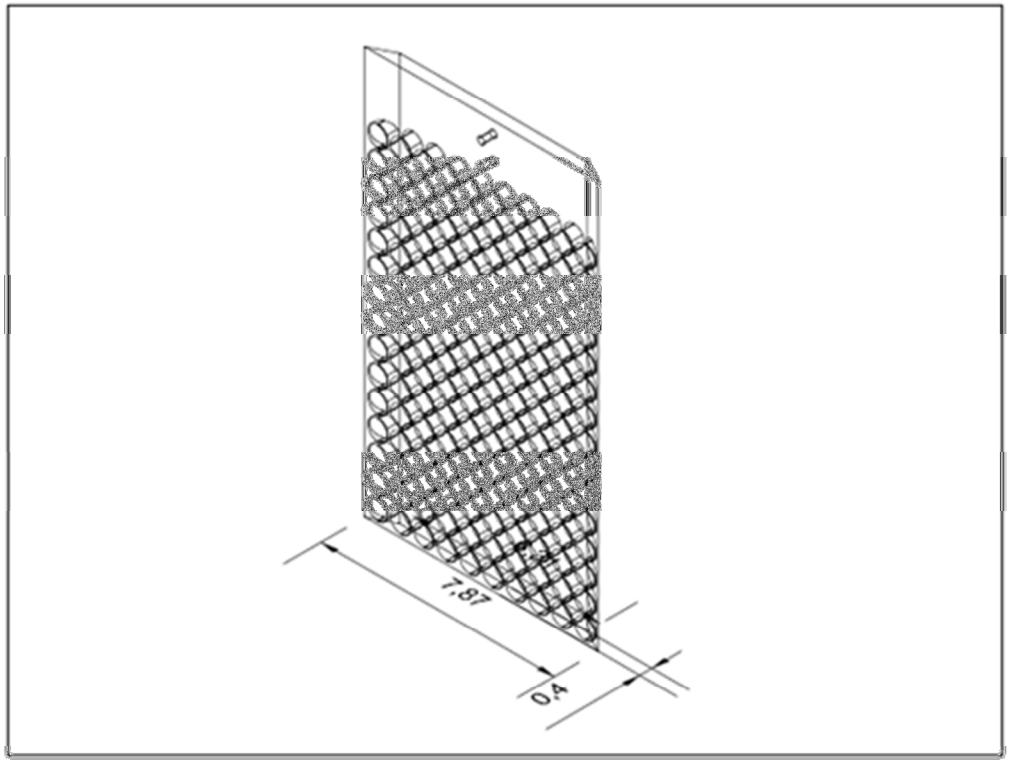

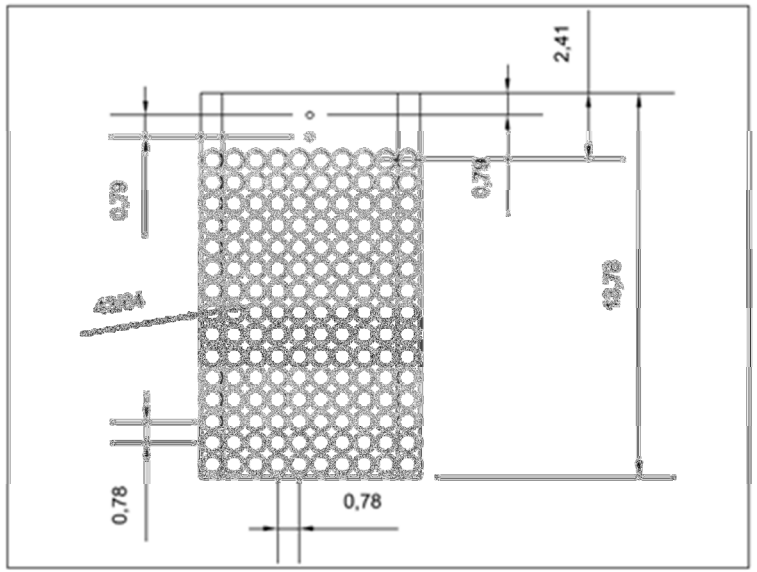

Holed test plate (200 mm width)

Top view – 3D view – Front view

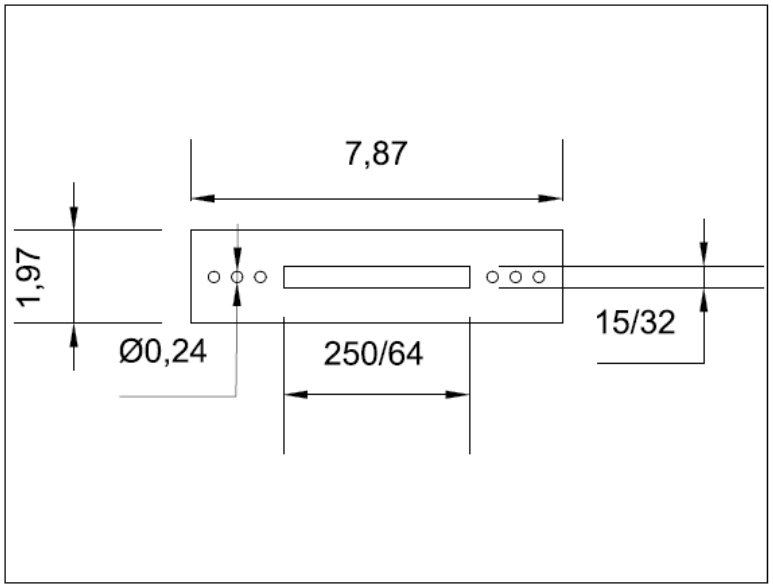

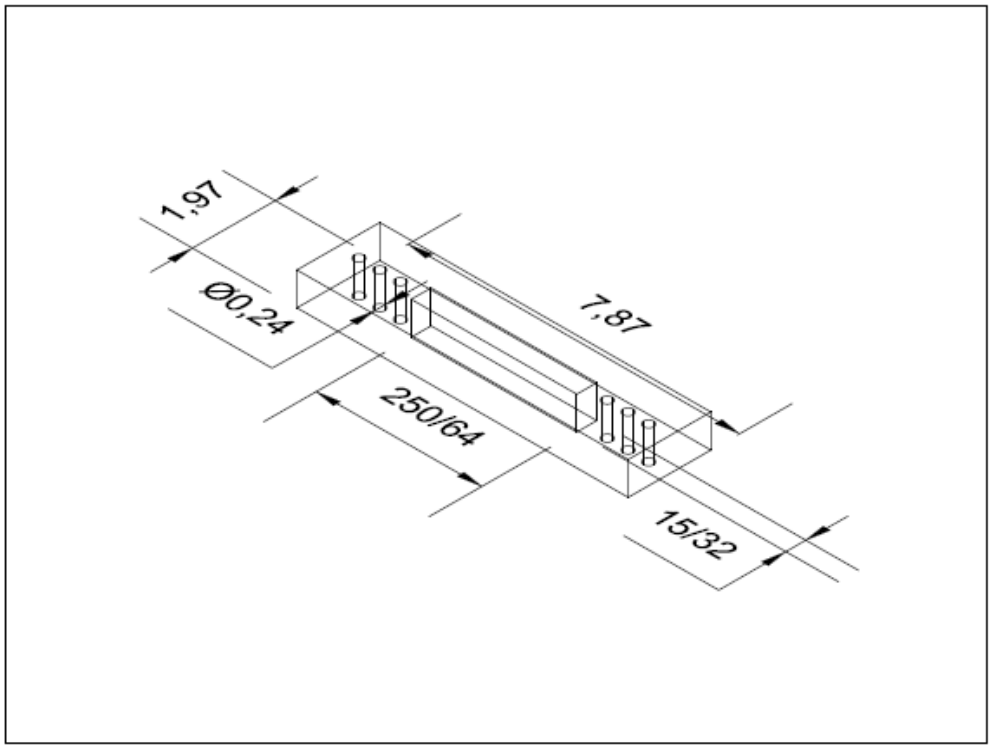

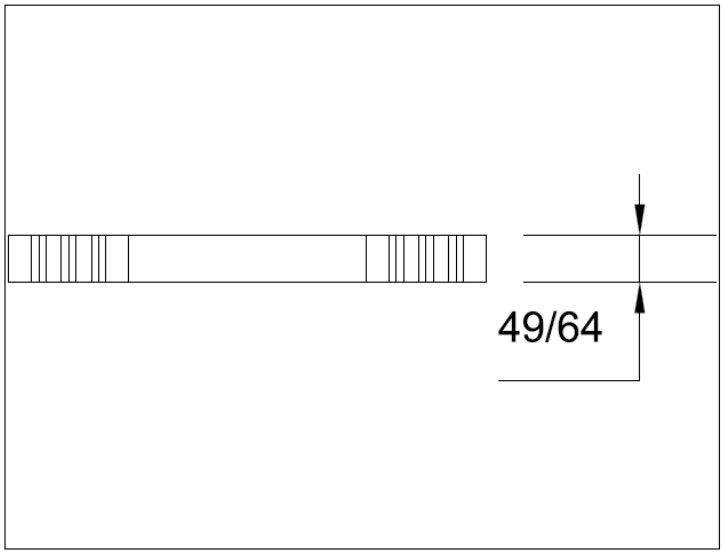

Parallel support bars

Top view – 3D view – Front view

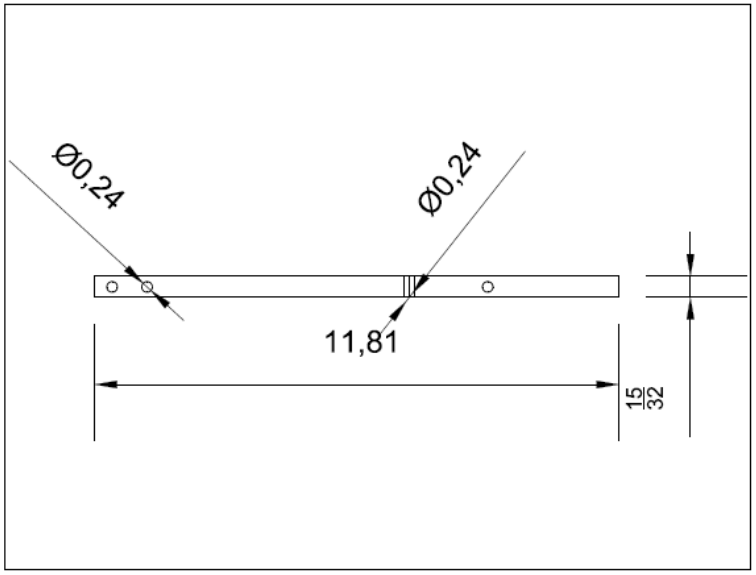

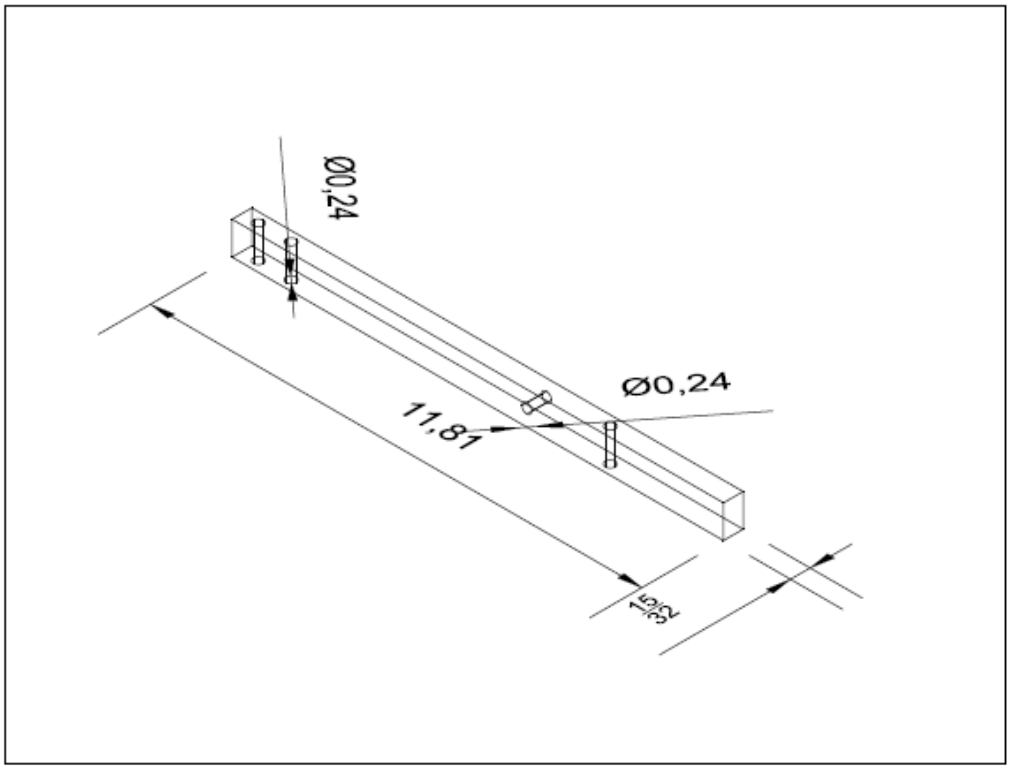

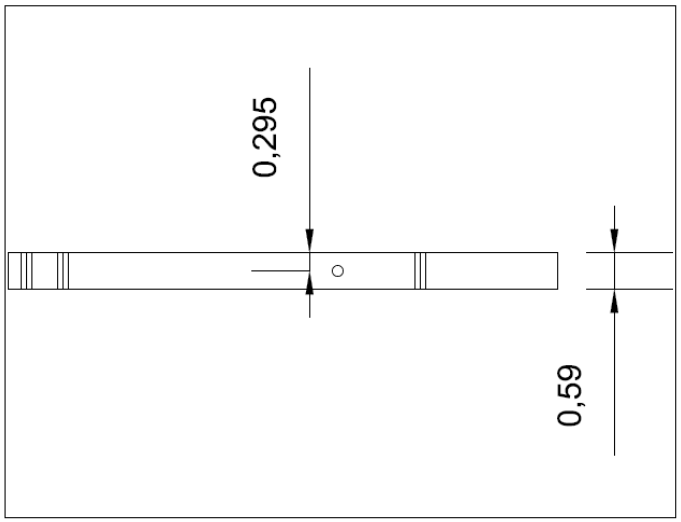

Support strut

Top view – 3D view – Front view

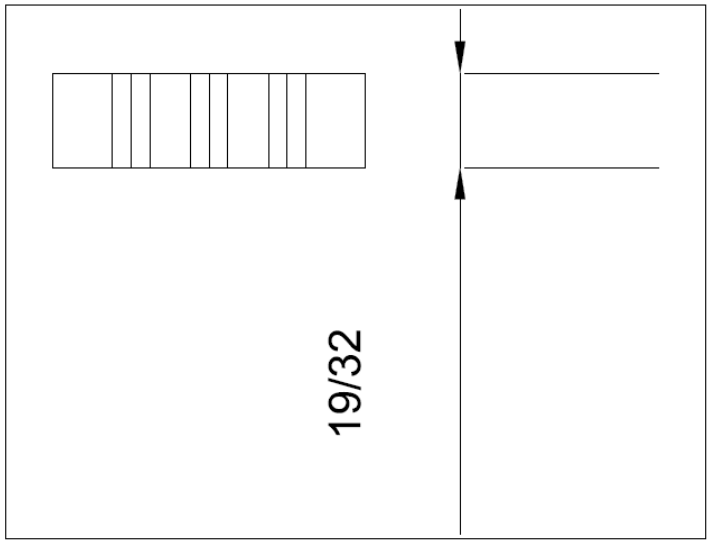

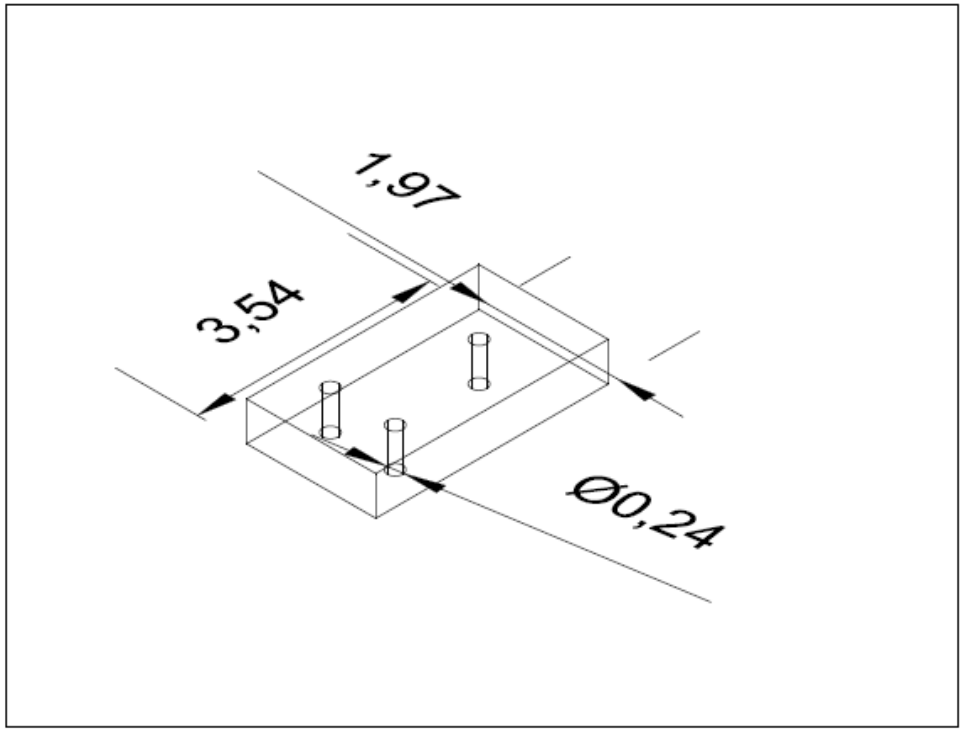

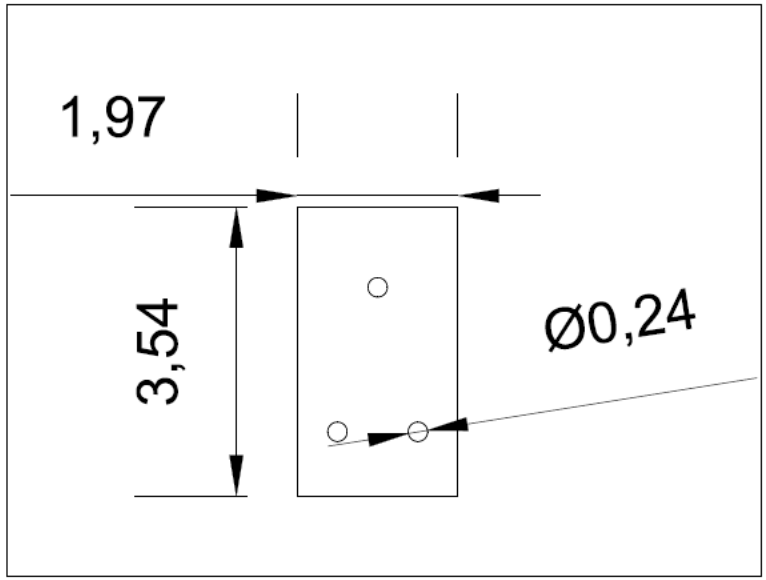

Load cell bracing support

Top view – 3D view – Front view

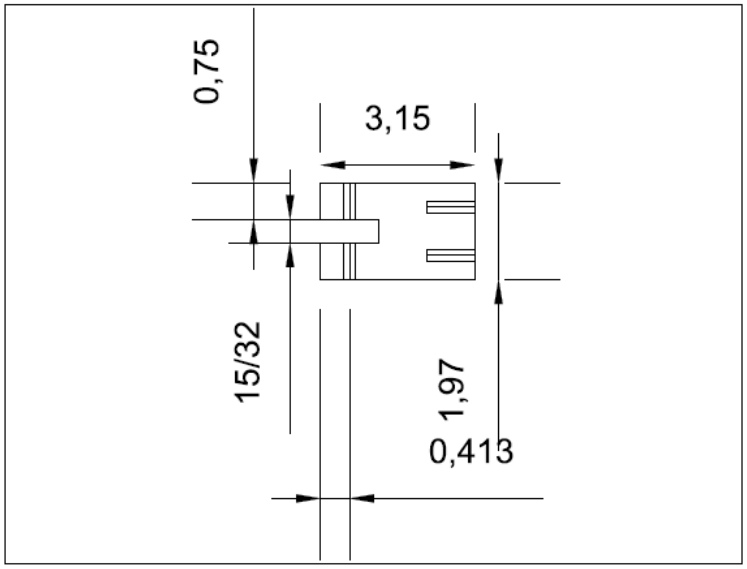

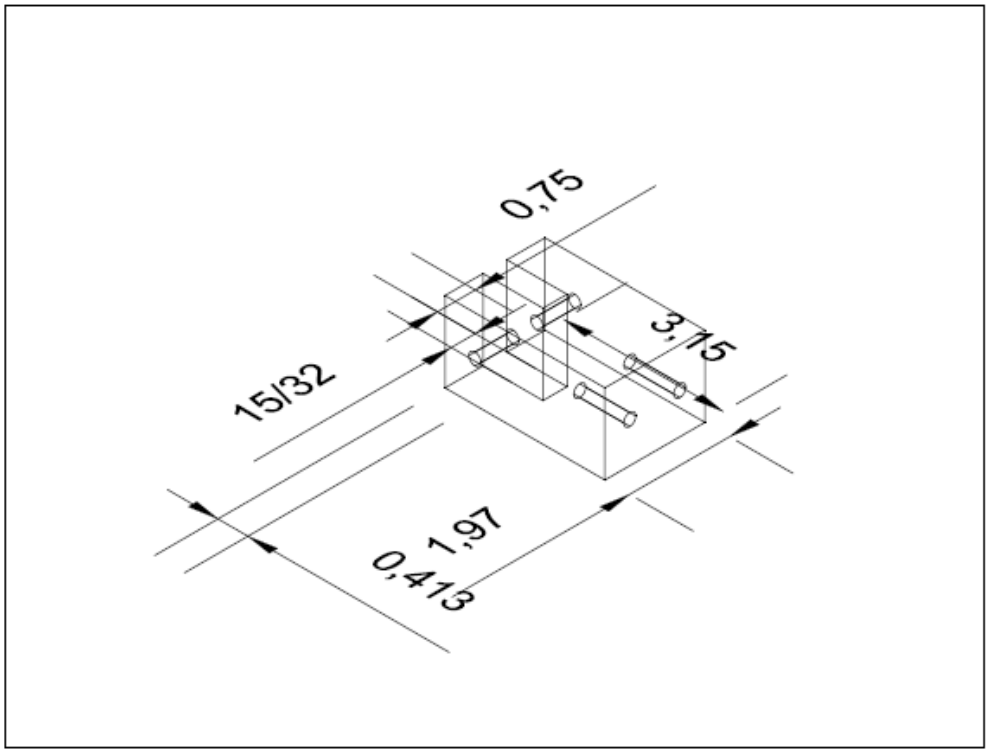

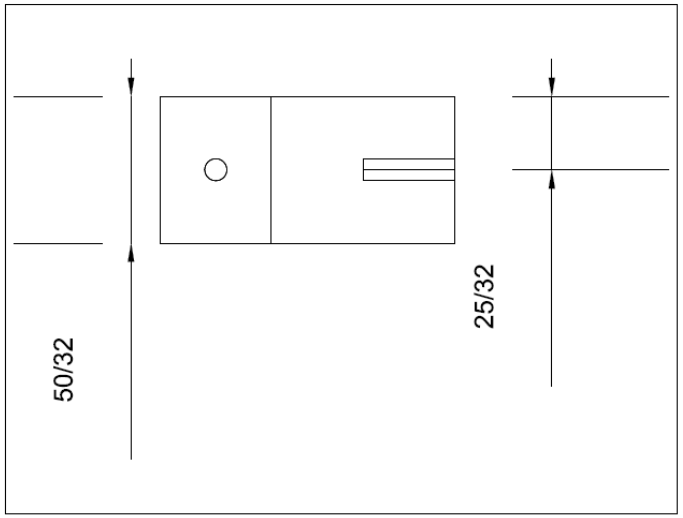

Bottom load cell support

Top view – 3D view – Front view

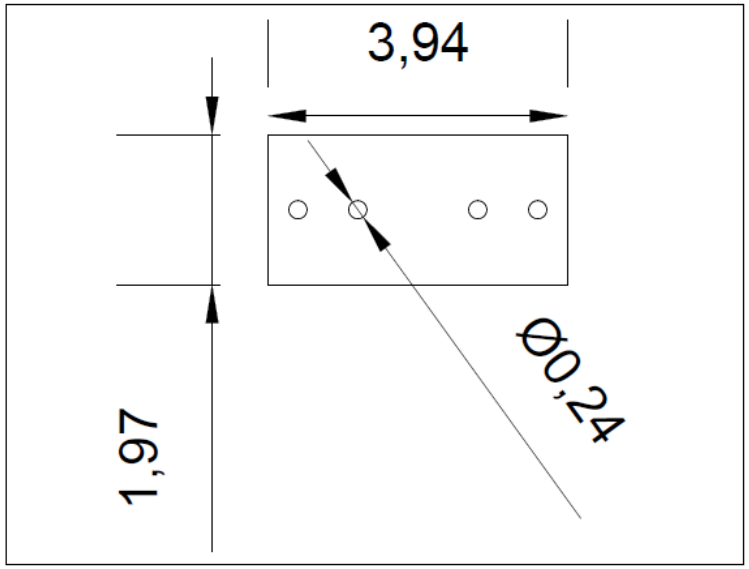

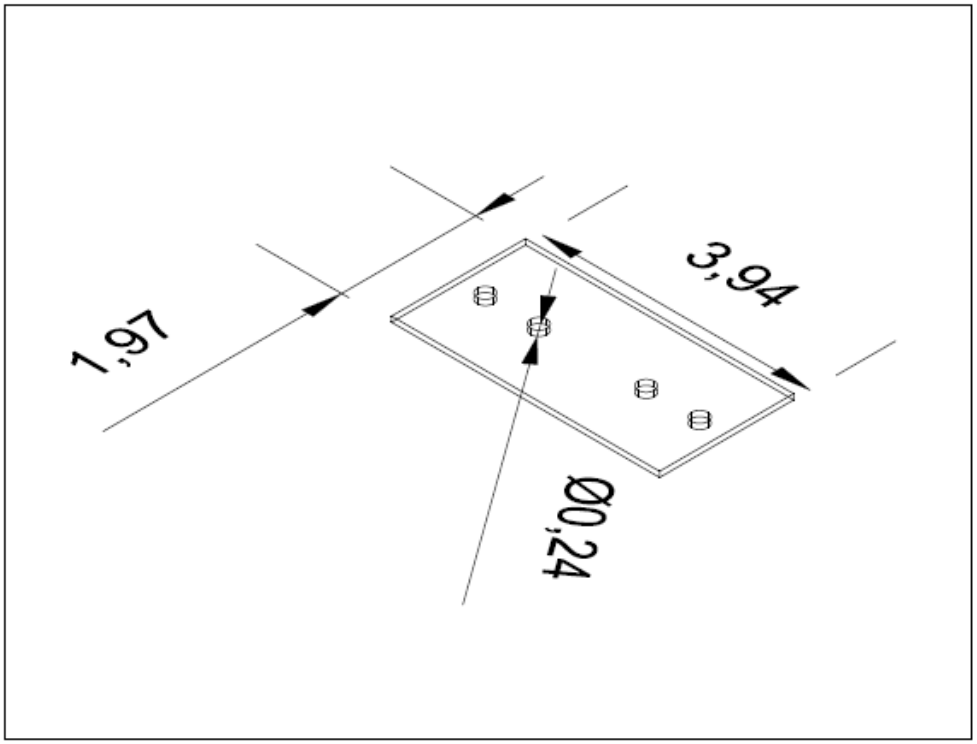

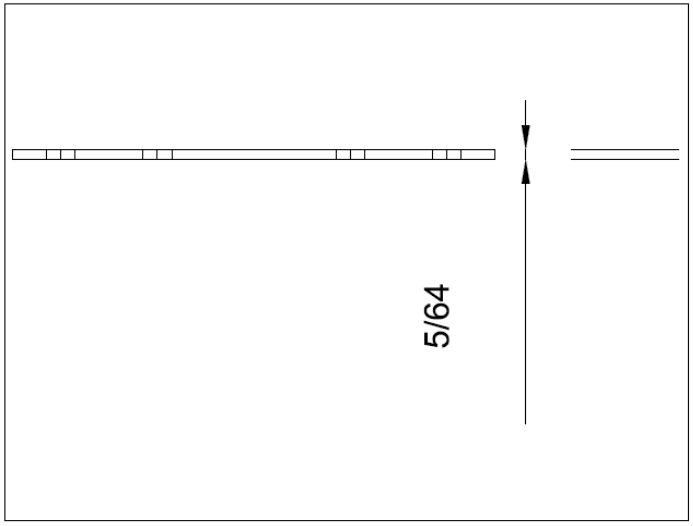

Attachment plates (2x)

Top view – 3D view – Front view

Appendix IV: Force on Plate Centroid Calculations

The depth of the drag force centroid was determined using a number of different tests. For each test the centroid was computed using a basic centroid calculation with a weighted average being attributed to the velocity or velocity squared. In the end, the velocity squared was chosen as the weighted centroid parameter over simply the velocity because the drag force acting on an object is related to the velocity squared in the drag force equation (Batchelor 2000):

$$F_D = \frac{1}{2}\rho v^2 C_D A \qquad \textbf{(AIV-1)}$$

Where:

- F_D is the drag force
- ρ is the density of the fluid
- v is the fluid velocity
- C_D is the dimensionless drag coefficient
- A is the cross section area

The drag force centroid location above the bed is calculated using the following equation:

$$Centroid_{DF} = \sum A_i * d_i(v_i^2) / \sum A_i \qquad \textbf{(AIV-2)}$$

Where:

- A_i is the area of a sub-section
- d_i is the distance to the middle of this sub-section
- v_i is the average velocity in this sub-section

In the following table, the drag force centroid locations were computed for various tests using both *v* and v^2.

Table AIV-1: Force On Plate Centroid Calculations

Test: 20contr_30open_crv1							
Depth (cm)	v (m/s)	v^2	Area * (v)	Area * (v^2)	D: centroid of each area (cm)	Area (v)*d	Area (v^2)*d
0	0.065655	0.004311	0.695673	0.123789	2.5	1.739183	0.309471
5	0.212614	0.045205	1.08436	0.235258	7.5	8.132699	1.764434
10	0.22113	0.048898	0.563012	0.126835	11.25	6.333887	1.426889
12.5	0.22928	0.052569	0.575064	0.132281	13.75	7.907128	1.81886
15	0.230771	0.053255	1.733627	0.400729	18.75	32.50551	7.513677
22.5	0.23153	0.053606	1.732712	0.400307	26.25	45.48368	10.50806
30	0.230527	0.053143					
						centroid (with v)	**17.64227 cm**
						centroid (with v^2)	**17.77964 cm**
Test: 20contr_40open_crv1							
Depth (cm)	v (m/s)	v^2	Area * (v)	Area * (v^2)	D: centroid of each area (cm)	Area (v)*d	Area (v^2)*d
0	0.049678	0.002468	0.662373	0.122024	2.5	1.655933	0.305059
5	0.215271	0.046342	1.113838	0.248408	7.5	8.353785	1.86306
10	0.230264	0.053022	0.573739	0.131672	11.25	6.454563	1.48131
12.5	0.228727	0.052316	2.26676	0.513862	17.5	39.6683	8.992586
22.5	0.224625	0.050456	1.696864	0.383933	26.25	44.54269	10.07824
30	0.227872	0.051926					
						centroid (with v)	**17.52182 cm**
						centroid (with v^2)	**17.54099 cm**
Test: 15contr_30open							
Depth (cm)	v (m/s)	v^2	Area * (v)	Area * (v^2)	D: centroid of each area (cm)	Area (v)*d	Area (v^2)*d
0	0.163571	0.026756	0.941928	0.180525	2.5	2.354821	0.451311
5	0.2132	0.045454	1.090834	0.238107	7.5	8.181256	1.785804
10	0.223134	0.049789	0.560818	0.12581	11.25	6.309205	1.415367
12.5	0.225521	0.05086	0.561385	0.126063	13.75	7.71904	1.733373
15	0.223587	0.049991	1.676995	0.374975	18.75	31.44365	7.030778
22.5	0.223612	0.050002	1.679443	0.376071	26.25	44.08539	9.871873
30	0.22424	0.050284					
						centroid (with v)	**17.54897 cm**
						centroid (with v^2)	**17.59606 cm**
Test: 15contr_25open_crv1							
Depth (cm)	v (m/s)	v^2	Area * (v)	Area * (v^2)	D: centroid of each area (cm)	Area (v)*d	Area (v^2)*d
0	0.117314	0.013763	0.834735	0.151674	2.5	2.086836	0.379184
5	0.21658	0.046907	1.111008	0.247026	7.5	8.332559	1.852693
10	0.227823	0.051903	0.572676	0.131187	11.25	6.442605	1.475854
12.5	0.230318	0.053046	0.579588	0.134375	13.75	7.96934	1.847654
15	0.233353	0.054454	1.74707	0.406968	18.75	32.75757	7.630659
22.5	0.232532	0.054071	1.74225	0.404725	26.25	45.73405	10.62403
30	0.232068	0.053855					
						centroid (with	**17.59835**

						v)	**cm**
						centroid (with v^2)	**17.69329 cm**
Test: 15contr_25open							
Depth (cm)	v (m/s)	v^2	Area * (v)	Area * (v^2)	D: centroid of each area (cm)	Area (v)*d	Area (v^2)*d
0	0.080691	0.006511	0.76138	0.141562	2.5	1.90345	0.353905
5	0.223861	0.050114	1.15498	0.26705	7.5	8.66235	2.002877
10	0.238131	0.056706	0.594459	0.141353	11.25	6.687668	1.590222
12.5	0.237437	0.056376	0.595483	0.141842	13.75	8.187893	1.950321
15	0.23895	0.057097	1.794435	0.429334	18.75	33.64566	8.050006
22.5	0.239566	0.057392	1.793313	0.428798	26.25	47.07447	11.25594
30	0.238651	0.056954					
						centroid (with v)	**17.57354 cm**
						centroid (with v^2)	**17.64398 cm**
Test: 10contr_25open							
Depth (cm)	v (m/s)	v^2	Area * (v)	Area * (v^2)	D: centroid of each area (cm)	Area (v)*d	Area (v^2)*d
0	0.065941	0.004348	0.774861	0.159715	2.5	1.937153	0.399287
5	0.244003	0.059538	1.259533	0.317597	7.5	9.446499	2.381978
10	0.25981	0.067501	0.645127	0.166483	11.25	7.25768	1.872937
12.5	0.256292	0.065685	0.641385	0.16455	13.75	8.819041	2.262562
15	0.256816	0.065955	1.916043	0.489509	18.75	35.9258	9.178303
22.5	0.254129	0.064581	1.912028	0.487452	26.25	50.19073	12.7956
30	0.255745	0.065406					
						centroid (with v)	**17.51455 cm**
						centroid (with v^2)	**17.52678 cm**

As one can see from the results above there is not much difference between tests or even between using v or v^2. The average of the v^2 drag force centroid values of the tests above was used to modify the force on the load cell for all tests. **Therefore, a drag force centroid value of 17.63 cm above the bed was used.**